UNIVERSITA' DEGLI STUDI DI PADOVA

DIPARTIMENTO DI INGEGNERIA INDUSTRIALE
CORSO DI LAUREA MAGISTRALE IN INGEGNERIA ELETTRICA

TESI DI LAUREA MAGISTRALE

Analysis of the control system of a high tension test laboratory on composite materials for aeronautic applications

RELATORE: *Prof. Roberto Caldon*
Dipartimento di ingegneria industriale

CORRELATORE: *Prof. Manu Haddad*
School of Egineering, Cardiff University

LAUREANDO: *Giuseppe Mastrolembo*

ANNO ACCADEMICO 2012/2013

INDEX

ABSTRACT

As everybody know energy delivered by a lightning is much higher than energy managed daily by humans and so a lightning lab should satisfy two requirements: first and most important safety for people for buildings and for electrical circuits. From the first requirement follows the second: as much as simplicity in the design of the circuits.

INTRODUCTION

Nowadays, global efforts to reduce Green House Gas (GHG) emissions across all sectors have reinforced use of novel Carbon Fibre Composite (CFC) materials in airframe structures. However, as each commercial aircraft is struck by lightning at least once a year, flight safety of these next-generation aircraft becomes critically important. Consequently, Cardiff University made a collaboration with aircraft manufacturer, EADS®, and the Welsh Government, to establish a lightning simulation and research facility, called the ***Morgan-Botti Lightning Laboratory (MBLL)***. From the two requirements of the abstract the first led to build a pneumatic safety control system that has characteristic to be almost immune from electromagnetic disturb and it can manage safety of the entire lab during experiments and during the rest of the time for example during the maintenance of the main circuit. The addition of a control chamber, from where is possible to manage all the lab, that has characteristic to be a Faraday cage and an optical transmission I/O system to communicate from control chamber to the circuit and vice versa ensures maximum safety for the people within the lab. The second led to have simple RLC circuit that were designed to manage properly high currents and tension. Necessity to manage the main circuits in remote (to ensure safety for people) prompted design and construction a control system that allows control of all operating modes of the main circuit from control chamber through LabVIEW Interface software. Once again to guarantee simplicity control system operates in DC mode and open loop and this ensure to have very simple circuits. In the first part of this work will be explained the lightning phenomena from the physics point of view, considering as a lightning flash can born and as it can propagates and electrical characteristics. The CFRPs structural, mechanical and electrical characteristics and the interactions between lightning and CFRPs consideration too. The MBLL will be able to make tests that reproduce faithfully a natural lightning. The correct shape of the waveforms for the tests have been studied by ***The European Organisation for Civil Aviation Equipment (EUROCAE)*** and they are included in the ED84 report. The MBLL will be able to reproduce the EUROCAE waveforms. In the first part of this work a brief description of the EUROCAE waveforms will be done. In the chapter two will be discussed the characteristics of the MBLL considering the main electrical circuits and their operation which are able to reproduce the different types of waveforms. The waveforms made by main circuits have to be properly coordinated in order to simulate a lightning for this reason the Lab is equipped by a control system that are able to manage the operation of the electric circuits. The chapter three will be focused to the control system in particular the electrical circuit and the operation of the three control chassis. After description of the control system in the chapter four will be explained the simulations of the operation of the control system correlate of graphs and argumentation of the results. Simulations made by the known software Orcad PSpice 9.1 for windows.

CHAPTER ONE

Lightnings, Interactions, CFRP, Test waveforms

1.1 Lightning mechanism

Lightning struck the Earth long before human life, and may even have played a crucial role in the evolution of life on our planet. In the earth planet, lightning lights up the sky about one hundred times per second, and while not every lightning reaches the ground – about 75% of lightning discharges remain in the clouds.

Lightning usually occurs in the charge centre of the cumulonimbus clouds. The charge centres, as illustrated in Fig. 1-1, are formed by several meteorological interactions, which transport positive charges on the upper layer of the cumulonimbus cloud, thereby forcing negative charges to accumulate at the lower part of the cloud [1].

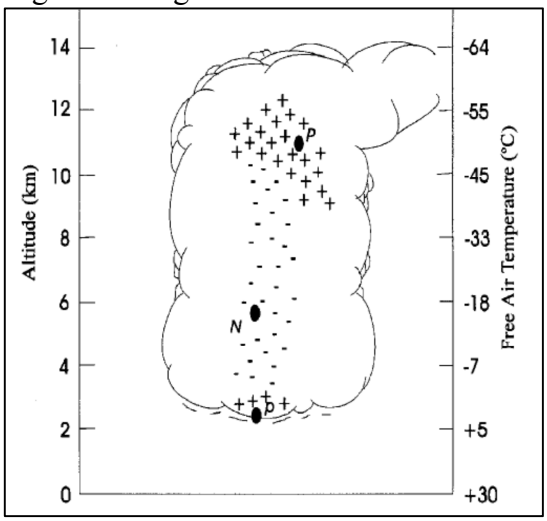

Figure 1.1: Generalized diagram showing distribution of electrical charge in a typical cumulonimbus cloud

Consequently, a potential difference is created between charged regions and between a charged region and ground [2]. When electric fields due to these charges become large enough, the air between regions of opposite polarity becomes ionized to form an electrically conducting channel and is possible to see the lightning flash. The ionized column is called a leader, and movement of the charged particles produces the electric current [2]. Lightning flash could be intra-cloud, inter-cloud or cloud-to-ground discharges [1]. In cloud-to-ground flashes the process that finish in a lightning flash begins with the formation of an ionized column called a leader which travels out from a region where the electric field is sufficiently high that it initiates progressive ionization. This occurs when the field is about 500kV/m. This kind of flash can contain between one to twenty-six strokes each flowing in the same channel [2]. Typically, the leader advances in steps each about 50 meters long, which are separated in time by about 40ms to 100ms; hence it is called a stepped-leader [1]. The diameter of the stepped leader is between 1m and 10m although the current, which is low (about 100A), is concentrated in a small highly ionized core, about 1 cm diameter., travelling at a velocity of about 1,5X10^5 m/s . The leader may form branches when it approaches the ground resulting in ionization of the air at extremities of ground objects, due to amplification of the electric fields at pointed surfaces [1]. The process of discharging the leader is known as the return stroke,

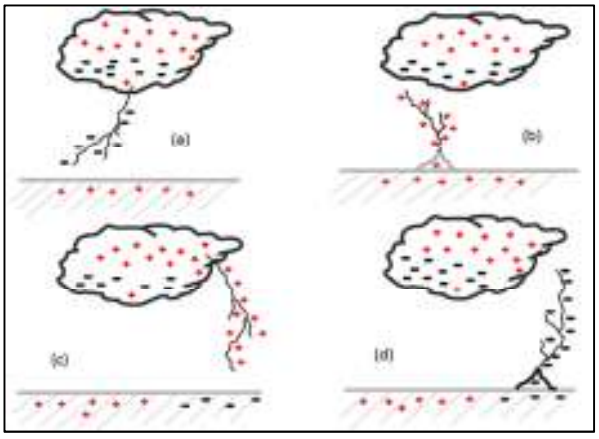

which proceeds at a velocity of about 5X10^7 m/s . A return stroke rapidly attains very high peak currents that heats up the conducting channel to peak temperatures of about $50{,}000^0$F, hence increasing channel pressure to about ten times normal atmospheric pressure [2]. These events culminate in visible light to the human eye and sets up shock waves that become the audible thunder sound wave [2] [1]. A negative downward lightning discharges electron through the lightning channel, and 90 per cent of cloud-to-ground strikes is in this category. The remaining 10 per cent occur as either positive downward, positive upward or negative upward discharges [2], and studies have shown that cloud-to-ground flashes produce higher electrical currents than intra-cloud flashes. A positive flash is one that lowers positive charge to earth while a negative flash lowers negative charge. It is common for a negative flash to discharge several charge centers in succession, with the result that the flash contains several distinct pulses of current, and these are usually referred to as subsequent strokes. Return stroke modeling indicates that there is a decrease of the value of the return stroke current versus altitude. This is typical of a negative flash to open ground, but over mountains and tall buildings, the leader may be of the upward moving type, originating from a high point such as a mountain peak. When such a leader reaches the charge pocket in the cloud, a return stroke is also initiated and subsequent events follow the same pattern as for initiation by a downward moving leader. Thus the "switching" point is near the ground for downward leaders but near the charge pocket in the cloud for upward leaders. This can make a significant difference to the waveform and amplitude of the current experienced by an airborne vehicle which may be intercepted by a flash. There is evidence that cloud-to-ground flashes produce more intense currents than intracloud lightning.

1.1.1 The negative flash to ground

An example of the return stroke current is shown in Fig 1.3. There are about between 1 and 24 strokes in a negative flash, with the mean value being 3; very few flashes contain more than 24 strokes. The total duration of the flash is between about 20ms and 1s, with a mean value of 0.2s. The time interval between the strokes is typically about 60ms. There is some correlation among these parameters, the flashes with the most strokes tend to have the longest duration. The rise time of the first stroke is about 6μs, with a decay time (to half the peak amplitude) of about 70μs. Subsequent strokes in the flash tend to have higher rates-of-rise although lower peak amplitudes than the initial stroke and they can therefore be significant for inducing voltages in aircraft wiring, where the inductively coupled voltages are proportional to the rate of change of the lightning current.

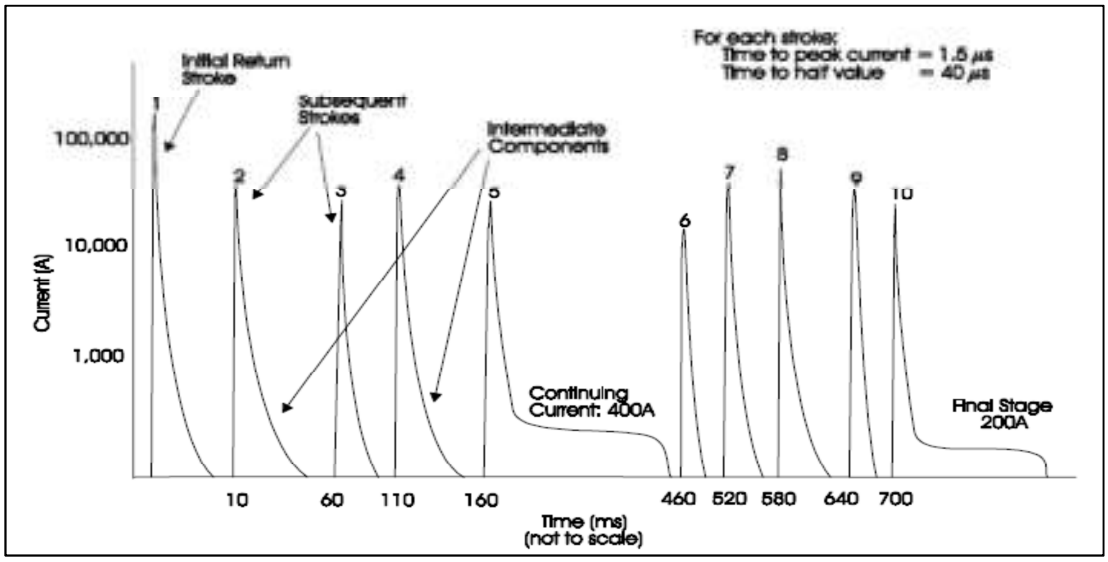

Fig 1.3: Model of a severe negative lightning flash waveform

Close the end of some of the strokes in a negative flash, there are often a lower level current of a few kA persisting for several milliseconds, known as an 'intermediate current', as shown in Fig 1.3. After some strokes a "continuing current" of 100-400A flows with duration of 100-800ms, so that there is substantial charge transfer in this phase. It is particularly common for there to be a continuing current after the last stroke. It is generally thought that before a restrike can occur the continuing current must cease, as illustrated after stroke 5 in Fig 1.3.

There are three different modes of charge transfer to ground in lightning discharges. It is convenient to illustrate these for the case of negative subsequent strokes. In negative subsequent strokes these three modes are represented by (a) dart-leader-return-stroke sequences, (b) continuing currents and (c) M-components:

In a leader-return-stroke sequence, the descending leader creates a conductive path between the cloud charge source and ground and deposits negative charge along this path. The following return stroke traverse that path, moving from ground toward the cloud charge source, and neutralizes the negative leader charge. Thus, both leader and return-stroke processes serve to transport effectively negative charge from the cloud to ground.

(a) The lightning continuing current can be viewed as a quasi-stationary arc between the cloud charge source and ground. The typical arc current is tens to hundreds of amperes, and the duration is up to some hundreds of milliseconds.

(b) Lightning M-component can be viewed as perturbations (or surges) in the continuing current and in associated channel luminosity. It appears that an M-components involves the superposition of two waves propagating in opposite directions.

(c) For all the processes mentioned, the channel conductivity is of the order of 10^{-4} S/m, except for the channel section between the dart-leader tip and ground shown by a broken line in Fig 1.4. For this latter channel section, the conductivity is about 0.02 S/m. (1)

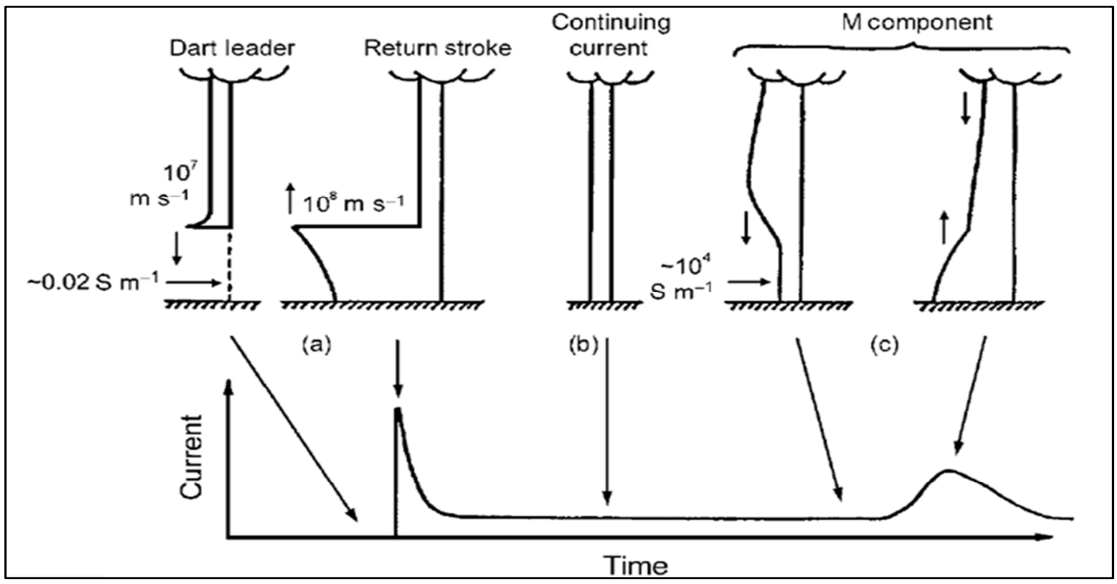

Fig. 1.4: modes of charge transfer to ground

1.1.2 The positive flash to ground

Positive flashes to ground generally occur less frequently than negative flashes, however in certain geographic locations there may be more positive flashes to ground. Present standards have assumed an average of 10% of flashes to ground are of positive polarity. Positive flashes are usually initiated by upward moving leaders and more commonly occur over mountains than over flat terrain. Normally they consist of one stroke only followed by continuing current. Positive strokes have slower rise times than negative strokes, with higher peak currents and charge transfers. The stroke duration is longer than most negative strokes. An example of the current in a positive flash is shown in Fig 1.5; it is a moderately severe example although not the "super flash" which occurs occasionally. Typically the rise time of a positive flash is 20μs and the total duration 0.1s. Although positive flashes are less frequent than negative, they have been considered in formulating the lightning environment for design and certification purposes.

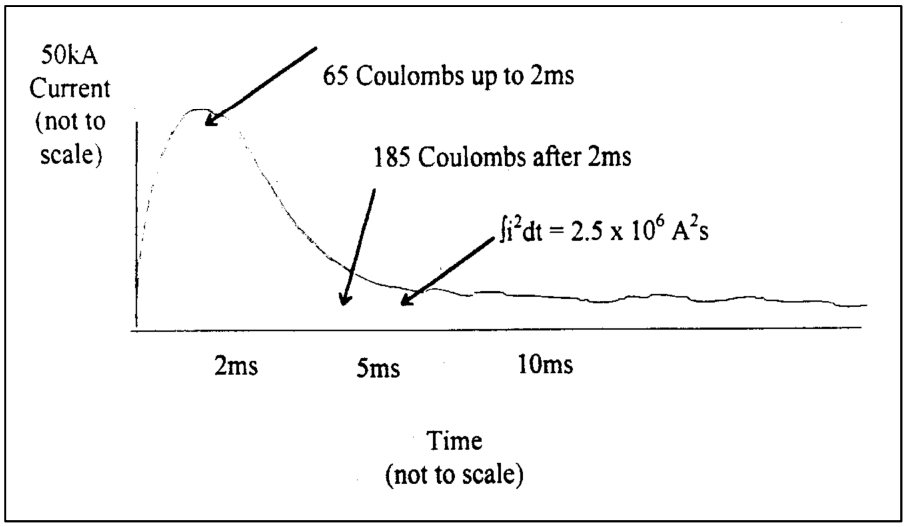

Fig 1.5: Typical Positive Flash

1.1.3 Inter and Intra-Cloud Flashes: The preceding discussion relates to flashes of either polarity to ground since most available knowledge relates to flashes of that type. Instrumented aircraft have been employed in U.S.A. and France to record the characteristics of cloud flashes. Generally speaking, the conclusion is that intracloud flashes are less severe than flashes to the ground, certainly with respect to peak current, charge transfer and action integral. However, the airborne measurements show some evidence that over a portion of some pulse wavefronts the rate-of rise for a short time (less than 0.4μs) may be higher than the cloud to ground flashes. Short pulses of low amplitude but high rate-of-rise have been observed during intra-cloud flashes. Similar pulses due to charge redistribution in a cloud have been observed between return strokes in flashes to ground. For intra-cloud discharges up to 60kA peak currents have been recorded, but are more typically 20-30kA. The pulses occurring during the initial lightning attachment phase occasionally occur in negative cloud to ground flashes. For the designer of aircraft, the difference between cloud to ground and cloud to cloud lightning may be academic. Aircraft may, after all, be expected to encounter all types of flashes. Whether the high current striking an aircraft is associated with the upper end of a cloud-to-ground flash or with a intra-cloud flash makes no difference. Protection designs and test data presented here are expected to account for each of these lightning environments.

1.1.4 Lightning Parameters: Most of the available statistical data are from cloud to ground and ground to cloud lightning flashes. The relevant data are presented in Fig. 1.6 is divided into negative and positive flashes. The tables include statistical data for the lightning currents and all related parameters of interest for the definition of the lightning environment. For a given flash or stroke parameter, the tables show that as the magnitude increases, the percentage of occurrence decreases. The extreme parameters do not occur together in one flash.

Parameters Positive Flashes	Unit	Lightning Parameters 95%	 50%	 5%
Flash duration	ms	14	85	500
Total charge	C	20	80	350
Positive Stroke		**95%**	**50%**	**5%**
Peak current	kA	4.6	35	250
Peak rate-of-rise	A/s	2×10^8	2.4×10^9	3.2×10^{10}
Time to peak	μs	3.5	22	200
Time to half value	μs	25	230	2000
Impulse charge	C	2	16	150
Action integral	A^2s	2.5×10^4	6.5×10^5	1.5×10^7

–Note: The individual parameters listed above do not necessarily occur together in one flash.

Parameters Negative Flashes	Unit	Lightning Parameters 95%	 50%	 5%
Number of strokes		1 - 2	3 - 4	12
Time intervals between strokes	ms	8	35	140
Flash duration	s	0.03-0.04	0.2	1
Charge in flash	C	1.3	7.5	40
Negative first stroke				
Peak current	kA	14	30	80
Peak rate-of-rise	A/s	5.5×10^9	1.2×10^{10}	3.2×10^{10}
Time to peak	μs	1.8	5.5	18
Time to half value	μs	30	75	200
Impulse charge	C	1.1	5.2	24
Action integral	A^2s	6×10^3	5.5×10^4	5.5×10^5
Negative subsequent strokes				
Peak Current	kA	4.6	12	30
Peak rate-of-rise	A/s	1.2×10^{10}	4×10^{10}	1.2×10^{11}
Time to peak	μs	0.22	1.1	4.5
Time to half value	μs	6.5	32	140
Impulse charge	C	0.2	1.4	11
Action integral	A^2s	5.5×10^2	6×10^3	5.2×10^4
Continuing current		**98%**	**50%**	**2%**
Amplitude	A	33	140	520
Duration	s	0.058	0.16	0.40
Charge	C	7	26	110

Note 1: The above lightning parameters do not necessarily occur together in one flash.
Note 2: The percentage figures represent percentiles, that is, the percentage of events having a greater amplitude than those given.

Fig 1.6: Tipical parameters of positive and negative flash

The available data indicate that the cloud to ground flashes represent the most severe lightning threat to the aircraft as regards with physical damage to composite structures. The high rate of rise pulse currents measured during the initial and the final attachment phases to instrumented aircraft may constitute a severe indirect effects threat. Similar pulses with fast rates of change have also been reported in cloud-to-earth flashes which convey negative charge to the earth. In addition to the lightning currents, electric fields exist before and during a lightning strike event. Initially, these fields result in breakdown of the air to form the attachment and may also cause breakdown of dielectric materials on an aircraft. The magnitudes of these fields are dependent upon air breakdown thresholds and range between 400 and 3000 kV/m, with rates of rise of up to 1000kV/m/μs.

1.2 Interaction between lightning and aircraft

1.2.1 Aircraft Lightning Attachment Points

A lightning flash initially attaches to, or enters, an aircraft at one spot and exits from another. Usually these are extremities of the aircraft such as the nose or a wing tip. For convenience, these are called initial entry and initial exit points. At any one time, current is flowing into one point and out of another. The "entry" point may be either an anode or a cathode; that is, a spot where electrons are either entering or exiting the aircraft. The visual evidence after the strike does not allow one to resolve the issue and usually no attempt is made. Instead, by convention, attachment spots at forward or upper locations have usually been called entry spots and those at aft or lower locations on the aircraft have been termed exit points. Since the aircraft flies more than it's own length within the lifetime of most flashes, the entry point will change as the flash reattaches to other spots after of the initial entry point. The exit point may do the same if the initial exit spot is at a forward portion of the aircraft. Thus, for any one flash, there may be many "entry" or "exit" spots and the following definitions are used: **lightning attachment point:** The place where the lightning flash touches (attaches to) the aircraft. **initial entry point:** The place where the lightning flash channel first "enters" the aircraft (usually an extremity).

initial entry point: The place where the lightning flash channel last "enters" the aircraft (typically a trailing edge).

initial exit point: The place where the lightning flash channel first "exits" from the aircraft (usually an extremity).

final exit point: The last place where the lightning flash "exits" from the aircraft (usually a trailing edge).

swept "flash"(or "stroke") points: Spots where the flash channel reattaches between the *initial* and *final points*, usually associated with the *entry* part of the flash channel.

1.2.2 Aircraft Lightning Strike Mechanisms

The electrical conditions which produce lightning, together with the mechanisms of lightning strike attachment to an aircraft are discussed in the following paragraphs. While it is not impossible to anticipate or avoid these conditions all of the time, it is important to understand the strike attachment process in order to properly assess the ways in which lightning effects aircraft.

1.2.2.1 Electric Field Effects: At the beginning of lightning flash formation, when a stepped-leader propagates outward from a cloud charge center, the ultimate destination of the leader, at an opposite charge center in the cloud or on the ground, has not yet been determined. The difference of potential which exists between the stepped leader and the opposite charge(s) establishes an electrostatic field between them, represented by imaginary equipotential surfaces, which are shown as lines in the two dimensional drawing of Fig. 1.6. The field intensity, commonly expressed in kilovolts per meter, is greatest where equipotential surfaces are closest together. It is this field that is available to ionize air and form the conductive spark which is the leader. Because the direction of electrostatic force is normal to the equipotentials, and strongest where they are closest together, the leader is most likely to progress toward the most intense field regions.

An aircraft will always assume the electrical potential of its location. Since the aircraft is typically a large conductor, whose surfaces are all at this same potential, it will divert and compress adjacent equipotentials, thus increasing the electric field intensity at its extremities, and especially between it and other charge sources, such as the advancing leader. If the aircraft is far away from the leader, its effect on the field near the leader is negligible; however, if the aircraft is within several tens or hundreds of meters from the leader, the increased field intensity in between may be sufficient to attract subsequent leader propagation toward the aircraft. As this happens, the intervening field will become even more intense, and the leader will advance more directly toward the aircraft.

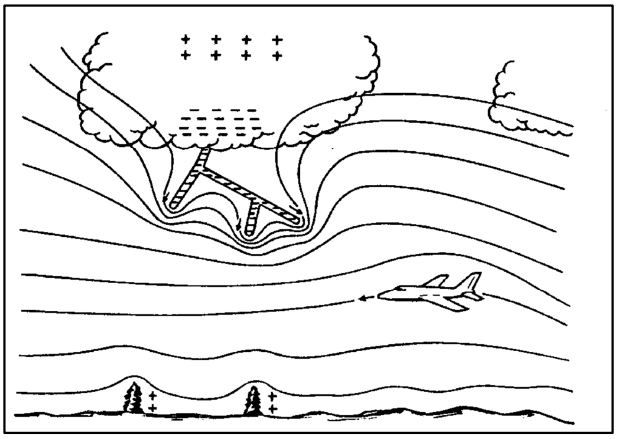

Fig. 1.6: Stepped leader approaching an aircraft.

The highest electric fields about the aircraft will occur around extremities, where the equipotential lines are compressed closest together, as shown in Fig. 1.7. Typically, these are the nose, wing and empennage tips, and also smaller protrusions, such as antennas or air data probes. When the leader advances to the point where the field adjacent to an aircraft extremity is increased to about 30 kV/cm (at sea level pressure), the air will ionize and electrical sparks will form at the aircraft extremities, extending in the direction of the oncoming leader. Several of these sparks, called streamers, usually occur nearly simultaneously from several extremities of the aircraft. These streamers will continue to propagate outward as long as the field remains above about 5 to 7 kV/cm. One of these streamers, called the junction leader, will meet the nearest branch of the advancing leader

and form a continuous spark from the cloud charge center to the aircraft. Thus, when the aircraft is close enough to influence the direction of the leader propagation, it will very likely become attached to a branch of the leader system.

1.2.2.2 Charge Stored on Aircraft: Streamers may propagate onward from two or more extremities of the aircraft at the same time. If so, the oncoming leader will have split, and the two (or more) branches will continue from the aircraft independently of each other until one or both of them reach their destination. This process of attachment and propagation onward from an aircraft is shown in Fig.1.8. When the leader has reached its destination and a continuous ionized channel between charge centers has been formed, recombination of electrons and positive ions occurs back up the leader channel, and this forms the high-amplitude return stroke current. This stroke current and any subsequent stroke or continuing current components must flow through the aircraft, which has now become part of the conducting path between charge centers. If another branch of the original leader reaches the ground before the branch which has involved the aircraft, the return stroke will follow the former, and all other branches will die out. No substantial currents will flow through the aircraft in such a case, and any damage to the aircraft will be slight.

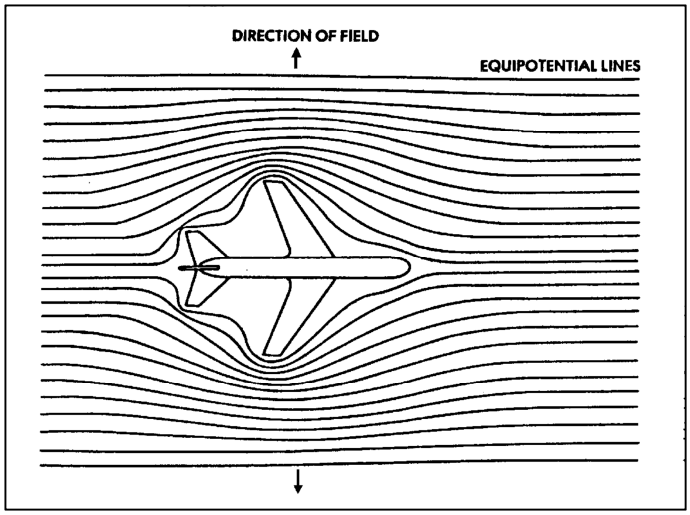

Fig. 1.7: Compression of electric field around an aircraft

1.2.2.3 Aircraft Inititiated Lightning Strikes: A question often asked is "If an aircraft cannot produce a lightning flash from its own stored charge, can it trigger a natural one?" Stated another way the question might be "Would the lightning flash have occurred if the aircraft were not present?" A second question would be "Even if aircraft do trigger lightning, would there be an impact on the criteria to which aircraft must be designed?" Some preliminary discussion of the mechanism by which aircraft triggers lightning is necessary. There is clear evidence that lightning flashes can be triggered by research aircraft that are intentionally flown into clouds to observe

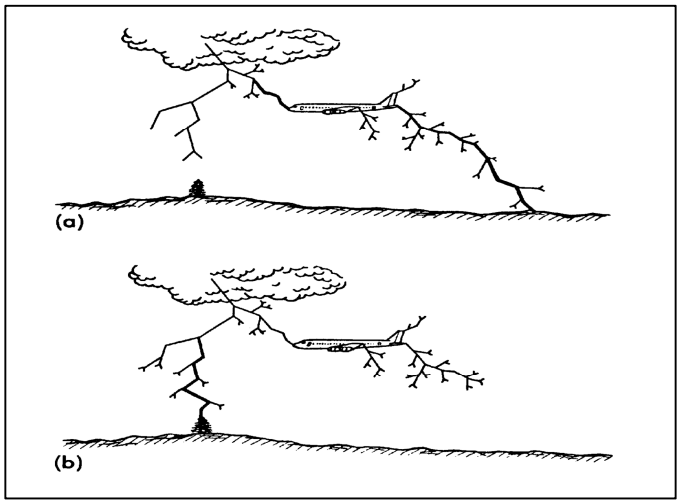

Fig.1.8: Return stroke paths

lightning phenomena, but it is not clear how often aircraft in normal service trigger lightning.

1.2.2.4 Swept Flash Phenomena

After the aircraft has become part of a completed flash channel, the ensuing stroke and continuing currents which flow through the channel may persist for up to a second or more. Essentially, the channel remains in its original location, but the aircraft will move forward a significant distance during the life of the flash. Thus, whereas the initial entry and exit points are determined by the mechanisms previously described, there may be other lightning attachment points on the airframe that are determined by the motion of the aircraft through the relatively stationary flash channel. In the case of an aircraft, for example, when a forward extremity such as the nose becomes an initial attachment point, its surface moves through the lightning channel, and thus the channel appears to sweep back over the surface, as illustrated in Fig.1.9. This occurrence is known as the swept flash phenomenon. As the sweeping action occurs, the type of surface can cause the lightning channel to attach and dwell at various surface locations for different periods of time. The aircraft does not usually fly out of, or away from, the channel. This is because the potential difference between charge centers (cloud and earth or another cloud) is sufficient to maintain a very long channel until the charges have neutralized each other and the flash dies.

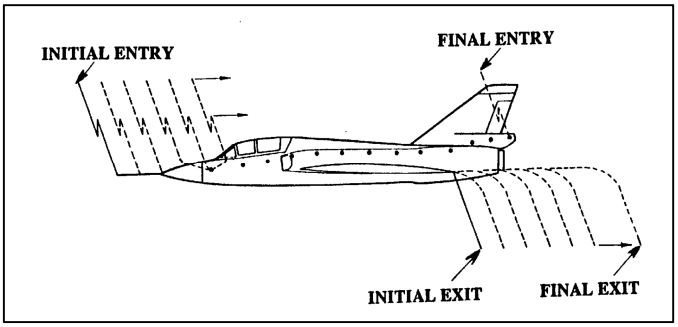

Fig.1.9: Typical path of swept flash attachment points.

1.2.5 Lightning zone location

The severity of the damage a direct lightning strike inflicts on an airborne vehicle is determined by: the lightning arc characteristics, the airframe strucure, the interaction between the aircraft and the lightning channel [22], and the zone or region of the aircraft under consideration [20].

Zoning is used to classify the areas that are susceptible to direct and indirect effects of lightning, and further used to differentiate areas prone to lightning attachment from areas acting as a conducitve path [15]. Following from Fig.1.10, three main regions that are considered are Zones 1, 2 and 3. 18

Each zone represents aircraft areas that are likely to be subject to a certain lightning current amplitude and lightning component in the lightning test environment. In [15], these zones are defined as follows:

Zone 1: Regions likely to experience initial lightning attachment and first return stroke;

Zone 2: Regions likely to experience subsequent return strokes; typically the areas where swept phenomenon occurs;

Zone 3: Regions unlikely to experience arc attachment but where conduction of lightning current between attachement points occur.

Further subdivisions include Zones 1A and 2A where long arc attachment is unlikely as a result of relative motion between the aircraft and the lightning channel which causes a swept phenomenon in a direction opposing aircraft motion. In addition, Zones 1B and 2B define the regions where lightning channel is unlikely to move, because the relative motion cannot sweep the attachment further, hence long hang on of arc is envisaged. Lastly, Zone 1C represents all the areas of the aircraft surface where a first return stroke of reduced amplitude is envisaged, usually having low likelihood of attachment [15] [16].

Typically, a leading-edge location will be subjected to the current components A and possibly the intermediate current component B. Components C and D will not be experienced by a leading edge because the aircraft will have flown past the lightning attachment point. The converse is also true, as a trailing edge will most likely experience all the four current waveform components and the arc will tend to hang on there for the duration of the flash [20].

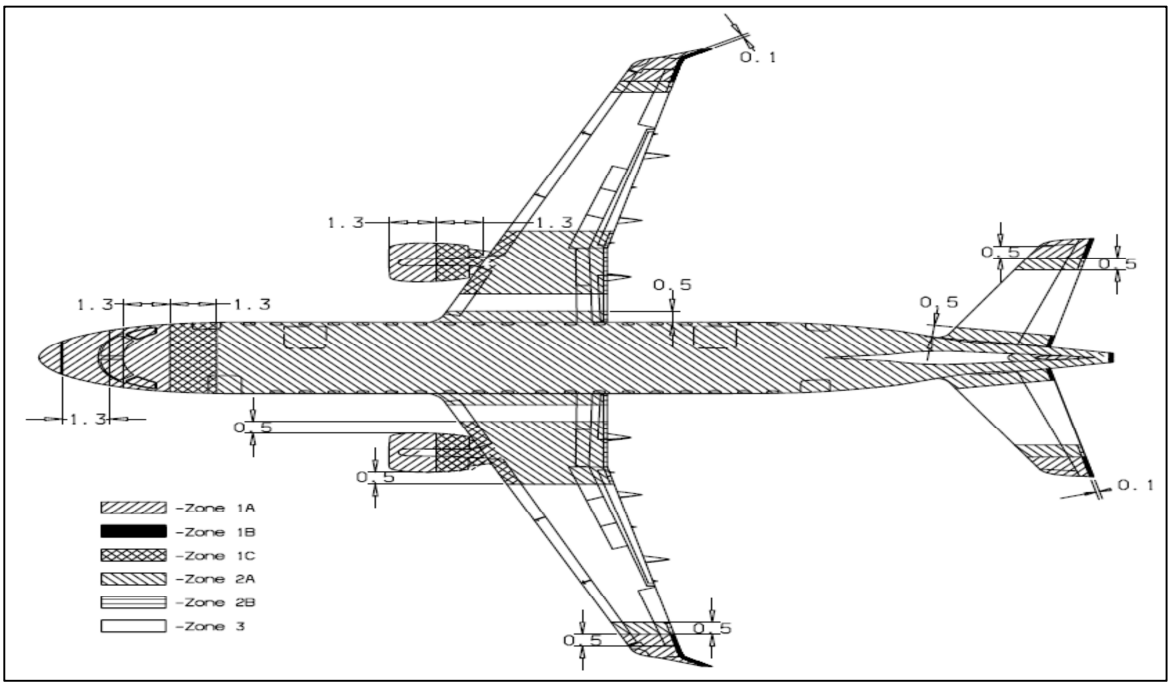

Fig.1.10: Example of lightning strike zone detail of typical transport aircraft

1.3 Carbon composite for aerospace applications

In practice, CFCs are manufactured from carbon fibres embedded in an epoxy matrix, and its robust strength is derived from the strength of individual strands of carbon [3]. Over the last decade, CFCs have progressively supplanted conventional metal alloys in aerospace applications [4] [5].

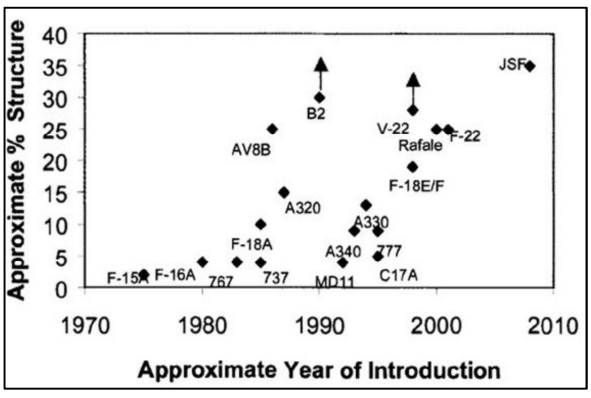

Several authors agree that a major driver behind this rapid transition from conventional alloys to CFCs is the substantial weight savings they evidence; hence, resulting in lower fuel consumption with consequent emissions reduction [4] - [6]. In addition, other advantages of using CFCs include: availability in a wide range of forms, ability to form complex shapes easily, plus resistance to radar and radio signals which make them suitable for use as radomes and antenna covers [7].

1.3.1 Progress in Carbon Composite Development

In the 1960s, the simultaneous invention of graphite fibre reinforced plastic (GFRP) in the UK and boron fibre reinforced plastic (BFRP) in the US marked the entry of composite materials into the aerospace industry [5]. By 1970, the development of BFRP had proceeded more rapidly in the US [5], and military aircraft manufacturers had started to make very little use of fibrous composite materials [4] - [3]. Although development of GFRP proceeded rather slowly, the cost of BFRP had risen to about five times an equivalent GFRP material in 1980.

This economic reality informed the decision of the US to switch over to GFRP [5], paving the way for use of composites in secondary and tail components such as rudder and wing trailing-edge panels [3].

Today, new materials now used include: carbon and graphite fibres, organic material fibres such as Kevlar, new matrix material such as polyimide, and improved metals such as Aluminium, Titanium and Nickel. As these new fibre and matrix materials have undergone different stages of maturity over the years [4], the latest generation of airliners will extensively deploy them for use in primary load carrying structures [5] [3].

Fig.1.11 reveals the upward trend of growth in advanced composite materials used in airframe structures over a forty year period until 2010. Following from the development trend between 1990 and 2000, authors in [8] inferred that costs considerations kept composite application low in commercial transport, while a peak uptake of about 35 per cent composite structure was evident in the Joint Strike Fighter (JSF) and other military aircraft [9]. However, today the world's largest aircraft, Airbus® A380, using composite materials in its wings, has achieved a stellar 17 percent lower fuel consumption per passenger than comparable aircraft [3]. Following these more recent advances, Fig. 1.12 [10] reveals that fully half of the Boeing® 787-Dreamliner airframe structure has been designed with composites, and the 250-seater jetliner will burn 20 per cent less fuel and have maintenance costs 10 per cent lower than any airplane of its size [6]. Markedly, these novel composite materials will provide improved fuel efficiencies with consequent increased profits to airliners, while reducing pollution to the environment.

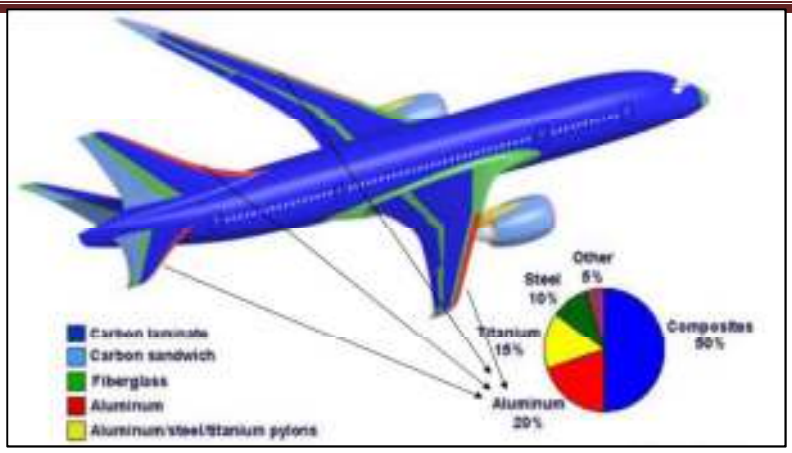

1.3.2 Characteristics of carbon composite materials

Carbon fibres have inherent high strengths and small diameters of about 6 to 10 microns [4]. Comparatively, the ultimate strength of CFC is about five times that of aluminium

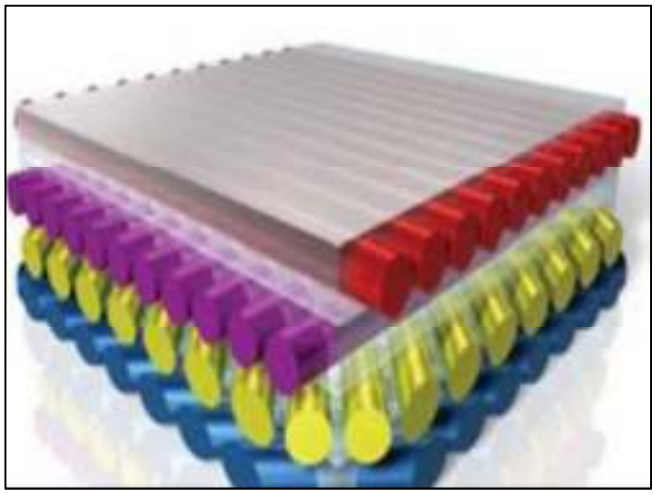

Fig 1.13: Arrangement of Carbon fibre composite to form laminate

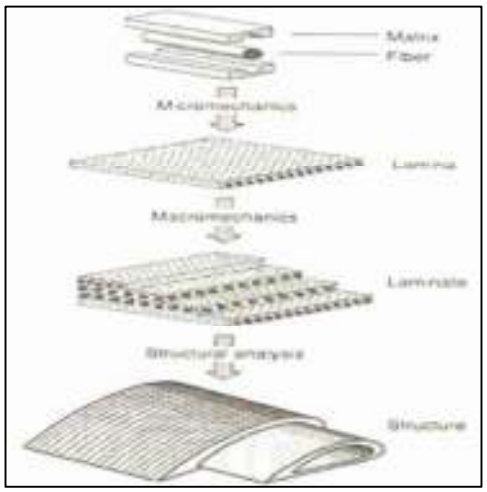

Fig 1.14: Flow diagram showing various stages of manufacturing composite materials

alloys, and its density about 60% that of aluminium alloys [3]. Also, CFC is generally lighter, stronger and more resistant to fatigue and corrosion, compared to metal alloys [6].

In twenty-first century military and commercial aircraft, the CFCs used, which are otherwise known as pre-pregs, come in the form of uni-directional (UD): thin (~0.125mm - 0.25mm thick) sheets or tapes of parallel fibres, supplied with resin squeezed around the fibre [5] [3] [11]. The aforementioned parallel fibres have straight fibre strands which are laid side by side to run in the form of a ribbon [9]. Pre-pregs are stored in refrigerators to prevent premature curing of resin at room temperature [3]. To form a single compact piece or sub-component, pre-pregs can be laid into moulds by hand or by robotic tape-laying machines, such that successive sheets or plies are arranged over each other in different directions, as in Fig.1.13 [3] [11]. The high-strength pre-preg system is cured in a large pressure chamber called autoclave, subject to heat and pressure [11]. Fig.1.14 depicts the flow of a typical CFC manufacturing process

A piece of composite having parallel fibres is much stronger when pulled in the direction of the fibre than when pulled to the side. Thus, the mechanical and physical properties of CFCs vary with direction; hence, they are anisotropic [4]. Consequently, the desired stiffness, strength and weight can be achieved by adjusting the direction of orientation of the successive layers, dependent on design [3].

1.3.3 Lightning in CFRP

Lightning strike is very dangerous to all structures, whether metallic or composites, and requires careful consideration from a certification standpoint. Lightning can induce damage on an aircraft structure, both metallic and composite, by melting or burning at lightning attachment points, resistive heating, magnetic force effects, acoustic shock, arcing and sparking at joints, and ignition of vapors in fuel tanks, so recent work is being conducted to assess the use of novel protection systems, such as the introduction of conductive carbon nanotubes, to reduce the lightning strike damage and to replace current protection systems, such as copper strips and interwoven conductive wires.

One of the major causes of CFRP damage was considered to be shockwaves due to supersonic-speed expansion of the ionized leader channel when a return stroke occurs. However, focusing on the lightning attachment point, it can be observed that most of the resin was burned off or evaporated by the heat. The arc root burning voltage of carbon is higher than that of metals. This effect, plus the high bulk resistivity, generates more heat in the immediate arc root area and the hot spot remains for a longer period than for most metals. Thus, short duration high action integral pulses as well as low current long duration pulses produce high thermal inputs, and so all phases of the lightning flash are significant in producing arc root damage in carbon fiber composites. [12].

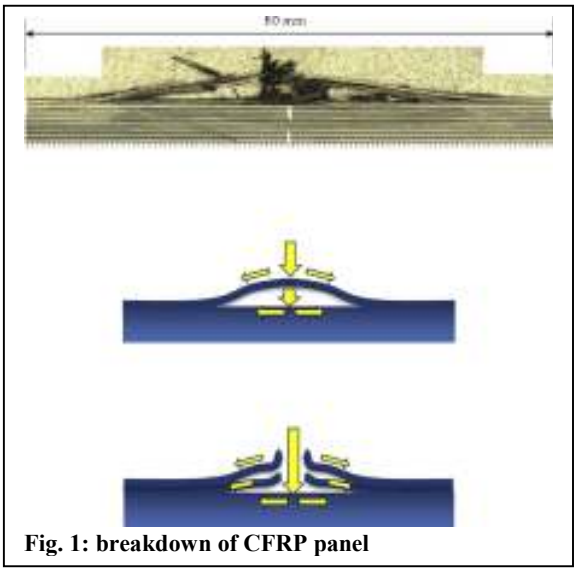

Fig.1.15: breakdown of CFRP panel

A possible phenomenon occurring with through-thickness electrical conduction is dielectric breakdown at the interlayer gaps. As temperature rises through resistive heating, the burning or pyrolysis of resin advances, and reacted resins release gas. The rapid evaporation of trapped gas in interlaminar layers results in an explosive fracture in the vicinity of the lightning stroke attachment point. Dielectric breakdown of pyrolysis gases at the interlayer gaps is shown in Fig.1.15. Therefore, the combination of a shockwave event and a rapid evaporation of resin through

resistive heating is a major cause of explosive fractures of surface fiber. The other most important phenomenon, the delamination, occurs because of matrix resin decomposition. The surface temperature exceeds 3,000 °C within 1μs, consequently, surface recession caused by carbon sublimation occurs. Once the surface layer is lost because of sublimation, the next layer is exposed directly to the electrical current. Consequently, surface recession also causes apparent electrical conduction in the thickness direction. Both dielectric break down at the interlayer gaps and surface recession occur above decomposition temperature (>600 °C), resulting in electrical conduction to thickness direction [13].

Generally, damage manifests as visible fiber fracture in the outer ply, as well as longitudinal splitting and bulging of the area around the strike. In some cases the upper ply or plies even separate in small chips or fragments and leave an empty space on the surface. In general however, the damage appears to be confined to the surface of the specimen and in the region immediately surrounding the strike zone. The shape of the damage area is elongated in the direction of the fibers in the outer ply. In carbon fiber composites the thermal effects are more pronounced then in metal ones, but the lower thermal conductance and higher electrical resistance affects the proportions of vaporizing and propagation processes and lead to an increase in area in relation to the depth of damage [12].

A lightning damage region in the thickness direction is limited to the vicinity of the damaged surface because of the strong orthotropic electrical properties of graphite/epoxy laminate. These strong orthotropic electrical properties generate a similar electrical current distribution in the thickness direction near the lightning attachment surface. As a result, varying the thickness of a specimen does not affect the size of damage in each damage mode.

Each damage mode shows strong correlation with a particular lightning parameter; the fiber damaged area and damage thickness is governed by the peak current of the lightning stroke, while the resin deterioration area and the delamination projection area are determined by the electrical charge and the action integral of the waveform, respectively.

Unnotched and filled-hole CFRP specimens were subjected in some laboratories [14] to simulated lightning strike damage at different current levels (10, 30, 50 kA). Although there appear to be a clear trend of increasing projected damage area for increasing current intensity, the size of the damage areas for the 30 and 50 kA strikes are relatively similar. Beyond 10 kA, the damage area reaches the boundaries of the specimen and is then forced to grow longitudinally. For the unnotched specimen it appears that the projected damage area increases linearly up to 30 kA, and then levels off. The filled-hole specimens were tested to see the effect of discontinuities or the effect of a fastener in a panel. For filled-hole specimens the results are dramatically different. For 10 kA strikes, the only damage visible is surface pitting of the fasteners on the head side, where the strike takes place, however, for the 30 and 50 kA strike the surface damage is much more extensive than in the unnotched specimens. In general it appears to be mostly due to acoustic shock, hence

the large bulging of the upper plies, rather than burning of the matrix on the surface, as for the unnotched specimens.

From the mechanical point of view it is interesting to observe that at the maximum energy level, 50 kA, the reduction in tensile strength is approximately 20%, while in compression it is slightly over 30%. Unnotched residual strength for both tension and compression decreases in a relatively linear fashion with current intensity Fig.1.16

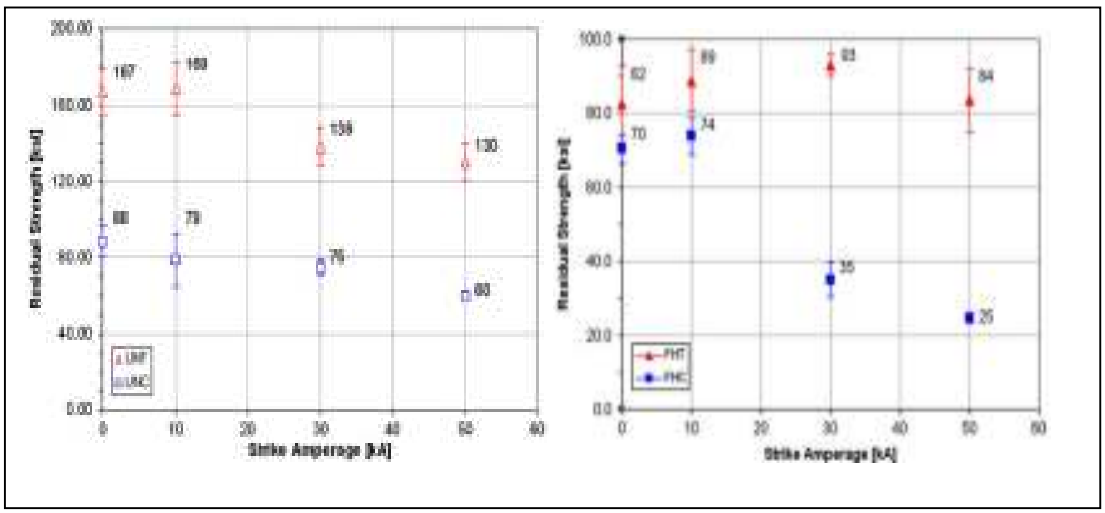

Fig.1.16: residual strength for tension and compression in unnotched and filled-hole panels

Optical microscopy confirms that for unnotched specimens the damage is confined to the upper two–four plies, while for filled-hole specimens it is either confined to the fastener alone at the lowest applied current, or it affects the entire thickness of the laminate up to the backface at the higher applied currents. The complex damage state inside the laminate comprises pyrolized fibers, vaporized resin, and traces of inter- as well as intra-ply arcing [14] [15].

1.4 Waveforms for lightning tests

1.4.1 General

The environment waveforms presented in this section represent idealized environments which are to be applied to the aircraft for purposes of analysis and testing. The waveforms can't replicate a specific lightning event, but they are intended to be made of different waveforms whose effects upon aircraft are similar of that from natural lightning. The standard lightning environment is composed of different voltage waveforms and current waveform components which is the important characteristics of the natural lightning flashes. In the following waveform descriptions, parameters of particular importance to the effects to be considered, are included whereas other parameters are omitted. For example, for direct effects evaluations, peak current amplitude, action integral and time duration are the main parameters, whereas for indirect effects evaluations, rates of current rise and decay as well as peak amplitude are considered. Not all surfaces of an aircraft need to be

designed to survive the same lightning threat. This section presents waveforms and their related parameters to be applied for aircraft structures and equipment lightning protection design and verification purposes.

1.4.2 Idealised Voltage Waveforms

The idealized Voltage Waveform represents that portion of the electric field important for assessment of lightning attachment to aircraft structures.

The basic Voltage Waveform that airplane are subjected for analysis or test is one that represents an electric field which increases until breakdown occurs either by puncture of solid insulation such as the fiberglass skin of a radome, or flashover through the air or across an insulating surface. The path that the flashover takes, either puncture or surface flashover, depends in part on the waveshape of the electric fields.

It is sometimes necessary to determine the critical voltage amplitude at which breakdown occurs. This critical voltage level depends upon as the rate-of-rise of voltage as the rate of voltage falling. Two examples are: (1) determining the strength of the insulation used on electrical wiring; and, (2) determining the points from which electrical streamers appear on a vehicle as a lightning flash approaches. Since there is a several kind of possible electric field waveforms produced by natural lightning, two voltage waveforms have been established, representing fast and slow rates of field rise. These are Waveform A and Waveform D. Two other high voltage Waveforms designated B and C are described below. The first is a full voltage Waveform to be used wherever an impulsive field that does not reach breakdown is required, i.e. streamer testing. The second Waveform is employed for fast front model tests. Waveform D can also be used for slow front model tests.

It has been determined in laboratory testing that the results of attachment point testing of aircraft models are influenced by the voltage Waveform. Fast rising waveforms (rise in the order of a few microseconds) produce a relatively small number of attachment points, usually to the apparent high field regions on the model and may produce a greater likelihood of puncture of dielectric skins. Slow front waveforms (in the order of hundreds of microseconds) produce a greater spread of attachment points, possibly including attachments to lower field regions.

The voltage waveforms presented in this document are intended for evaluation of possible lightning attachment locations and/or dielectric breakdown paths through nonconducting surfaces or structures.

Voltage Waveform A

This waveform has a dv/dt of 1000 kV/μs (± 50%) until its increase is interrupted by puncture of, or flashover across, the object under test. At that time the voltage collapses to zero. The rate of voltage collapse or the decay time of the voltage if breakdown does not occur (open circuit voltage of a lightning voltage generator) is not specified.

Voltage Waveform B

Waveform B is a 1.2 x 50μs waveform which is the electrical industry standard for impulse dielectric tests. It rises to crest in 1.2μs (± 20%) and decays to half of crest amplitude in 50μs (± 20%). Time to crest and decay time refer to the open circuit voltage of a lightning voltage generator, and assume that the waveform is not limited by puncture or flashover of the object under test.

Voltage Waveform C

This is a chopped voltage waveform in which breakdown of the gap between an object under test and the test electrodes occurs at 2μs (± 50%). The amplitude of the voltage at time of breakdown and the rate-of-rise of voltage prior to breakdown are not specified.

Voltage Waveform D

The slow fronted waveform has a rise time between 50 and 250μs so as to allow time for streamers from an object to develop. It should give a higher strike rate to the low probability regions than otherwise might have been expected.

All the waveforms are shown in Fig1.17

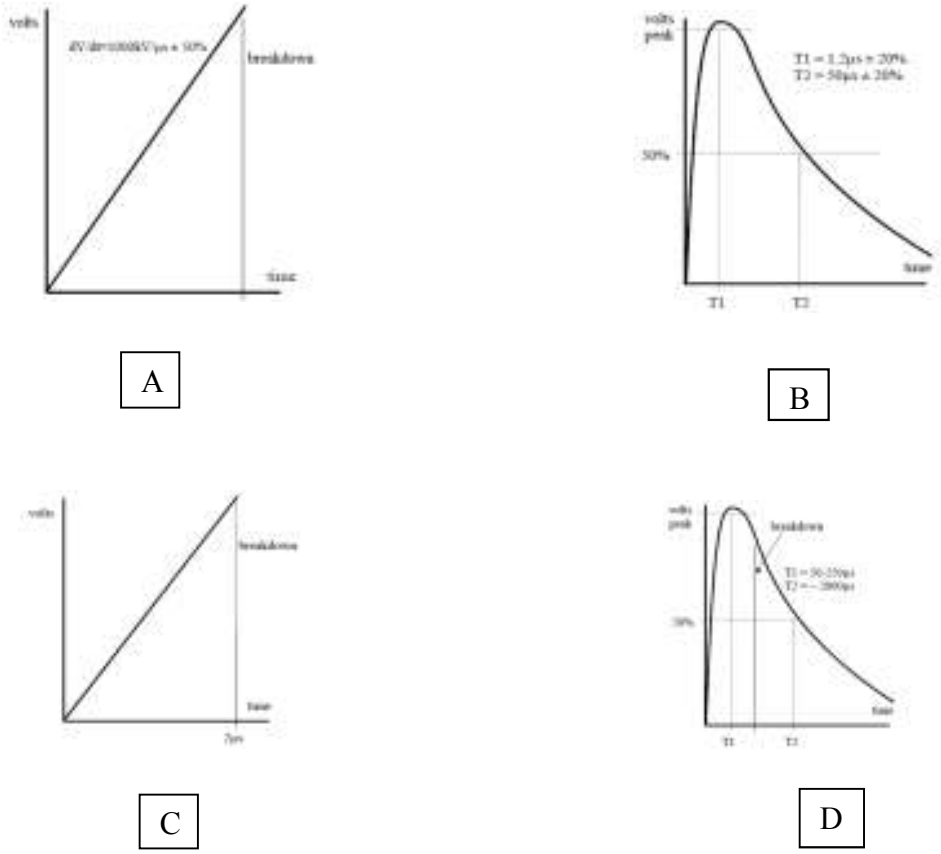

Fig.1.17: Voltage waveform A-B-C-D

1.4.3 External idealized current component

The external lightning environment is comprised of current components A, Ah, B, C, D and H, and the multiple stroke (MS) and multiple burst (MB) Waveform sets. The MS is comprised of components A and D/2, and the MB is comprised of component H pulse sequences. Current components A, B, C, and D comprise the lightning flash current waveform for evaluating direct effects and are shown in Fig.1.18. Current components A and D, and Waveform sets MS and MB are applicable for evaluating indirect effects. In this report only A B C D waveforms will be analysed because by the MBLL only that ones are possible to reproduce right now.
This waveform combines the severe parameters of both the negative and the positive first return strokes. It occurs most frequently to aircraft flying at lower altitudes for example during the take-off or landing.

Current component A – first return stroke current

For analysis purposes and indirect effect considerations the double exponential waveform shown in Fig.1.19 shall be applied.
This waveform is defined mathematically by the double exponential expression shown below:

$$i(t) = I_0\left(e^{-\alpha t} - e^{-\beta t}\right)$$

Where

$I_0 = 218\ 810$ A
$\alpha = 11\ 354\ s^{-1}$
$\beta = 647\ 265\ s^{-1}$
t is time (s)

For direct effects testing purposes component A can be simulated by an oscillatory or unidirectional waveform like those presented in the Fig.1.20 A and B. The current must have an amplitude of 200kA (± 10%) with a rise time of up to 50μs (the time between 10% and 90% of peak amplitude). The action integral has to be 2 x 10^6A^2s (± 20%), and the total time to 1% of peak value shall not exceed 500μs.
The action integral, ∫i2dt, is a critical factor in the extent of damage. It relates to the energy deposited or absorbed in a system. However, the actual energy deposited cannot be defined without a knowledge of the resistance of the system. For example, the instantaneous power dissipated in a resistor is Ri^2, and is expressed in Watts. To find the energy it has to be integrated the value of the power. Action integral can be applied to any resistance value to find the total energy deposited.

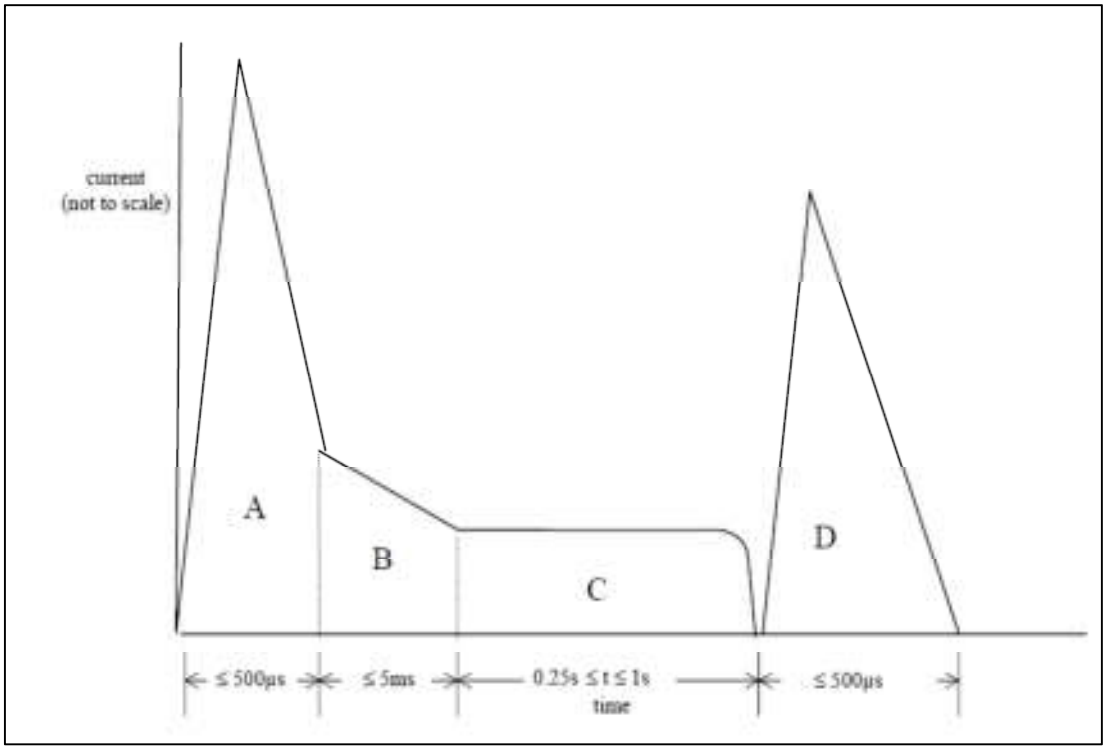

Fig.1.18. Current components A through D for Direct Effects testing.

COMPONENT A (First Return Stroke)

Peak Amplitude	:	200kA (± 10%)
Action Integral	:	2 x $10^6 A^2s$ (± 20%) (in 500µs)
Time Duration	:	≤ 500µs

COMPONENT B (Intermediate Current)

Max. Charge Transfer	:	10 Coulombs (± 10%)
Average Amplitude	:	2kA (± 20%)
Time Duration	:	≤ 5ms

COMPONENT C (Continuing Current)

Amplitude	:	200 - 800A
Charge Transfer	:	200 Coulombs (± 20%)
Time Duration	:	0.25 to 1 s

COMPONENT D (Subsequent Return Stroke)

Peak Amplitude	:	100kA (± 10%)
Action Integral	:	0.25 x $10^6 A^2s$ (± 20%) (in 500µs)
Time Duration	:	≤ 500µs

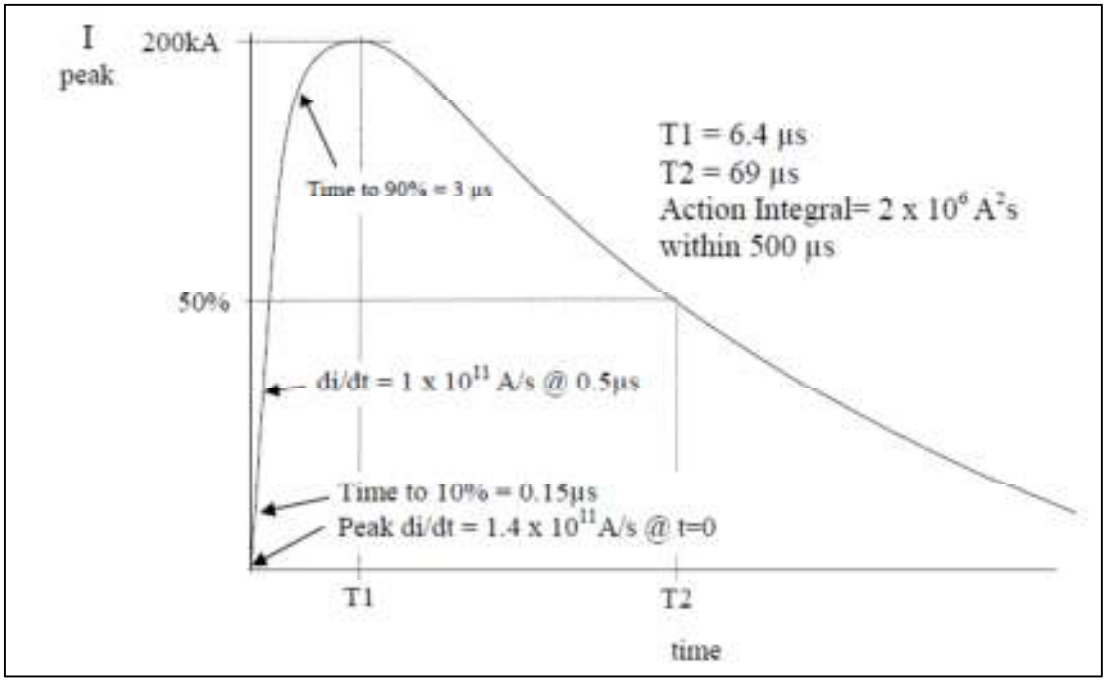

Fig.1.19. Current component A for analysis and indirect effects test purposes.

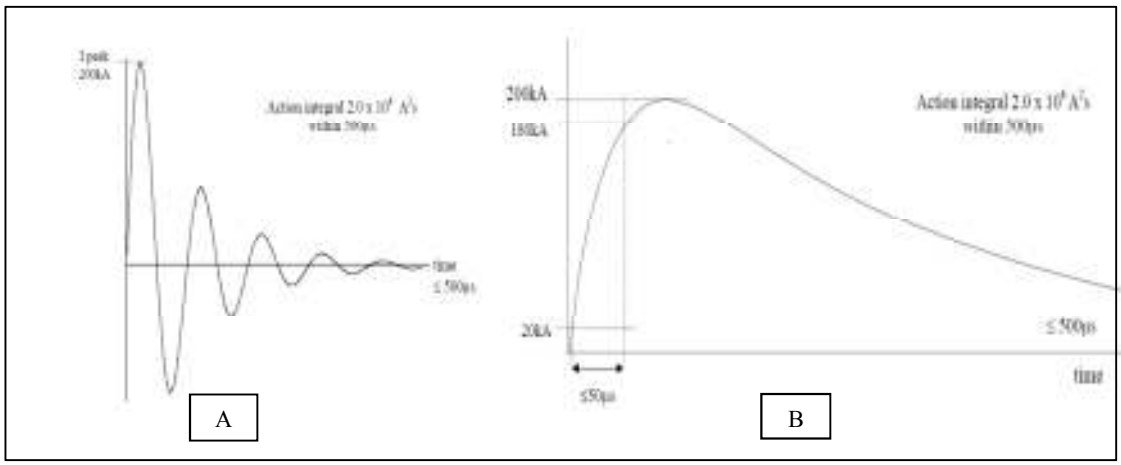

Figure 1.20: A. Damped sinusoidal current. B Unipolar current.

Current component B - Intermediate current

This component represents mainly the intermediate currents following some of the negative initial return strokes and/or restrikes.

This waveform is described mathematically by the following expression:

Where $$i(t) = I_0\left(e^{-\alpha t} - e^{-\beta t}\right)$$

$I_0 = 11\ 300$ A
$\alpha = 700\ s^{-1}$
$\beta = 2\ 000\ s^{-1}$
t is time (s)

For direct effects testing, this component should be unidirectional, e.g. rectangular, exponential, or linearly decaying. The average amplitude must be 2kA (± 20%) flowing for a duration of 5 milliseconds (± 10%) with a charge transfer of 10 coulombs (± 10%).

Current component C - continuing current

This current component represents the lightning environment that might be caused by the long duration currents which may follow some restrikes of the negative cloud to ground lightning strikes and also the return stroke of the positive cloud to ground lightning flashes. For analysis purposes, a square waveform of 400A for a period of 0.5s should be utilized. For direct effects testing, the Component C should have a current amplitude between 200 and 800A, a time duration between 0.25 and 1.0s and transfer charge of 200 coulombs (± 20%). This waveform should be unidirectional; e.g. rectangular, exponential or linearly decaying.

Current component D - subsequent stroke current

The current Component D represents a subsequent stroke in a negative cloud to ground lightning flash. For indirect effect investigations and analysis purposes, the double exponential current waveform presented in Fig.1.21 is used.

The waveform is defined mathematically by the double exponential expression shown below:

$$i(t) = I_0\left(e^{-\alpha t} - e^{-\beta t}\right)$$

Where

$I_0 = 109\ 405$ A
$\alpha = 22\ 708\ s^{-1}$
$\beta = 1\ 294\ 530\ s^{-1}$
t is time (s).

For direct effects testing, the component D can be simulated by either oscillatory or unidirectional waveforms like A waveform with a total time duration to 1% peak value of 500µs. The amplitude shall be 100kA (± 10%), the rise time shall not exceed 25µs (time between 10% and 90% of the amplitude). The action integral is 0.25 x 106A2s (± 20%).

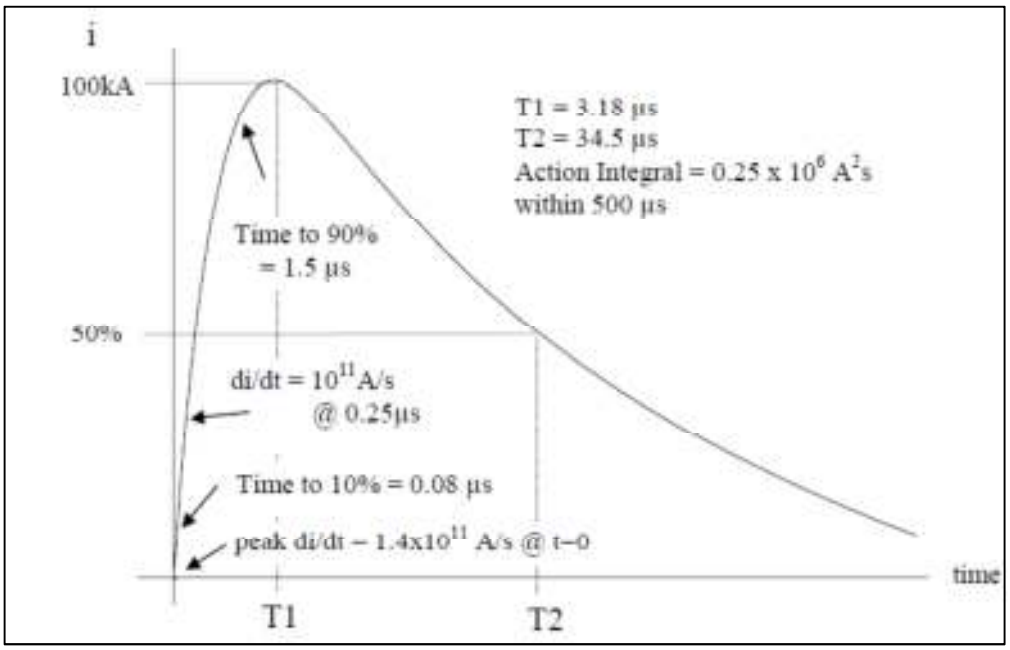

Fig: 1.21. Current component D for analysis purpose and indirect effects test purposes.

CHAPTER TWO

The Morgan Botti lightning laboratory

Introduction

Classically, protection systems in the aerospace industry are desgined for worst-case scenario. Hence, in a bid to ensure adequate lighning protection and flight safety for next-generation carbon composite airborne vehicles, Cardiff University in collaboration with aircraft manufacturer, EADS, and the Welsh Government, has established a lightning simulation and research facility, called the Morgan-Botti Lightning Laboratory (MBLL) [16].

MBLL has been designed to generate full-threat current waveforms in accordance with international aeronautical standards EUROCAE - ED14, ED84, and ED 105. It is envisaged that this controlled lightning, when combined with advanced diagnostics, will be focused to develop and enhance electrical performance of carbon composite materials [16] [17].

Fig 2.1: MBLL 3-D Layout

This novel research facility, having a three dimensional layout illustrated as in Fig. 2.1, requires a maximum current of 63 A from the grid to generate up to 200 kA at full capacity. It is the most advanced University-based lightning test facility in the UK [17] [18]. Pertinently, this laboratory employs RLC control circuits during the discharge of capacitor banks to generate desired component waveforms. When fully developed, the capabilities of this robust facility would be significantly relevant for robust research in any of the following areas [16]:

- Direct effect of lightning strikes on aerospace materials and components.
- Effect of lightning currents on power system components including wind turbines.

- Conduction mechanisms, degradation effects and failure mechanisms of carbon composite materials under lightning strike currents.
- Discharge phenomena and electric and magnetic field distributions in carbon composite materials and components under lightning strikes.
- Characterisation of degradation phenomena in carbon composite materials under the combined mechanical and lightning current stresses.
- Development of optimized designs for carbon composite materials and components for airborne vehicles,
- Investigate performance of coating and paints in combination with carbon composite materials.

Presently, the D-waveform generator is in operation, and installations are underway for B and C generators. The A-component generator remains a futuristic consideration as two more capacitors have yet to be sourced.

2.1 The D Component generator

Following from ED-84, the D-component waveform, which emulates a subsequent return stroke, has a peak current amplitude of 100kA and action integral of $0.25 * 10^6\ A^2s$ in 500μs. To achieve this, a 60kV 20kW charger charges three series connected D bank capacitors, each rated at 20kV, 200μF. Subsequently, the capacitor bank is discharged through a test sample, which is fitted firmly to the mounting plate of a test rig within an enclosed test chamber, using a pneumatic spark gap trigger to achieve excellent personnel safety.

Fig 2.2 is the schematic diagram of the D-waveform generator at MBLL, and a detailed examination of the physical implications of its component parts are presented in following sub-section.

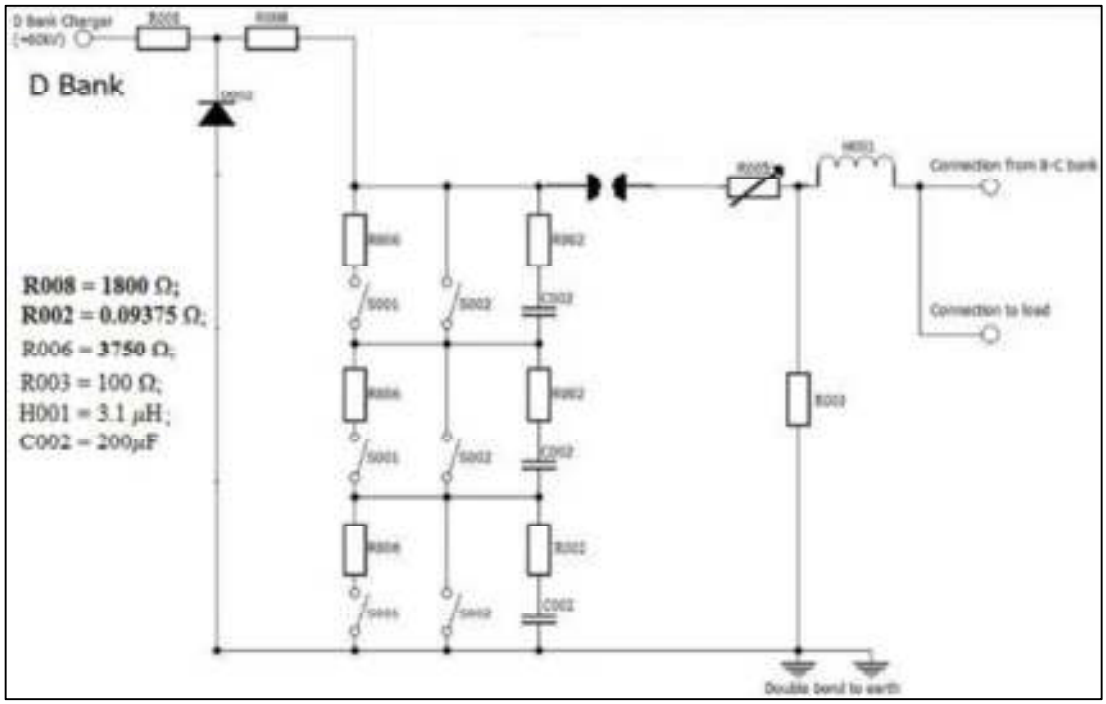

Fig 2.2: Schematic diagram of D-component generator

The 20kW TECHNIX® SR60-P-20000 capacitor charger operates on 400V AC mains supply to deliver 0 - 60kV output voltage, at output current ranging from 0 – 500mA [19] [20]. Both voltage and current outputs are continuously adjustable from 0 to 100% full scale mode.

The charging process is governed by the equation 3.1:

$$I\Delta T = C\Delta V$$

Where;

I: Current setting;

V: Voltage setting;

T: Time needed to reach voltage (V); and

C: Capacitive value of the capacitor connected to the generator.

Remarkably, this air-cooled device has a positive polarity and achieves a rated efficiency of 88% at full load [19]. Considerably, for allowance of a robust safety margin, the charger is typically operated at about 54kV and 330mA. In addition, the equipment is safely grounded to earth and remote control and communication signals with the resident LabVIEW® driver is via optic fibres. Fig 2.3 and 2.4 show the front and rear views of the D-bank charger.

To insure the charger against poor power quality, the supply circuit employs an isolation transformer and power line condition filtering. Also, an Uninterrupted Power Supply (UPS) is employed to safeguard the control system. Novel Double Resonance Technology (DRT) at high frequencies (50kHz) allows smooth switching for all components with significant reduction to harmonics, ripples and internal power loss.

Fig 2.3: Front View of D-bank Charger

Also, the 60kV sub-assembly is immersed in a mineral-oil tank to enhance insulation performance [20].

Fig 2.4: Rear view of D-bank Charger

2.1.2 The Charger Protection Circuit

This circuit, shown in Fig. 2.5, utilizes a stack of sixty DSI 45-16A rectifier diodes to provide protection for the D-bank charger against any feedback from the charging circuit. Each diode has a reverse blocking voltage (VRRM) of 1600V, with forward voltage (VFO) equals 0.85V; the root mean square (rms) forward current is rated at 70A, while the internal resistance of the diode is a negligible 90mΩ [21]. Collectively, the stack, denoted by D002 in Fig. 2.2, withstands 96kV in the reverse direction, and allows conduction in the forward direction at forward voltages above 51V.

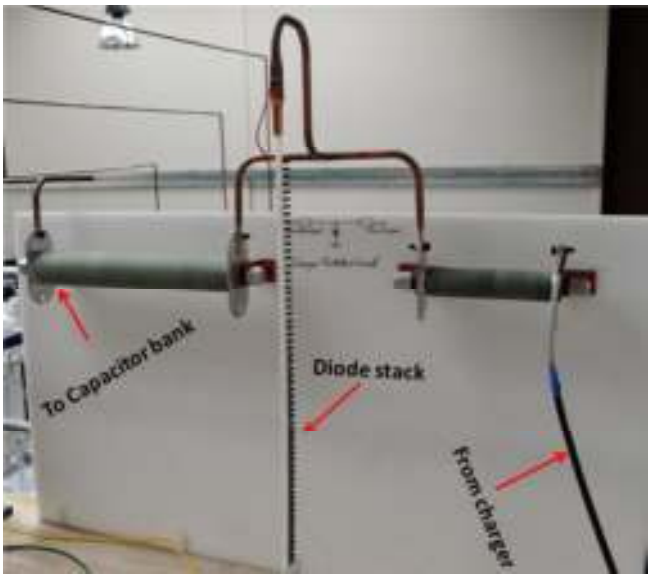

Fig 2.5: Charger protection circuit

Following from Fig. 2.2, R008 is implemented as a 1800Ω ± 20% HVR® Ceramic Carbon Resistor (CCR) assembly in the AD-bank charger filter circuit. Both High Voltage Resistors (HVRs) are air-cooled with design working voltages of 60kV. These HVRs are fastened to a

Polytetrefluoroethylene (PTFE) board to ensure excellent insulation. The one on the charger side can withstand impulse energy of 100kJ, while that on the capacitor side withstands 478.8kJ.

2.1.3 Dumping and Earthing Switches

Dumps are represented by a resistor-switch combination (S001 and R006) in Fig. 2.2, while switch S002 is the short-circuit to earth. During capacitor charging, the pneumatically controlled switches S001 and S002 must be open. Upon capacitor discharge, dumps are closed firstly followed by the earthing switch. This delay is a safety consideration for ejection of excess charges within the system, whilst preventing arcing at the bronze-plated switch terminals.

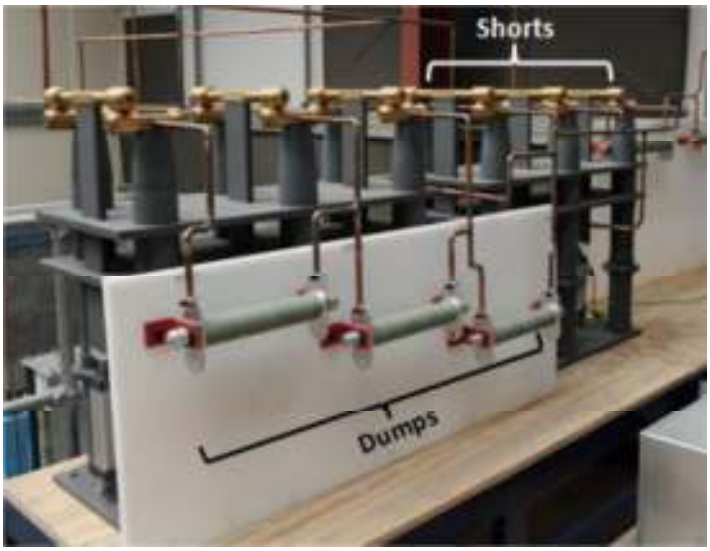

Fig 2.6: Dumping and Earthing switches for AD-banks

Fig 2.6 is the physical connection of the dumping and earthing switches situated together with the D-bank charger and charger protection circuit, by design, on the rooftop of the test chamber for optimal space utilization. Expectedly, the dumping resistors (R006) valued at 3750Ω are HVRs, and firmly fixed to PTFE board so to achieve excellent insulation. Each HVR is rated at 20kV peak voltage and 180kJ impulse energy. Interestingly, electrical connections from the charger via dumps and shorts to the capacitors are implemented using round copper pipes. Anecdoctally, this design preference is due to copper's characteristic high resistance to heat which prevents melting when subjected to high voltages. To achieve robust linkages at HVR terminals, these copper pipes are flattened until the interior surfaces meet (without any crack or flaw). According to BS 1977:1976 [22], the standard value of volume resistivity of annealed copper pipes used in high voltage installations at 20^0C is 0.017241μΩ.m. Consequently, in line with specifications by the International Electrotechnical Commission (IACS), their conductivity value translates to 100 per cent of high conductivity copper.

2.1.4 The D-bank Capacitor Assembly

Basically, the D-bank capacitor arrangement is one-quarter of the A-bank array. In practice, the D-bank generator incorporates three sub-assemblies of series-connected 0.09375Ω resistors with

200μF capacitors, linked in series using long flat aluminium bars. These GAEP® castor oil-impregnated capacitors are rated at 20kV and have Direct Current (DC) life of about 100 hours. The battery life is about 3000 charge/discharged cycles. Undoubtedly, these bespoke energy storage products are built to last. Each capacitor has a single bushing having estimated equivalent series inductance of 40nH. Also, the rated voltage reversal is 20% and maximum peak current rating is about 150kA, while the rated energy is roughly 50kJ [23]. The high voltage stored in the capacitor is lethal and can be retained for long periods. Hence, for personnel safety, grounding sticks are connected to discharge the capacitors when not in use, as in Fig. 2.7. Several HV 12.7cm diameter Linear Disc Resistors, each valued at 0.125Ω ± 10%, are combined uniquely to give an equivalent of 0.09375Ω. This is achieved by connecting six discs in series across eight parallel branches.

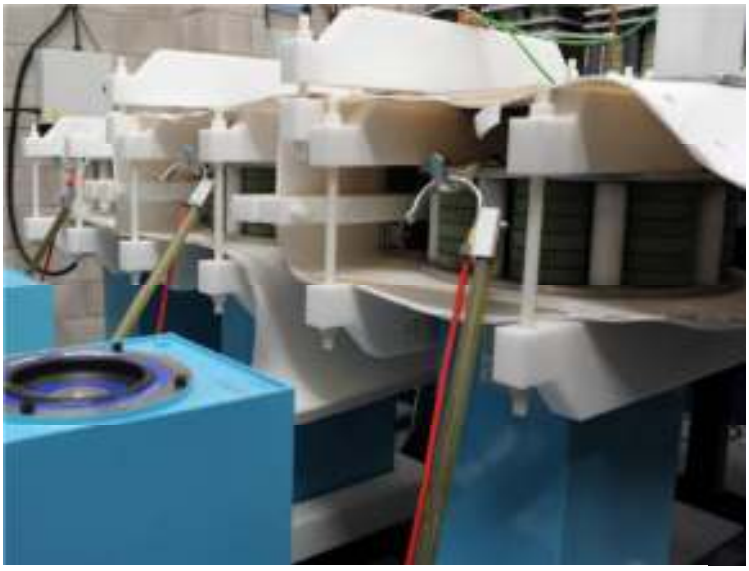

Fig 2.7: D-bank Capacitor Assembly with grounding sticks connected

Interestingly, these HVR® ceramic resistors are manufactured from a carefully blended mix of clays, alumina and carbon, which is subsequently pressed to shape and fired up in a kiln, under a controlled environment [24]. Furthermore, the surface of resulting product (Ceramic Carbon Resistor) is then flame-sprayed with aluminim for electrical contact. Markedly as in Fig 2.7, PTFE sheets are employed for secure insulation levels between busbar layers and this ultimately provides a compact design with minimal construction footprints.

2.1.5 Spark gap, Variable Resistor Array, and Fault Load Resistor

A pneumatic spark gap trigger mechanism assist the arc during direct effect testing of CFCs. The ram houses two electrodes, one on each side, and the arcing proceeds rather very rapidly. Consequent upon this, a blast of air is fed into the ram to cool the spark gap. The metal frame structure, which bears the resistors and capacitor doubles as a pressure chamber for storing the cooling air. The variable resistor (R005) is implemented as three stacks of resistors, which are

combined appropriately to compensate for the test sample resistances. The resistances of stacks A, B, and C respectively are within the range of 0.125Ω – 0.7708Ω, 0.1875Ω – 1.1563Ω, and 0.375Ω – 2.3125Ω. These three stacks are linked together in a parallel connection. Desired equivalent resistance can be achieved by adjusting flat conductive sheets on each stack, which have been designed to specific values. The HVR discs are similar to those earlier described and Fig.2.8 is the pneumatically-controlled spark gap and variable resistor array.

Fig 2.8: The pneumatically-controlled spark gap and variable resistor array

The choice of HVRs in applications of this nature is due to their capability to withstand energy within the range of joules to megajoules and frequencies up to mega-hertz [24]. Following from Fig.2.2, the fault load resistor (R003) is implemented as shown in Fig.2.9.

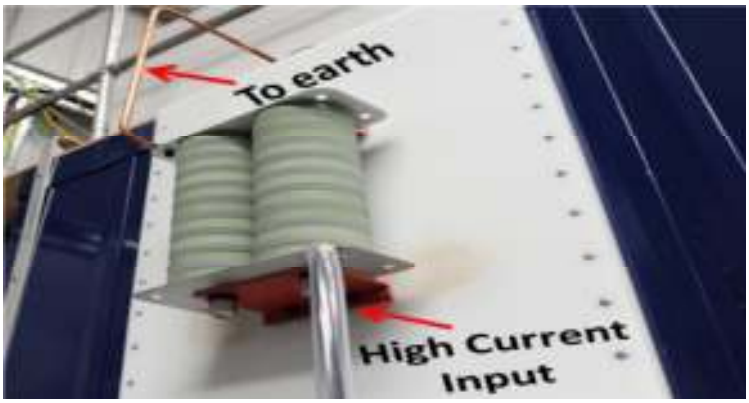

2.1.6 HV Bushing and Cables

The inductor (H001) in Fig.2.2 represents the cumulative inductance of the circuit and is envisaged to be about 3.1μH. Figure 3.10 is the HV bushing linking the variable resistor stack and the test chamber, via eight 50 mm2 H01N2-D welding cables at both input and return paths. However, within the test chamber, only six of these cables are actively connected to the test bed. Certainly, a future upgrade of the two remnant conductors is desirable as this will reduce the overall circuit

inductance. Markedly, this welding cable together with flat aluminum bars were uniformly employed thoroughout the HV area for making connections and linkages.

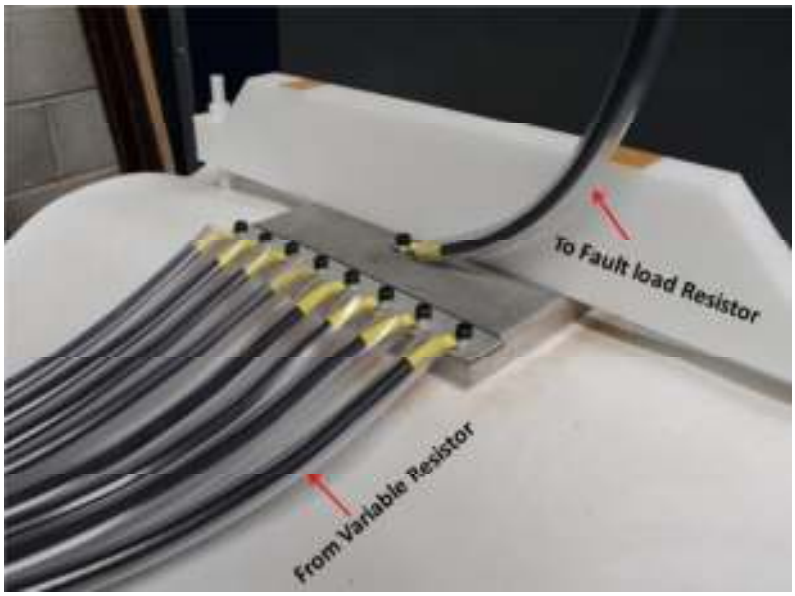

Fig 2.10: High Voltage (HV) bushing

Typically, the H01N2-D welding cable has a core made from Class 5 flexible plain copper conductors. The cable sheath is HOFR (Heat and Oil Resistant and Flame Retardant) with voltage rating of 450V for non-welding applications and thermal ratings between -20^{0}C and +85^{0}C [30]. At 100% duty cycle for a single cycle operation over a maximum period of 5 minutes, the implemented 50mm2 cable has a maximum loading capacity (I100) of 285A. However, following equation 3.1 [25], higher maximum loading capacities can be estimated for duty cycles within timescales on the order of standard lightning current waveforms.

$$I = \frac{I_{100} * \sqrt{100}}{F}$$

Where:

I: is the maximum permissible loading current for the required duty cycle

I100: is the maximum permissible loading current for a duty cycle of 100%

F: is the required duty cycle calculated as a percentage of 5 minute operating period. 35

From the foregoing, considering a typical AD-waveform with duty cycle of about 500µs, the maximum permissible loading current can be estimated:

$$F = \frac{500 * 10^{-6}s}{5 * 60s} * 100\% = 1.667 * 10^{-4}$$

Thus,

$$I = \frac{285 * \sqrt{100}}{1.667 * 10^{-4}} \approx 17 * 10^{6} A$$

Clearly, this current rating is more than enough to withstand the A-bank's peak current estimated at 250kA.

2.2 The test rig

The test rig (as in Fig. 2.11) is located inside a test chamber, which is a two-layered steel wall construction, designed to absorb the sound and evacuate any debris produced whilst testing samples. The test sample mounting frame has dimension $550 * 550\ mm$, upon which the test sample is firmly fitted.

Fig.2.11: The test rig

Fig 2.12 illustrates a two-dimensional layout of the test rig and the current is supplied to the test rig via six (6) single core 50 mm2 conductors, ditto for the return path. To prevent escape of stray fields, the test rig is designed such that aluminum conductors dropping down within four plastic legs guide the high current unto the bottom aluminum plate from the top aluminum plate.

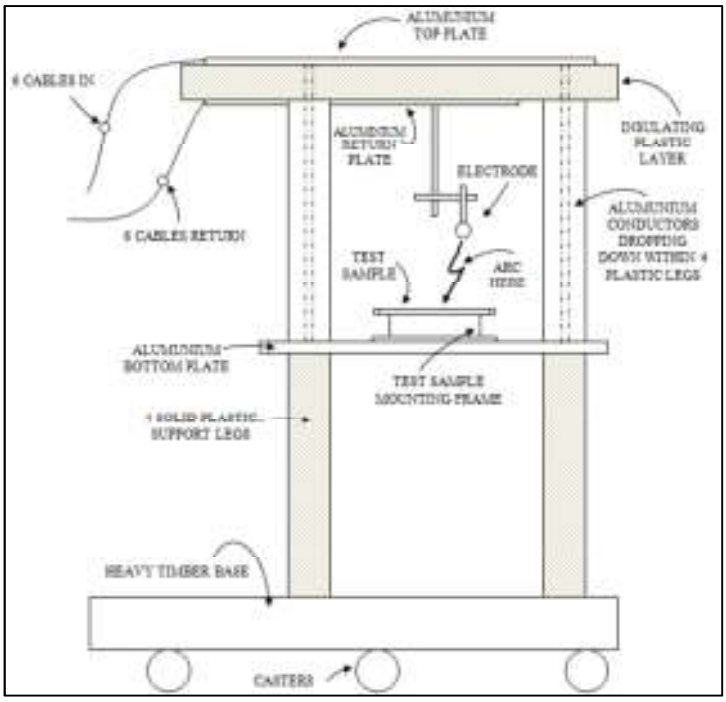

Fig 2.12: 2-D Layout of the test rig

Thus, the test sample mounting frame acts as the point of entry and the electrode serves as the exit point enroute the aluminum return plate. Additionally, the electrode is used to direct the point of attachment and an insulating plastic layer effectively separates the top aluminum plate from the aluminum return plate. The four solid plastic legs, which provide insulation and support, are mounted on a heavy timber base for stability and the entire construction is borne by casters for ease of maneuvering. When testing CFC samples having a layer of copper mesh, test samples are drilled at the edges and screwed to the mounting frame, through a square aluminum frame. This ensures reliable contact between the mesh and the mounting frame.

2.3 The test chamber

A shot of the lightning current will be usually accompanied by a loud noise with consequent physical burn-through and/or in some cases obliteration of test sample. Hence, the test chamber has been carefully designed to remedy these consequences for excellent personnel safety. This test cell, with an overall dimension of 5.0m × 4.0m × 4.0m high, has a thick inner perforate. The inner layer is painted black and the 4m side has a full width and height double doors. The roof is also designed to support external loading for optimal space utilization. The fan blower in Fig. 2.13 circulates fresh air for removal of any smoke and dust emanating after each shot. Akin, an air extractor located on the roof of the test chamber also bolsters circulation.

Fig.2.13: The Fan blower

The fan shown in Fig. 2.13 belongs to the class of F-type Forward Curve Multivane Fans. They are well suited for low pressure high volume applications and its airstream can be modified to handle gases at up to 200^0C. Typical applications are in heating, ventilating, cooling and hot gas recirculation processes [26].

2.4 Rogowski Coil

Rogowski coils (Rocoil) are governed by Faraday's Law of electromaganetic induction. In agreement with [29], they have been employed for non-invasive measurement of the high speed current pulse flowing through the conductors at the HV bushings. Fig 2.14 is the main Rocoil implemented at MBLL. The output signal from this Rocoil is fed directly to an oscilloscope via an integrator circuit for signal processing and display of current waveform.

Fig.2.14: The main Rocoil

In addition, the output of four Rocoils used for non-invasive current measurement at the platic-insulated legs of the test rig are connect to an integrator for signal amplification from where they are relayed to a digital oscilloscope.

2.5 Diagnostics and safety consideration

To guarantee flawless safety, the laboratory is constructed upon a solidly earthed ground plane. Since it is important to contain any stray voltages and curtail any flow of fault current between the HV area and the control room; fibre optic- and pnematic controllers have been implemented for signal transmission and control.

2.5.1 Data Acquisition System

The data acquisition system (DAS) resides near the test chamber and houses: two Tektronix® TDS 3034C Digital Phospor Oscilloscopes, one rack-mounted National Instrument (NI) single PXI chassis (see Fig.2.15), plus a breakout board and a Rocoil integrator (as in Fig.2.16). To remedy poor power quality, these electronic devices are connected to a UPS module situated within the DAS housing. The PXI unit, dubbed Gargamel, has the following modules [28]:

Chassis: PXI-1031 (4 slot with 400W PSU)

Controller: PXI-8108 (2.53GHz Dual Core)

Module: PXI-5105 (60 MS/s, 12-Bit, 8-Channel Digitizer/Oscilloscope)

Module: PXI-6251 (Multichannel ADC, DAC and DIO)

Fig.2.15: TDS 3034C Oscilloscopes and NI PXI chassis

Presently, recorded signals are digitized by the oscilloscopes and transferred via removable Universal Serial Bus (USB) disks for further data analysis on personal computer (PC). When fully operational, the NI-PXI chassis will be fully linked to the control room such that digitized signals can be acquired directly. Furthermore, for ease of connection to its various terminals, the NI-PXI chassis was supplied with a breakout board situated on top of the integrator in Fig. 2.16.

Fig.2.16: PXI breakout board and Rocoil integrator

2.5.2 Fibre Optics

The fibre optic connections within MBLL are implemented using ethernet, RS232 and direct control technologies. For data exchange over ethernet links, fibre optic media converters were employed within the laboratory to achieve inexpensive electrical isolation for connections between: control room and main office area, control room and DAS housing, control room and AD bank controller etc. Hirschmann® fibre optic converter was implemented at the AD bank charger for conversion of standard RS232 signals to a pair of optical signals [19]. Pertinently, Fig. 2.17 is the OZDV2451G V.24/RS232 to fibre converter which operates in asynchronous full duplex mode for interference-free transmission [29].

Fig.2.17: RS to optic fibre converter

According to Hirschmann® [30], the converter in Fig. 2.17, which is line powered, has a wavelength of 870nm and achieves a bit rate of 20kbps. Also, having a rated current of 3.3mA, this robust device can transmit uninterrupted signals over a distance of about 20km. Direct control was achieved using the HFBR-0501 versatile link series. This series is composed of transmitters, receivers, connectors (as in Fig. 2.18) and specified cable for easy design. These reliable links find great use in applications where voltage isolation/insulation, signal security and Electromagnetic Interaction (EMI) immunity are deriable [31].

Fig.2.18: Transmitter, receiver and connector for HFBR-0501 series

Typically, at MBLL, HFBR-1522 transmitters and HFBR-2522 receivers were chiefly implemented [28] for extensive use with thyristor gate triggers. The transmitter operates on a 600nm LED and the receiver houses a monolitic dc coupled, digital IC with open collector Schottky output transistor [31].

2.5.3 Photographic Diagnostics

Advanced photographic techniques such as still cameras, high-speed cameras and thermal cameras, may be effectively combined with analytical tools to further understand intricate voltage, current and temperature changes during a high current test. Considering the hazard that sparks pose to aircraft wing skins, it critically important to identify spark sources during a test. In ED-105 [32], film cameras (35mm or Polaroid) which are capable of detecting 200μJ voltage sparks have been recommended. However, owing to obsolete film processing techniques, a Nikon® D700 DSLR is used instead at MBLL. Thermal cameras are capable of recording the temperature of sample layers as lightning currents flow through the laminate. The FLIR® SC7600-MB infrared camera as in Fig. 2.19 [33] is implemented at MBLL.

Fig 2.19: The FLIR® infrared camera

The extremely swift timescales wherein lightning flashes occur require dedicated high speed cameras that can record and analyze the ensuing interactions. Figure 2.20 reveals the Photron® FASTCAM SA5 which is taken on at MBLL.

Fig 2.20: Photron® FASTCAM SA5

This ultra high-speed video system in Fig. 2.20 uses its unrivalled sensitivity, frame rate and resolution, to achieve desireable image quality and colour reproduction [34]. The mega-pixel resolution is rated at 7,500 frames per second (fps) and a maximum frame rate of 775,000 fps at an exceptional exposure time of about 1µs. Furthermore, UVIRCO® CoroCAM 504 in Fig. 2.21 is a veritable tool for identifying overstressed HV equiment and/or test samples that are on the verge of producing a spark [35]. Undoubtedly, this will aid improved sample and HV equipment designs and allow for robut analysis.

Fig. 2.21: UVIRCO® CoroCAM 504

2.5.4 Personnel Safety

Grounding sticks used for earthing purposes provide visible sign to personnel. These grounding sticks are designed to protect different zones within the HV area of the laboratory. Furthermore, Castell® Trapped Safety Key Interlocks are installed at the entrance to the HV area, to provide the safest environment possible. Fig.2.22, reveals a grounding stick mounted on its hanger and the

interlock key system. The hangers incorporate a pneumatic switch which appropriately signals the control room for further processing. If these grounding sticks are not in postion, an alarm signal is relayed to the control room such that the capacitor banks will not be charged.

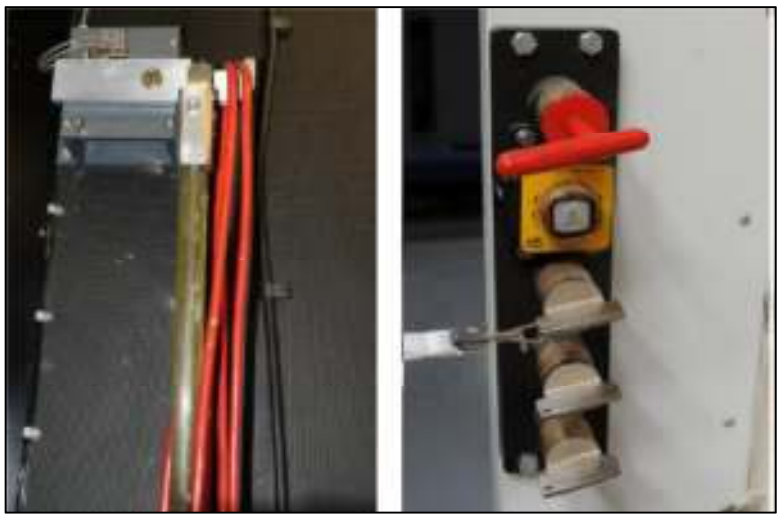

Fig 2.22: Some personnel safety devices

The interlock key system operates such that when all personnel keys are returned, the main door leading to the HVarea can be shut, and only then is the control key removeable. Consequently, the control key is inserted into a disconnector box to power on the HV area.

2.6 The Control room

All signals are relayed to a control room wherein a resident computer controller, LabVIEW®, has been implemented. LabVIEW, which stands for Laboratory Virtual Instrument Engineering Workbench, is a graphically-based programming language developed by National Instruments [36]. Thus, it is aptly preferred for test and measurement applications such as at MBLL.

2.6.1 The Screened Room

The screened room is where personnel sit when the test is carried out and it has been so designed for optimal safety. The room is fabricated from a 6.0m long container with both ends closed, having a single personnel sized steel door which closes against a rubber strip to prevent infiltration of sound. The space between the outer and inner wall is filled with foam which absorbs sound. The floor of the container has been retrofitted with steel and covered by a hard wearing grey carpet with underlay for further sound absorption. Clearly, the metal work acts as a Faraday cage shielding personnel from any stray fields during tests. Two vents fitted on the roof continuously recirculate fresh air within the cubicle thus providing excellent and safe working conditions.

2.6.2 The Patch Panel

The patch panel is located within the control room and houses mostly pnematic and fibre optic relays. Notably, one hard-wired connection between the control PC and the LabVIEW® hardware driver exists. At present, the spark gap trigger and dumping switches are controlled using a mechanical switch from the control room. However, this temporary solutions will be upgraded for full control using LabVIEW® driver in the near future. Fig.2.23 is the pneumatic and fibre optic terminations within the safety system control panel of the control room.

Fig 2.23: The control box connections

2.6.3 Control Interface

Remote monitoring of visual signals from earthing and dumping switches situated on the test chamber's rooftop is achieved using wireless CCTV cameras. This novel monitoring technique eliminates the need for a window at the wall closest to the HV area and enhances the protective capabilities of the screened room. Fig 2.24 is the Technix® Graphical User Interface (GUI) used for operation and control of the AD-bank charger. This interface summarily emulates the operational controls physically present on the charger. Hence, the desired charging voltage and current are set from the control room and visual signals obtained from CCTV images serve as a backup for monitoring the charger.

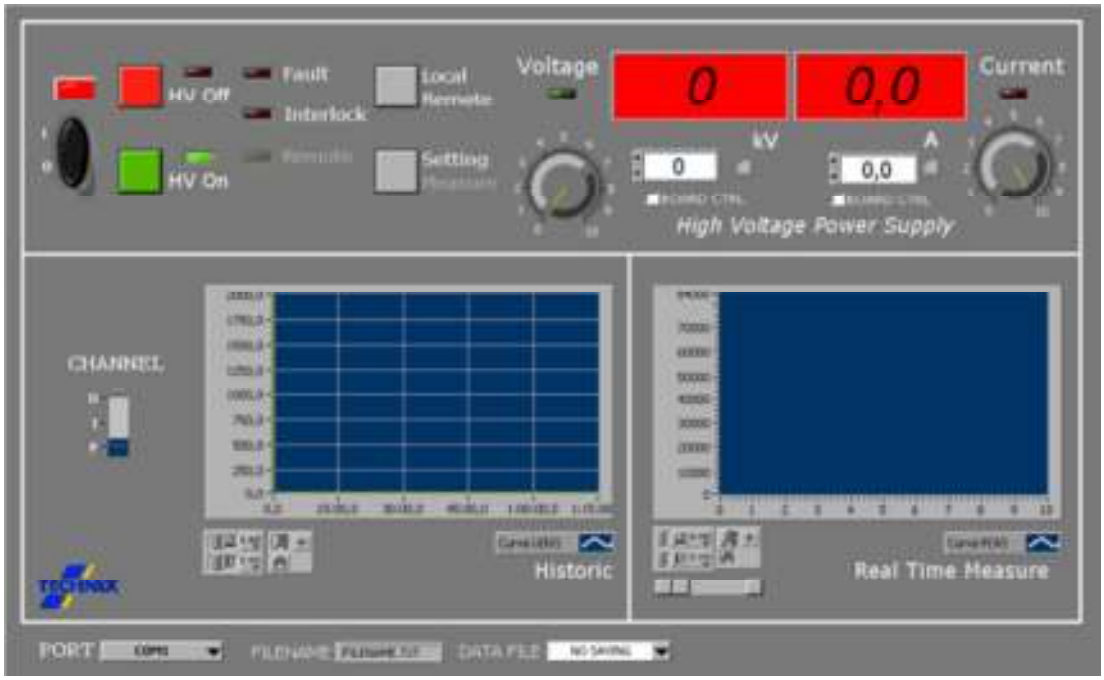

Fig 2.24: GUI for AD-bank Technix® charger

CHAPTER THREE

The control system

Introduction

It's important to ensure a relevant safety level for all the components of the system (main circuit, sensors, pneumatics actuators for dump earth and fire switch) and for all the staff which works within the laboratory. Operator necessarily has to control and eventually modify all the main parameters of the system, from remote position (control chamber) therefore it needs to implement a control system with the following characteristic:

- Control and monitoring by NI LabVIEW interface.
- Control of capacitors banks charge (4 banks, one for each waveform, D bank is a part of A bank).
- Control of pneumatics dump earth and fire switch.
- Protection against any feedback or noise current signals or electromagnetic interference from the main circuit.

3.1 NI LabVIEW interface

LabVIEW (short for Laboratory Virtual Instrumentation Engineering Workbench) is a system design platform and development environment for a visual programming language from National Instruments. The graphical language is named "G" (not to be confused with G-code). Originally released for the Apple Macintosh in 1986, LabVIEW is commonly used for data acquisition, instrument control, and industrial automation on a variety of platforms including Microsoft Windows, various versions of UNIX, Linux, and Mac OS X. The latest version of LabVIEW is LabVIEW 2012, released in August 2012 [37]. In the MBLL is used a special LabVIEW interface for the charger made by Technix.

3.2 Chargers control, switches control, trigger

Charge for A/D capacitors bank is provided by a 60 kV 20 kW DC Tecnix charger [38] while for B and C capacitors banks is used two chargers LAMBDA EMI MODEL 402L 20kV DC and LAMBDA EMI LC SERIES respectively. The pneumatics switches are used to interrupt the main circuit and they are actuated by pneumatic actuator. Along the main circuit there are three groups of pneumatics switches which are used for:

- **Fire switch**: a pneumatic switch that operates to fire the discharge through the testing material in the main test chamber.
- **Dump switch**: a pneumatic switch which ensures a link between the main circuit and the ground/earth through a resistive link. This allows, for the safe, dissipation of accumulated residual energy in the main capacitors and/or inductance to ground/earth. There are three dump switches in parallel for A/D bank and one B/C. This link is maintained when the circuit is not in operation to provide complete safety of the circuit.
- **Earth switch**: a pneumatic switch which supplements the dump switch and ensures a direct short circuit connection between the main circuit and ground/earth.there are three dump switches in parallel for A/D bank one for B bank and one for C bank. This link is maintained when the circuit is not in operation to provide complete safety of the circuit.

As mentioned before in the MBLL is possible reproduce all the four part of a natural lighting called in the ED-84 A,B,C,D. Through the control system it is possible to select which of the four waveform can be used for testing or use all the waveforms in sequence. At the moment isn't possible to use the complete sequence of all four waveform because the lab isn't provided of the sufficient capacitors to create the A waveform. By the operation of the control system will be possible to make a D-B-C sequence for testing. In order to use the automatic sequence, system control needs a trigger signal taken during D waveform discharge by a Rogowsky coil sensor. Through the trigger signal LabVIEW can commands B and C fire switches at the same time. Presence of high current values and high di/dt gradients especially in A and D waveform produce high electromagnetic variable fields that can induce interferences in all the circuits of the lab. It's important that propagation of the interferences is limited within control circuits to ensure the correct work. For these reasons, as shown in Fig.1, all the control chassis have optic fiber links with the control chamber. Fiber optics links ensure a very good level of insulation between main circuit and control chamber. After a panoramic of the control system, a detailed analysis of the control system will be done from both components and function point of view.

As shown in Fig.1 the control system is composed of three chassis with the function of:

- **A/D chassis**: control charger and control of fire, dump, earth switches.
- **B/C chassis**: control charger and control of dump, earth switches.
- **Trigger**: automatic or manual control of B and C fire switches and power supply for B and C switches.

3.2.1 A/D chassis

A/D chassis is a electric/pneumatic circuit which receives and sends out electric signals from LabVIEW interface and from the charger and send pneumatic signals to fire dump and earth switch. In

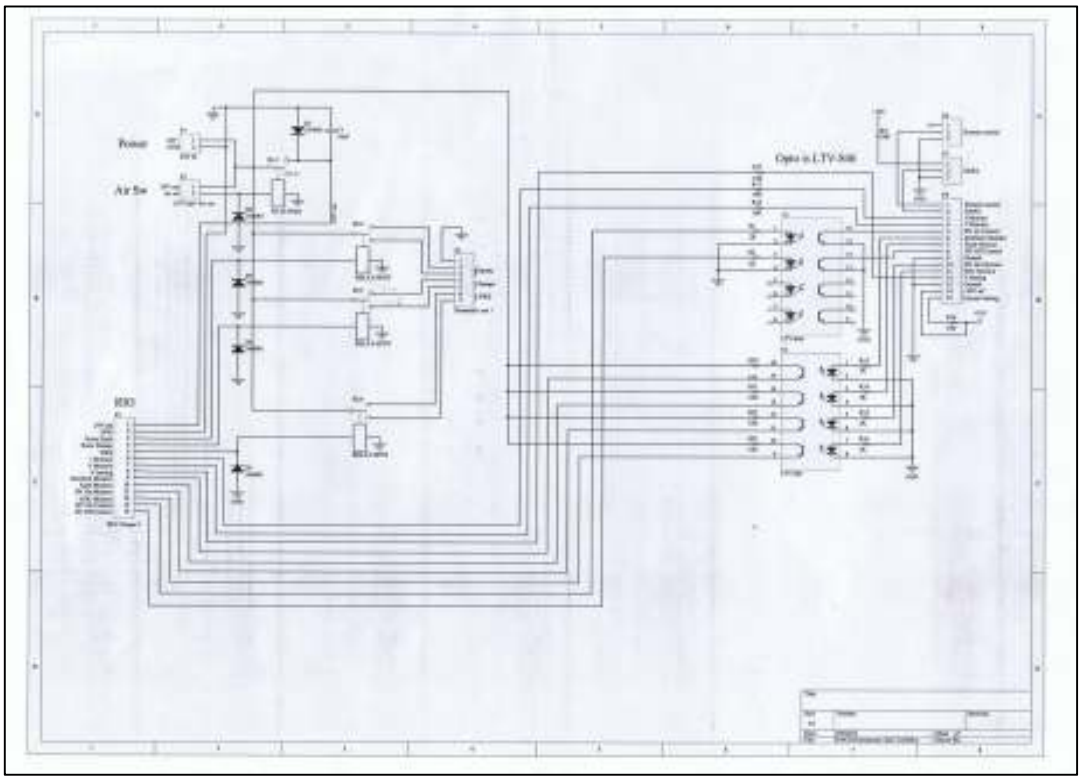

Fig.3.2 Electrical schematic of A/D chassis circuit

Fig.3.2 is possible to see an electrical schematic of the circuit within the chassis.

3.2.1.1 Circuit description

- **Power supply**: entire circuit within the chassis is alimented by a 24V/5A DC Power supply by Siemens (Siemens SITOP SMART 5A)[39].
- **Air switch**: current switch which is operated from a pneumatic signal from safety panel. It is used to abilitate the function of the RIO gate through the RL1 single state relay.
- **D1-D5 diodes**: protection against current feedback.
- **RL2-4**: single state relays operated by the RIO gate. They are used to deflecte power between two power line which are used for the air valves of the pneumatics fire, dump, earth switches.
- **Air valves**: set of three air valves which provide to send pneumatic power to actuators of the fire, dump, earth switches. Each actuators needs two pneumatic power signals, one for the up position and one for the down position. Air valves provide, behind commands of the RIO gate, to deflecte the pneumatic power, from the main pneumatic power circuit, in each actuator [40].
- **Optocoupler**: LTV-846 is a 4 channel digital optocoupler which provide two functions, unidirectional switch and galvanic isolation between RIO gate and charger gate. Optocoupler is provided of resistances in input and output gates to ensure the proper current level for both input and output [41].

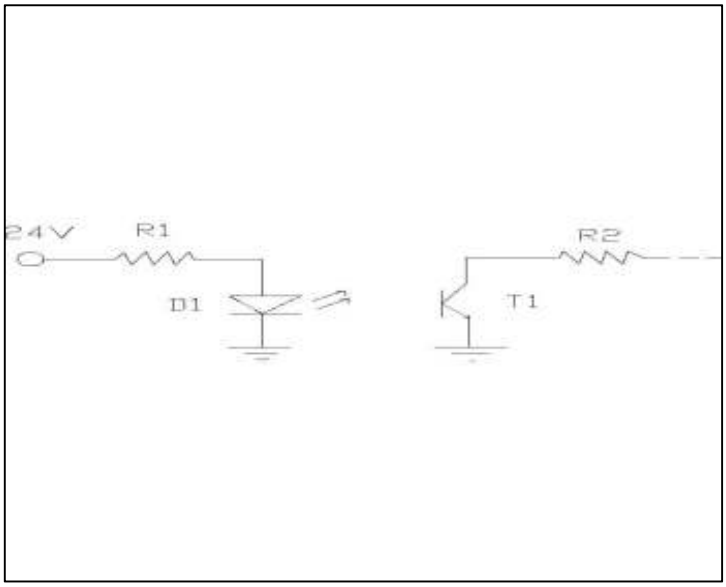

Fig.3.3 Electrical schematic of octocoupler

Fig 3.3 shows a simple equivalent electrical circuit of an optocoupler. R1 was sized to have 10-15 mA diode current. The voltage drop over the diode during its close state is about 1,2V and the R1 value can be found by use the following formula:

$$\frac{Vd - Vf}{If} = R1$$

Vd is the input voltage, Vf is the drop voltage over the diode during the on state and If is the nominal current of the diode. R1 is of 2K. Resistance R2 of the output gate have the same function of R1, that is current limiting of the transistor current. Its value is of 10K.

- **RIO gate**: CompactRIO is a reconfigurable embedded control and acquisition system. The CompactRIO system's rugged hardware architecture includes I/O modules, a reconfigurable field-programmable gate array (FPGA) chassis, and an embedded controller. Additionally, CompactRIO is programmed with NI LabVIEW graphical programming tools and can be used in a variety of embedded control and monitoring applications. The main part of the RIO gate is The NI cRIO-9022 embedded real-time controller is part of the high-performance CompactRIO programmable automation controller (PAC) platform. It features an industrial 533 MHz Freescale MPC8347 real-time processor for deterministic, reliable real-time applications and contains 256 MB of DDR2 RAM and 2 GB of nonvolatile storage for holding programs and logging data [42]. RIO gate allows communications between LabVIEW software and A/D charger and pneumatics switches using modules with several functionality capable to manage both analogue and digital signals. In detail it has:

    - 2 X NI 9472: 8-channel Digital Output Modules (one for future expansion)

        - Raise earth
        - Raise dump
        - Fire
        - HV on control
        - HV off control

    - 1 X NI 9421: 8-channel Sinking Digital Input Module

        - Interlock monitor
        - Fault monitor
        - HV on monitor
        - End Of Charge Monitor

    - 1 X NI 9263: 4-channel 16 Bit Analog Voltage Output Module

        - V setting

    - 1 X NI 9215: 4-channel 16 Bit Simultaneous Analog Input Module

        - I monitor
        - V monitor

- **Output gate**: it is a 15 pin gate for the link between chassis and charger.

- **Gigabit Ethernet Bridge**: Planet GT-90x series Opto/Ethernet converter. It provides to convert all the opto input/output signals between LabVIEW and chassis.

3.2.1.2 Circuit operation

The entire chassis works through the input/output signals of the LabVIEW interface through the RIO gate. As it said, in order to ensure all the system safety, is required that all the safety protocols are respected. Safety protocols are managed by the safety panel through several pneumatic sensors in all the laboratory. One of the safety protocol is to enable the A/D chassis function through a pneumatic signal that allows the work of the RIO gate. The several function of the A/D chassis are shown below:

- **Activation of the RIO gate:** RIO gate needs a power supply for working of 24V that is provided from the main power supply but as it said before to be activated it needs of the pneumatic signals from the safety panel.As it can be seen from the electrical schematic the air switch provides the energy supply for the RIO gate, particulary we have: in "off" position the air switch doesn't receive no pneumatic signal from safety panel and the air switch is "normally open". In this condition the air switch relay has its output pin in floating position ("off "position) and RIO gate doesn't receive energy. When the air switch receives pneumatic signal from safety panel a short circuit born into the air switch between power supply and air switch relay that commutes from the floating pin to the RIO gate energy way therefore the RIO gate is actived. When the RIO gate is active is possible to manage all the functions of the A/D chassis through the commands of LabVIEW software.

- **Control of pneumatic switches:** pneumatic switches needs two pneumatic signals each one for "up" position and one for "down" position. For dump and earth switches "down" position is a short circuit between main circuit and earth/ground while for the fire switch is open circuit. For dump and earth switches "up" position is open circuit while for fire switch is short circuit. A/D circuit is designed in such a way that in "off" position RL2 RL3 RL4 provide 24V power supply for guarantee a "normally down" position or short circuit with earth/ground. Must to be added that dump and earth switches have a passive safety system due to gravity that is if pneumatic power off suddenly the switches come back to "down" position (short circuit with earth/ground) by the gravity The management of the pneumantic switches is left to NI 9472 Module of the RIO gate that provides through LabVIEW signals to send 24V power supply to RL2 RL3 RL4 according to necessity. The 24V power supply permits to RL2 RL3 RL4 to change their pin connection from "down" position power supply line to "up" position power supply line. In case of power failure from RIO gate relays de energize and their pin come back to the "down" position power supply line.

- **Charger control:** charger communicates with RIO gate through both input and output signals and both analogue and digital signals. Regarding digital input output signals, between RIO gate and charge gate there are two LTV-846 optocoupler to guarantee galvanic isolation between the two gates. RIO gate manages the following signals:
    - **I & V monitor**: monitoring of current and tension of the capacitors bank. Both analogue signals (from 0V to +10V) in input to RIO gate are managed by NI 9215 module.
    - **V setting**: it sets capacitors bank tension and then the energy stored in the capacitors bank. It is an analogue output signal from RIO gate (from 0V to +10V) and it is managed by NI 9263 module.
    - **Fault monitor**: failure during charge of the capacitors bank signal. Digital input managed by NI 9421 module.
    - **Interlock monitor**: proper functioning signal of charger. Digital input managed by NI 9421 module.
    - **EOC (End Of Charge) monitor**: end of charge signal from capacitors bank. Digital input managed by NI 9421 module.
    - **HV On & HV Off control**: Turn on & Turn off signals for the charger. Digital outputs managed by NI 9472 module.

3.2.2 B/C chassis

B/C chassis provides to manages dump and earth switches of B/C circuits and the two chargers for the B and C banks. B/C circuit is quite similar to A/D circuit.

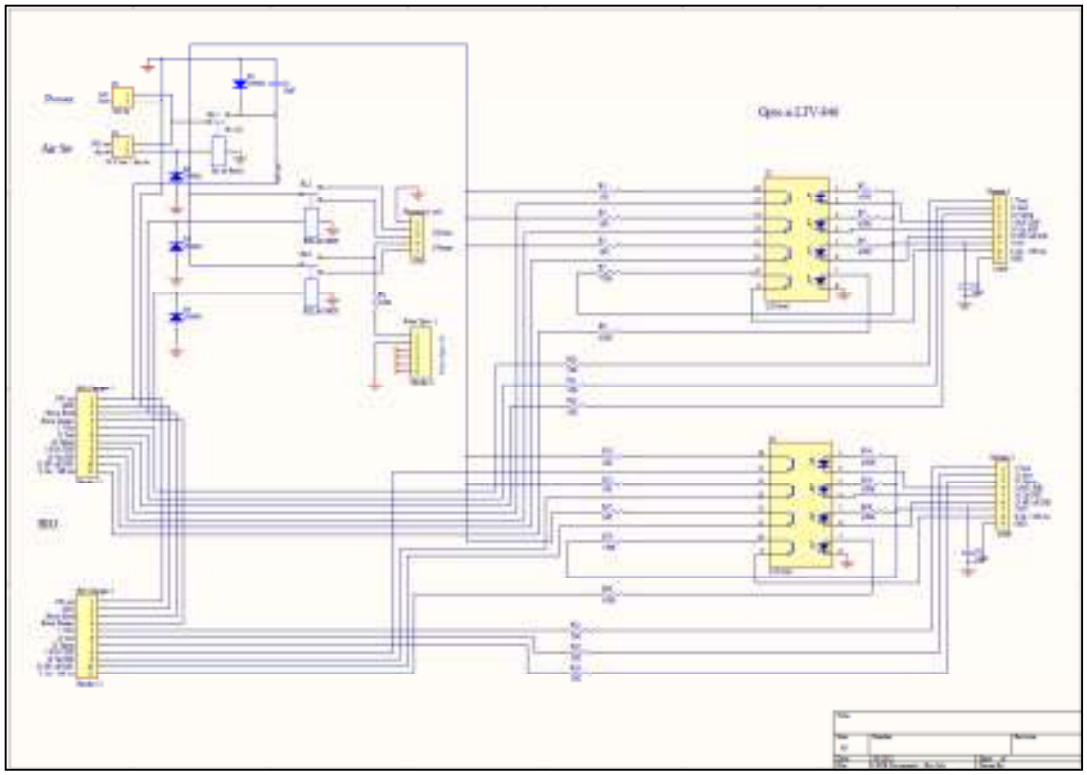

Fig.3.4 electrical schematic of B/C chassis circuit

3.2.2.1 Circuit description

- **Power supply**: entire circuit in the chassis uses a SIEMES SITOP SMART 5A 24V DC for the power [39].
- **Air switch**: current switch which is operated from a pneumatic signal from safety panel. It is used to abilitate the function of the RIO gate through the RL1 single state relay.
- **D1-D4 diodes**: protection against current feedback.
- **RL2-3**: single state relays operated by the RIO gate. They are used to deflecte power between two power line which are used for the air valves of the pneumatics dump, earth switches.
- **Air valves**: set of two air valves which provide to send pneumatic power to actuators of the dump and earth switches. Each actuators needs two pneumatic power signals, one for the up position and another one for the down position. Air valves provide, behind commands of the RIO gate, to deflecte the pneumatic power, from the main pneumatic power circuit, in each actuator [40].
- **Optocoupler**: LTV-846 is a 4 channel digital optocoupler which provide two functions, unidirectional switch and galvanic isolation between RIO gate and charger gate. Optocupler is provided of reisistors in the input and output gates to ensure the current level for both input and output [41].
- **RIO gate**: CompactRIO is a reconfigurable embedded control and acquisition system. The CompactRIO system's rugged hardware architecture includes I/O modules, a reconfigurable field-programmable gate array (FPGA) chassis, and an embedded controller. Additionally, CompactRIO is programmed with NI LabVIEW graphical programming tools and can be used in a variety of embedded control and monitoring applications. The main part of the RIO gate is The NI cRIO-9022 embedded real-time controller is part of the high-performance CompactRIO programmable automation controller (PAC) platform. It features an industrial 533 MHz Freescale MPC8347 real-time processor for deterministic, reliable real-time applications and contains 256 MB of DDR2 RAM and 2 GB of nonvolatile storage for holding programs and logging data [6]. RIO gate allows communications between LabVIEW software and A/D charger and pneumatics switches using modules with several functionality capable to manage both analogue and digital signals. In detail it has:

    - 2 X NI 9472: 8-channel Digital Output Modules (one for future expansion)

        - Raise earth
        - Raise dump
        - HV on/off control
        - HV on/off 2 control

    - 1 X NI 9421: 8-channel Sinking Digital Input Module

        - HV on monitor
        - HV on monitor 2

- HV off monitor
- HV off monitor 2
- EOC End Of Charge monitor
- EOC End Of Charge 2 monitor

o 1 X NI 9263: 4-channel 16 Bit Analog Voltage Output Module

- V Prog
- V Prog 2

o 1 X NI 9215: 4-channel 16 Bit Simultaneous Analog Input Module

- I Out
- V Out
- I Out 2
- V Out 2

➢ **Output gates**: two 15 pin gates for the link between chassis and the two chargers.

➢ **Optical output:** Avago technologies HFBR-1522 trasmitter. Fig 3.5 shows electrical schematic and main characteristics[43].

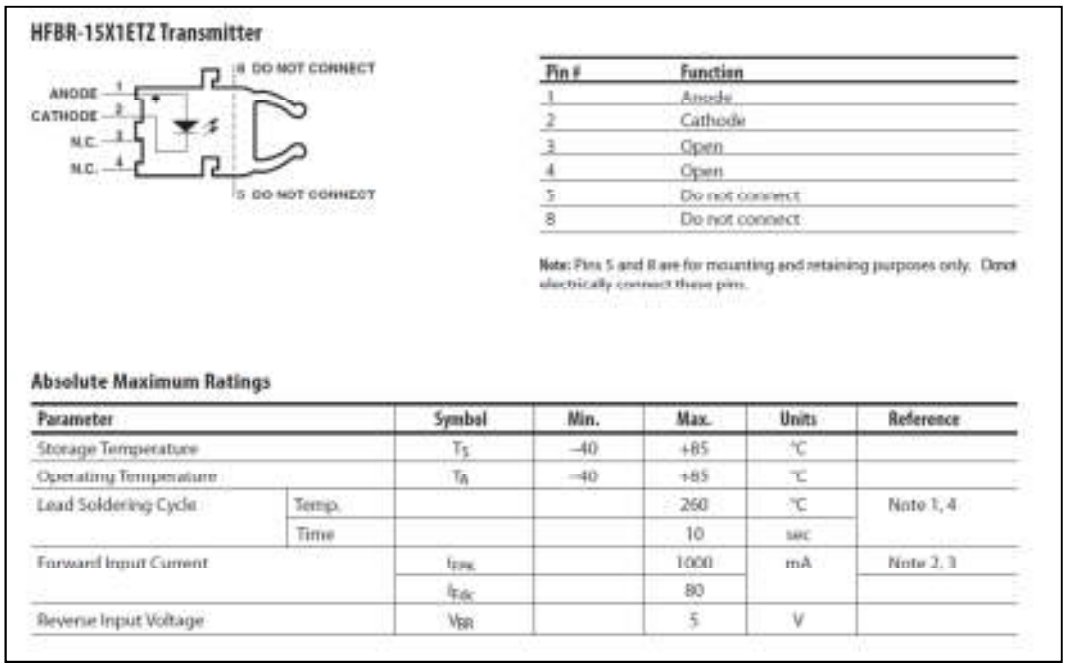

Fig.3.5 Electrical schematic and main characteristic of optical transmitter

3.2.2.2 Circuit operation

Operation B/C circuit operation is similar to A/D circuit operation due to a similar circuit structure. There is RIO gate that manages dump and earth switches through 24V power supply signals. Also there is the chargers control throught two differents gates, two optocoupler one for

each charger gate for the input output digital signals and the air switch for the RIO gate. There isn't control for the fire switch of B and C waveform. The B and C fire switches are not pneumatic switches, B fire switch is a seriers of seven tyristors while C fire switch is a a parallel of three IGBT, they need electrical impulses to them gate to be driven and this is managed by trigger chassis. Operation of optical output will be described after.

- **Activation of the RIO gate:** RIO gate needs a power supply for working of 24V that is provided from the main power supply but as it said before to be activated it needs of the pneumatic signals from the safety panel.As it can be seen from the electrical schematic the air switch provides the energy supply for the RIO gate, particulary we have: in "off" position the air switch doesn't receive no pneumatic signal from safety panel and the air switch is "normally open". In this condition the air switch relay has its output pin in floating position ("off "position) and RIO gate doesn't receive energy. When the air switch receives pneumatic signal from safety panel a short circuit born into the air switch between power supply and air switch relay that commutes from the floating pin to the RIO gate energy way therefore the RIO gate is actived. When the RIO gate is active is possible to manage all the functions of the B/C chassis through the commands of LabVIEW software.

- **Control of pneumatic switches:** pneumatic switches needs two pneumatic signals each one for "up" position and one for "down" position. For dump and earth switches "down" position is a short circuit between main circuit and earth/ground while for the fire switch is open circuit. For dump and earth switches "up" position is open circuit while for fire switch is short circuit. A/D circuit is designed in such a way that in "off" position RL2 RL3 provide 24V power supply for guarantee a "normally down" position or short circuit with earth/ground. Must to be added that dump and earth switches have a passive safety system due to gravity that is if pneumatic power off suddenly the switches come back to "down" position (short circuit with earth/ground) by the gravity The management of the pneumantic switches is left to NI 9472 Module of the RIO gate that provides through LabVIEW signals to send 24V power supply to RL2 RL3 according to necessity. The 24V power supply permits to RL2 RL3 to change their pin connection from "down" position power supply line to "up" position power supply line. In case of power failure from RIO gate relays de energize and their pin come back to the "down" position power supply line.

- **Chargers control:** chargers communicate with RIO gate through both input and output signals and both analogue and digital signals. Regarding digital input output signals, between RIO gate and charge gates there are two LTV-846 optocoupler one for each charger to guarantee galvanic isolation between the two gates. RIO gate manages the following signals:
  - **I & V monitor**: monitoring of current and tension of both B and C capacitors banks. All the four analogue signals (from 0V to +10V) in input to RIO gate and they are managed by NI 9215 module.

- **V setting**: it sets tension for both capacitors banks and then the energy stored in both of them. They are an analogue output signals from RIO gate (from 0V to +10V) and they are managed by NI 9263 module.
- **EOC (End Of Charge) monitor**: end of charge signals from both capacitors banks. Digital inputs managed by NI 9421 module.
- **HV On & HV Off monitor**: digital signals used to show the on or off state of the chargers. A couple for each charger. Digital inputs managed by NI 9421 module.
- **HV On & HV Off control**: turn on and turn off drive signals for each charger. Digital outputs managed by NI 9472 module.

- **Optical output:** header6 optical output drives a tyristor gate used for bypass of the dump switch of the B/C bank because after the fire of B and C waveforms a certain amount of charge remain stored in the C capacitors bank and this stored energy will flow through the dump and earth switches when them will be closed.To avoid that the high current from the C capacitors bank melt the dump switches, that close itself before the earth switches, there is a tyristor along which the current can flows during the closing time of the dump switches. In fact the the closing signal for both switches in parallel start at the same time but the closing time of the tyristor(some millisecond) is much less than the closing time of the dump switch (some second). The 24V digital output signal from RIO gate is changed is optical signal and sended to the gate driver circuit of the tyristor through optical link.

3.2.3 Trigger chassis

Functions of trigger chassis are:

1. To acquire trigger signal from D waveform
2. Power supply for gate driver circuit of B fire switch (seven tyristors in series)
3. Power supply for gate driver circuit of C fire switch (three IGBTs in parallel)
4. Closure drive signal for B fire switch
5. Closure drive signal for C fire switch
6. Automatic waveforms sequence

3.2.3.1 Circuit description

To acquire trigger signal from D waveform.

As said before control system is able to manage an automatic sequence of D-B-C waveforms (not now but for future tests). Trigger chassis is composed by severals sub-circuit. There will be a description of the severals sub-circuits before and a description of the operation of the entire chassis after. The first sub-circuit is not within the chassis but it excanges all the signals with the main chassis through optical links. It provides to create the trigger signal that is used by the LabVIEW to drive the B and C fire switches. Fig 3.6 shows an electrical schematic of the sub-circuit.

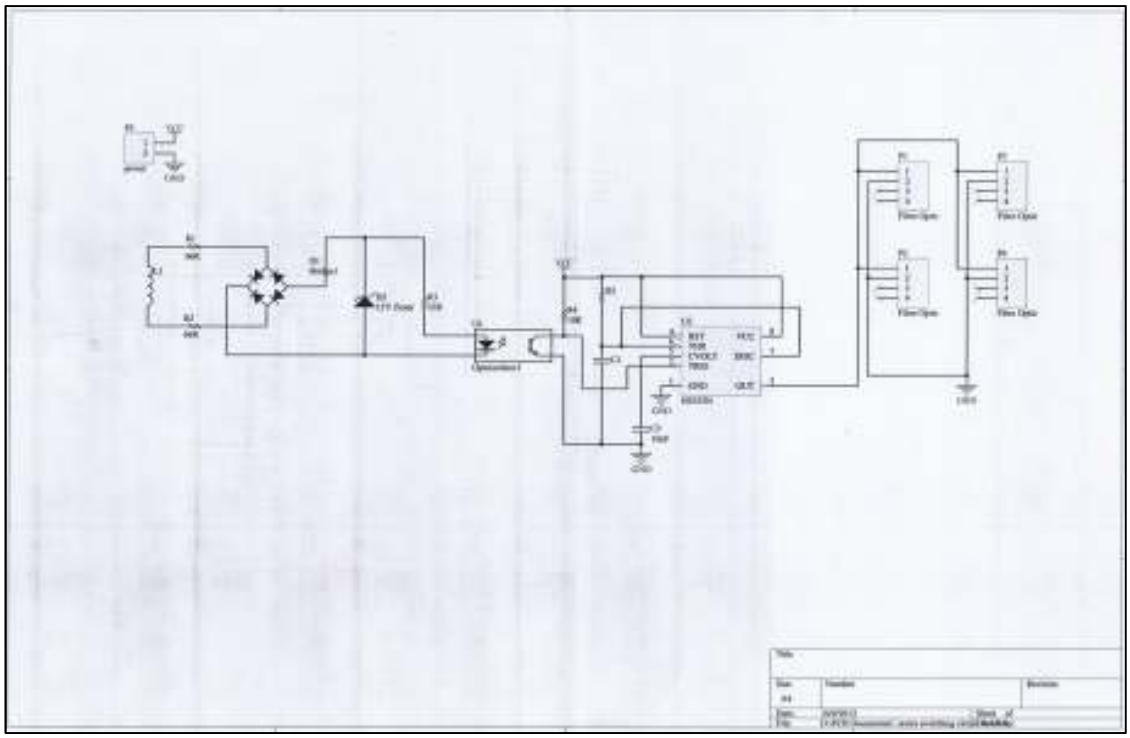

Fig.3.6 electric schematic of trigger sub-circuit

- **L1**: A Rogowski coil, named after Walter Rogowski, is an electrical device for measuring alternating current (AC) or high speed current pulses. It consists of a helical coil of wire with the lead from one end returning through the centre of the coil to the other end, so that both terminals are at the same end of the coil. The whole assembly is then wrapped around the straight conductor whose current is to be measured. Since the voltage that is induced in the coil is proportional to the rate of change (derivative) of current in the straight conductor, the output of the Rogowski coil is usually connected to an electrical (or electronic) integrator circuit to provide an output signal that is proportional to the current This type of coil has advantages over other types of current transformers. It is not a closed loop, because the second terminal is passed back through the center of the toroid core (commonly a plastic or rubber tube) and connected along the first terminal. This allows the coil to be open-ended and flexible, allowing it to be wrapped around a live conductor without disturbing it.It has an air core rather than an iron core, it has a low inductance and can respond to fast-changing currents. Because it has no iron core to saturate, it is highly linear even when subjected to large currents, such as those used in electric power transmission, welding, or pulsed power applications .A correctly formed Rogowski coil, with equally spaced windings, is largely immune to electromagnetic interference. The voltage produced by a Rogowski coil is

$$V = \frac{-AN\mu_0}{l}\frac{dI}{dt},$$

where $A = \pi a^2$ is the area of one of the small loops, N is the number of turns, and $l = 2\pi R$ is the length of the winding (the circumference of the ring). Di/dt is the rate of change of the current threading the loop. This formula assumes the turns are evenly spaced and that these turns are small relative to the radius of the coil itself. At high frequencies, the Rogowski coil's inductance will decrease its output. The inductance of a toroid is

$$L = \mu_0 N^2 (R - \sqrt{R^2 - a^2})$$

$\mu_0 = 4\pi \times 10^{-7}$ V·s/(A·m) is the magnetic constant, R is the major radius of the toroid, and a is its minor radius [44].

- **Double semiwave AC/DC converter**: it provides to convert the tension waveform across rogowsky coil. Zener D2 diode provides to maintain the output tension of the converter below 12V.
- **U1 optocoupler**: it provides a galvanic isolation between input and output of the sub-circuit.
- **KIA555P**: monolithic timing circuit that is highly stable controllers capable of producing accurate time delays or oscillation. In the time delay mode of operation, the time is precisely controlled by one external resistor and capacitor [45]. It provides to create a tension signal of 500ms that is the trigger signal for LabVIEW.

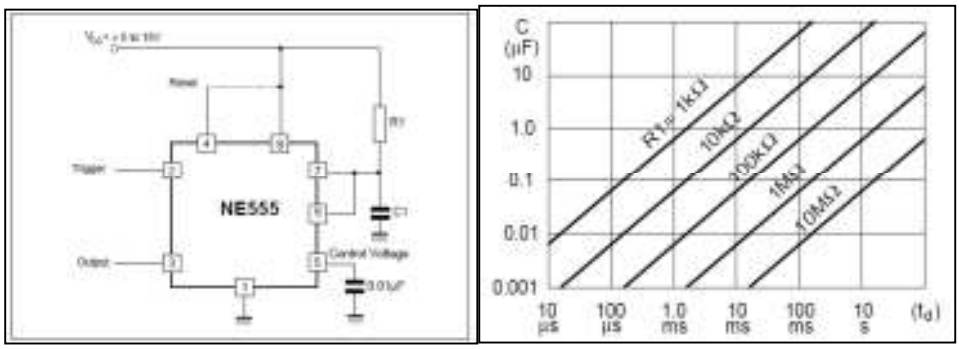

Fig.3.7 Tipical connection and value of R1 C1 for for monostable operation

- **Optical output**: four Avago technologies HFBR-1522ETZ transmitter in parallel. Only the first one is connected actually.
- **P5**: 5V power supply for integrated timer.

3.2.3.2 Operation of the circuit

By the operation of the Rogowski coil it is possible to say that the voltage drop across its depend by: characteristics of the measured current waveform, derivate of the current di/dt through the main conductor. D waveform has before a raise and after a fall therefore the coil voltage drop will be in a direction before and in the opposite direction after (positive and negative there is a reference for the

tension). These is the reason for using a double semiwave AC/DC converter. The zener diode D2 provides to maintain an input voltage for the optocoupler not above 12V. Output of optocoupler is linked directly with the trigger input of the integrated timer. The timer provides to create a 500ms voltage drop at its output, operating in monostable modality. The circuit triggers on a negative-going input signal when the level reaches 1/3 Vcc. Once triggered, the circuit remains in this state until the set time has elapsed, even if it is triggered again during this interval. The duration of the output HIGH state is given by t = 1.1 R1C1 and is easily determined by figure shown above [45]. The voltage drop at the output gate of timer is changed in optical signal by the opto transmitter and sended to trigger chassis through optical links.

3.2.3.3 Power supply for gate driver circuit of B fire switch (seven tyristors in series)

The gate driver circuit of the tyristors of the B fire switch needs a 12V power supply that is provided by a power pack contained within trigger chassis. Fig 3.8 shows an electrical schematic of the sub circuit.

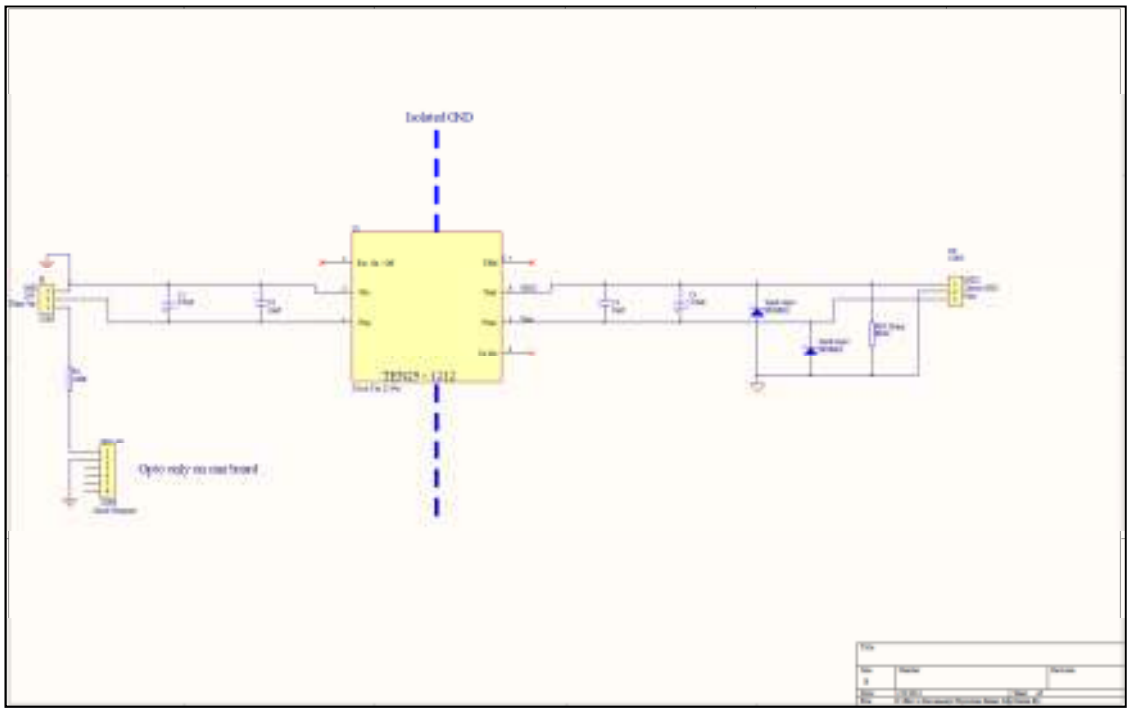

Fig.3.8 Electirc schematic of the power pack sub-circuit

The power pack is simply made of a DC/DC converter that provide to reduce the 24V tension of the main power supply (SIEMENS SITOP SMART 5A) to 12V. Capacitors in the input and output gates of the converter provides to maintain a levelled voltage waveform while Zener diodes at the outputs are against overvoltage [46]. CON6 optical output will be explained in the next paragraphs.

3.2.3.4 Power supply for gate driver circuit of C fire switch (three IGBTs in parallel)

The power supply for the gate driver circuit of the three parallel IGBTs is provided by a AC/DC converter TRACOPOWER TML402 15C. The output of the converter is 15V DC and 1333mA current [47].

3.2.3.5 Closure drive signal for B fire switch closure

The closure drive signal for B fire switch is sended by LabVIEW both manual set drive and automatic set drive. All the signals between LabVIEW and trigger chassis are managed by RIO gate as the other two control chassis. Trigger chassis has:

- 1X NI 9472
- 1X NI 9421
- 2X NI 9401
- 1X NI 9215

Only one of the two NI 9401 (digital TTL input/output module) are working now.All the others modules are for future applications. The closure drive signal for the gate driver circuit of the tyristors are sended from LabVIEW through the optical trasmitter which is in the B gate power pack sub circuit (Fig.3.8).

3.2.3.6 Closure drive signal for C fire switch

The closure drive signal for B fire switch is sended by LabVIEW both manual set drive and automatic set drive. The closure drive signal for the C fire switch is sended by LabVIEW. C fire switch is made by three parallel IGBTs and each of them receives a closure drive signal by the sub circuit shown below. Links are as the others optical type. At the moment the three IGBTs are driven by a unique signal from LabVIEW but in the future will be possible to to drive the three IGBTs indipendently.

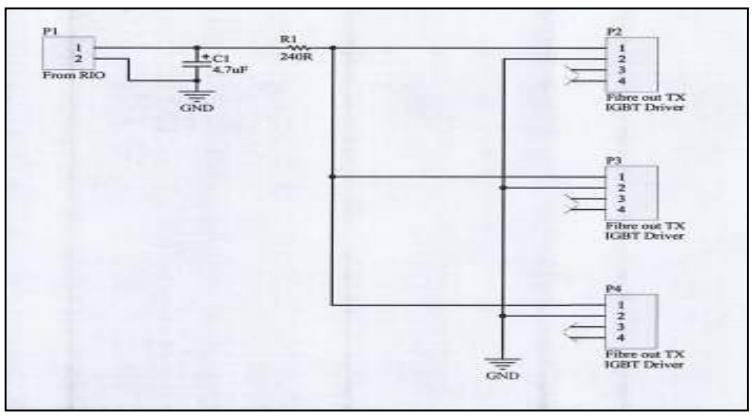

Fig.3.9 Electric schematic of C fire switch signal sub-circuit

3.2.3.7 Automatic waveforms sequence

In order to use automatic waveforms sequence system D-C-B LabVIEW needs of trigger signal from D waveform. The trigger signal is made by the sub circuit shown above. After that LabVIEW

receives trigger signal will send the closure drive gate signals to B and C fire switches at the same time. The trigger signal from sub circuit needs a power boost to be read correctly from LabVIEW. Therefore the optical trigger signal from sub circuit is changed by a opto receiver HBFR-2522Z in an electric signal. The electric schematic and the main characteristic of the opto receiver are shown below [43].

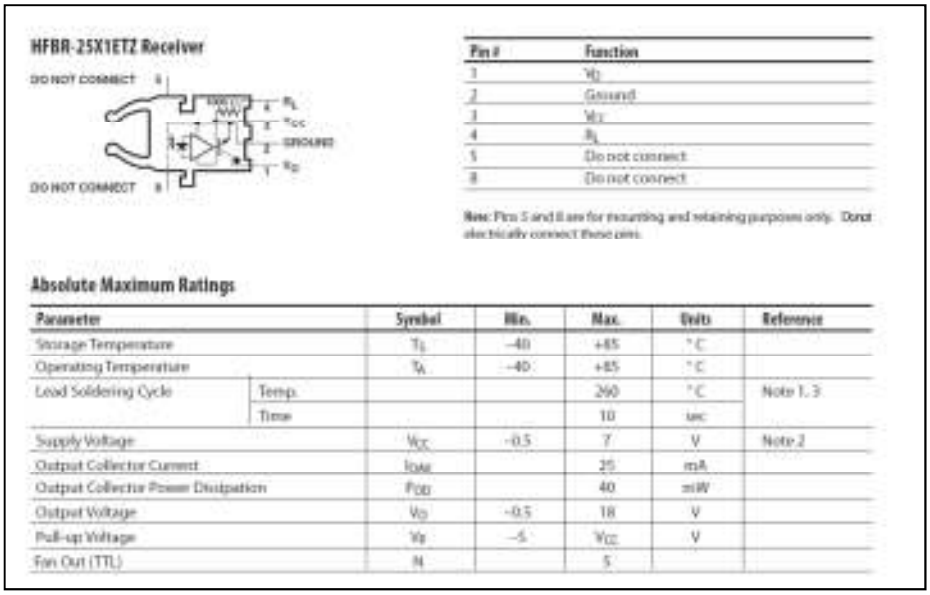

HFBR-25X1ETZ Receiver

DO NOT CONNECT

DO NOT CONNECT

Pin #	Function
1	V_O
2	Ground
3	V_{CC}
4	R_L
5	Do not connect
6	Do not connect

Note: Pins 5 and 6 are for mounting and retaining purposes only. Do not electrically connect these pins.

Absolute Maximum Ratings

Parameter		Symbol	Min.	Max.	Units	Reference
Storage Temperature		T_S	-40	+85	°C	
Operating Temperature		T_A	-40	+85	°C	
Lead Soldering Cycle	Temp.			260	°C	Note 1, 3
	Time			10	sec	
Supply Voltage		V_{CC}	-0.5	7	V	Note 2
Output Collector Current		I_{OAV}		25	mA	
Output Collector Power Dissipation		P_{OD}		40	mW	
Output Voltage		V_O	-0.5	18	V	
Pull-up Voltage		V_R	-5	V_{CC}	V	
Fan Out (TTL)		N		5		

Fig.3.10 Electric schematic and main characteristics of opto receiver

The receiver is in the sub-circuit shown in Fig3.11.

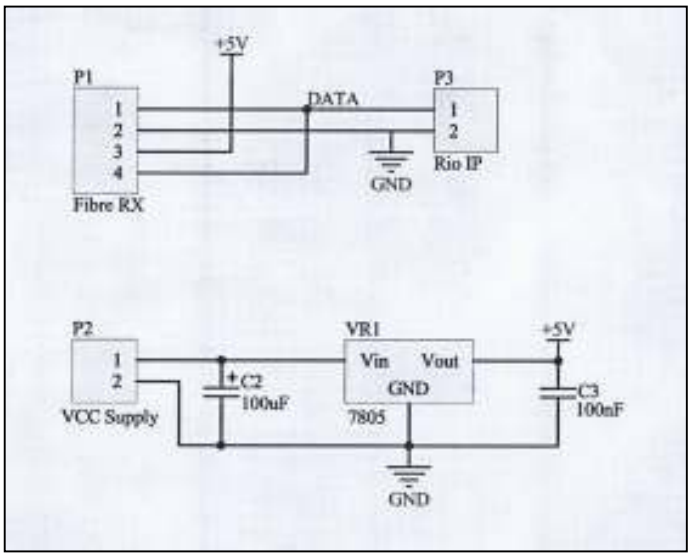

Fig.3.11 power booster for the trigger signal sub circuit

Opto receiver needs a 5V power supply which is provided by an integrated regulator Motorola MCT7805 (VR1 in the figure). The integrated regulator is powered by a 15V output tension of a

second AC/DC TRACOPOWER TML40215C converter. When the opto receiver receives the optical signal simply commutes its Vo output to Vcc tension value (5V). Vo is linked with one of the inputs of the RIO gate. Vcc signal in input to RIO gate is the trigger signal from D waveform.

Within the trigger chassis there is an opto/Ethernet converter that provides to convert all the input output signals of the LabVIEW. After there is an Ethernet switch that provides to send and receive signals to B/C chassis.

CHAPTER FOUR

Analysis of the control system

In order to understand if the control system will work properly, simulations by Orcad Capture software were done. In particular were analyzed the main currents and tensions of the circuits in order to assure that they are within the limits prescript in the datasheet of the single parts of the circuits. To understand if there is some possibility to improve operation of the system were made changes in some critical part of the circuit. Lastly, since it was not possible to know all the characteristics of the parts of the circuits for example on-off time of the switches or parasitic capacitance of the coils were done parametric analysis to show which solution could be the best.

Is possible to divide the analysis in different steps:

- Design of the circuits by Orcad Capture
- Sizing of the components of the circuits
- Chronological analysis in the main conditions
- Analysis of modified circuits
- Parametric analysis

4.1 Design of the circuits by Orcad Capture

Easy-to-use and powerful, Cadence® OrCAD® Capture is the most widely used schematic design solution, supporting both flat and hierarchal designs from the simplest to the most complex. Seamless bi-directional integration with OrCAD PCB Editor enables data synchronization and cross-probing/placing between the schematic and the board design. OrCAD Capture allows designers to backannotate layout changes, make gate/pin swaps, and change component names or values from board design to schematic using the feedback process. It also comes with a large library of schematic symbols and can export netlists in a wide variety of formats []. Each circuit chassis has been designed separately and the trigger chassis has been divided in different part. For the components of the circuits, some of these were chosen from the libraries of the software for example relay, optocoupler, switches, integrated circuits. For each of these components is possible to modify the main electrical characteristics using a mask of the OrCAD® software. Other components were made using their electrical equivalent at the output gate since was not possible to find them in the libraries of the software for example electrovalves or RIO gate. Each component has been sized using datasheet values where possible (for example for the relay or for the integrated timer). For the components that was not possible to have datasheets or electrical characteristics (for example electrovalves) they were sized using values as close as possible to the real values. Not all circuit was analyzed because some parts of this is only links between input and output for example I and V monitor in A/D bank are analogic links between RIO gate and charger made only by a wire and a resistance to restrict current through the wire and from datasheets of the two gates is possible to see that the limits of the tension and current I/O of the two gates are almost the same and so it is not necessary to simulate their operation.

4.2 A/D circuit sizing and analysis

4.2.1 A/D bank sizing

- **SPDT Relays**: A relay is an electrically operated switch. Many relays use an electromagnet to operate a switching mechanism mechanically, but other operating principles are also used. Relays are used where it is necessary to control a circuit by a low-power signal (with complete electrical isolation between control and controlled circuits), or where several circuits must be controlled by one signal. A simple electromagnetic relay consists of a coil of wire wrapped around a soft iron core, an iron yoke which provides a low reluctance path for magnetic flux, a movable iron armature, and one or more sets of contacts (there are two in the relay pictured). The armature is hinged to the yoke and mechanically linked to one or more sets of moving contacts. It is held in place by a spring so that when the relay is de-energized there is an air gap in the magnetic circuit. In this condition, one of the two sets of contacts in the relay is closed, and the other set is open. Other relays may have more or fewer sets of contacts depending on their function. When an electric current is passed through the coil it generates a magnetic field that activates the armature, and the consequent movement of the movable contact(s) either makes or breaks (depending upon construction) a connection with a fixed contact. If the set of contacts was closed when the relay was de-energized, then the movement opens the contacts and breaks the connection, and vice versa if the contacts were open. When the current to the coil is switched off, the armature is returned by a force, approximately half as strong as the magnetic force, to its relaxed position. Usually this force is provided by a spring, but gravity is also used commonly in industrial motor starters. Most relays are manufactured to operate quickly. In a low-voltage application this reduces noise; in a high voltage or current application it reduces arcing. When the coil is energized with direct current, a diode is often placed across the coil to dissipate the energy from the collapsing magnetic field at deactivation, which would otherwise generate a voltage spike dangerous to semiconductor circuit components.

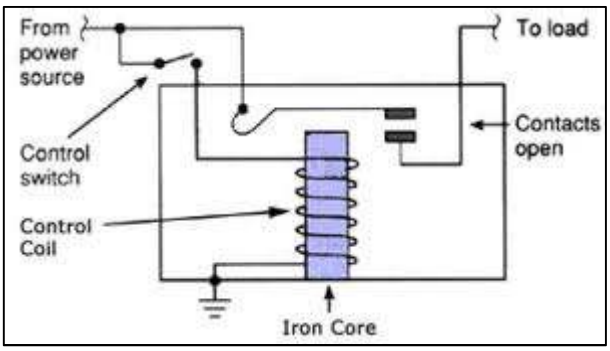

Fig 4.1: electrical schematic of relay

Relays used in the circuits are SPDT relays Omron G2R-1 (Single Pole Double Throw. A common terminal connects to either of two others. Including two for the coil, such a relay has five terminals in total). The main electrical characteristics of the relay, from datasheet, are:

TYPE	VALUE
I drop	10 mA
I pull	20 mA
Coil inductance	4,27 H @24 Vdc
Coil resistance	1100 ohm
R close	0,03 ohm
R open	100 Mohm
T Bounce	5 ms
T Break	5 ms
T Make	15 ms

TYPE	DESCRIPTION
I drop	Current flowing into the coil that allows changing of the state of the contacts from energized to de-energized
I pull	Current flowing into the coil that allows changing of the state of the contacts from de-energized to energized
Coil inductance	Value of the inductance of the coil driver of the relay
Coil resistance	Value of the resistance of the coil driver of the relay
R close	Value of the resistance between two close contacts
R open	Value of the resistance between two open contacts
T Bounce	Time of bounce of the contact due to mechanical inertia and friction of the armature
T Break	Minimum time to change the state of the contact, after coil current achieves “I drop”. This gap time is due to mechanical inertia and friction of the armature
T Make	Minimum time to change the state of the contact, after coil current achieves “I pull”. This gap time is due to mechanical inertia and friction of the armature

For the design of the relays was used a standard SPDT relay from MIX_MISC library of the software and were modified the main parameters using datasheet values.

- **Diodes**: A diode is a two-terminal electronic component with an asymmetric transfer characteristic, with low (ideally zero) resistance to current flow in one direction, and high (ideally infinite) resistance in the other. A semiconductor diode, the most common type today, is a crystalline piece of semiconductor material with a p–n junction connected to two electrical terminals**.** The most common function of a diode is to allow an electric current to pass in one direction (called the diode's *forward* direction), while blocking current in the opposite direction (the *reverse*direction). Thus, the diode can be viewed as an electronic version of a check valve. This unidirectional behavior is called rectification, and

is used to convert alternating current to direct current, including extraction of modulation from radio signals in radio receivers—these diodes are forms of rectifiers []. The Shockley diode equation relates the diode current I of a p-n junction diode to the diode voltage V_D. This relationship is the diode*I-V characteristic*:

$$I = I_S \left(e^{V_D/(nV_T)} - 1 \right),$$

where I_S is the *saturation current* or *scale current* of the diode (the magnitude of the current that flows for negative V_D in excess of a few V_T, typically 10^{-12} A). The scale current is proportional to the cross-sectional area of the diode. Continuing with the symbols: V_T is the thermal voltage (kT/q, about 26 mV at normal temperatures), and n is known as the diode ideality factor (for silicon diodes n is approximately 1 to 2).
When $V_D \gg nV_T$ the formula can be simplified to:

$$I \approx I_S \cdot e^{V_D/(nV_T)}.$$

This expression is, however, only an approximation of a more complex I-V characteristic. Its applicability is particularly limited in case of ultrashallow junctions, for which better analytical models exist.

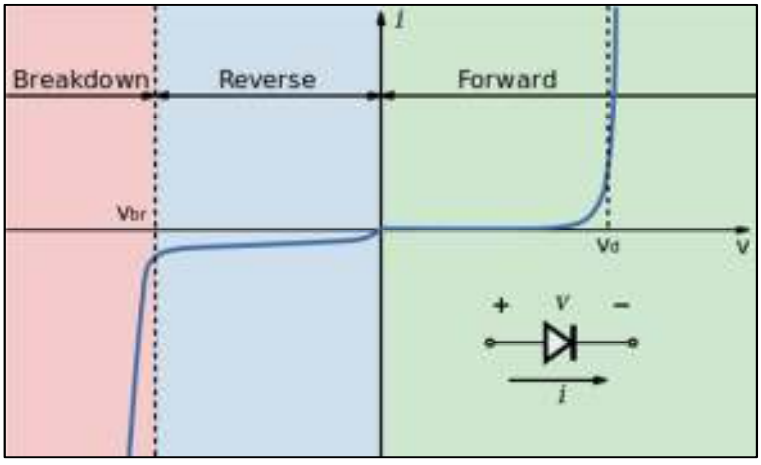

Fig. 4.2: V-I characteristic of p-n juction diode

In the circuits is used diodes 1N4001 that is possible to find in the DIODE library of Capture

- **RIO Gate:** As already said RIO gate is a series of input/output analog/digital gates. For this part of the circuit was not possible to find a model in the libraries of the software and neither an electrical schematic of the internal circuit and so for our purpose it was made using simple on off switches and resistances. The main electrical characteristics for the

simulations are: output voltage, input/output current, on-off switch time, output resistance. Values of voltage and current is possible to see in the datasheets. In the datasheet was not possible to find info about switch time and output resistance. Switch time info needs in case of work in frequency but the circuit works in DC and so switch time is not important for the purpose of simulation, however, since the output of the gate is a transistor probably the switch time is in the order of tens of microseconds (for the simulation it was 10 us). Output resistance is interesting in case of current that flows in the gate is so high to bring down output voltage. From datasheet is possible to see that if the current is within the limit, the voltage output remain constant , this means that is possible to avoid to simulate an output resistance (in case that current is within the limit in datasheet). For digital output gates it was used a switch that simulate the operation of an output transistor assuming a switch time of 10 us. For digital input gates it was used a resistance of 0.5 ohm but could be used a short circuit too since the input current and the output voltage depend both only by external circuit.

- **Electrovalve:** A solenoid valve is an electromechanically operated valve. The valve is controlled by anelectric current through a solenoid: in the case of a two-port valve the flow is switched on or off. A solenoid valve has two main parts: the solenoid and the valve. The solenoid converts electrical energy into mechanical energy which, in turn, opens or closes the valve mechanically.

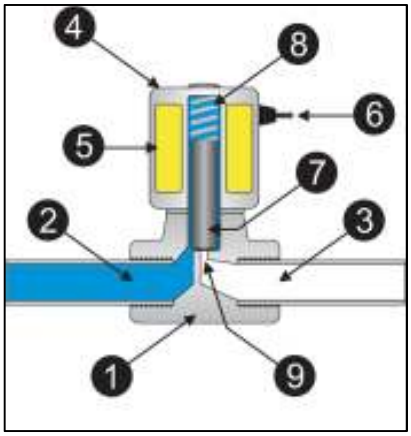

Fig.4.3: solenoid valve

1. Valve Body	4. Coil / Solenoid	7. Plunger
2. Inlet Port	5. Coil Windings	8. Spring
3. Outlet Port	6. Lead Wires	9. Orifice

For the analysis it was necessary to modeling the electric equivalent of the coil. A coil can be modeled as an ideal inductance in series with a resistance that takes into account joule losses and a capacitance in parallel that simulates capacitive coupling of each coil.

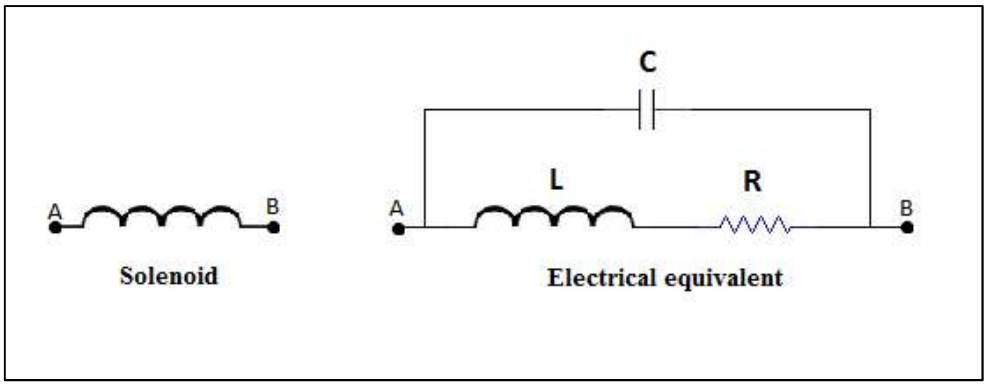

Fig 4.4: Solenoid and electrical equivalent

An RLC circuit has different parameters that describe the dynamic of the circuit. The most important are: *natural frequency, damping factor, Q factor, bandwidth.*

The resonance frequency is defined in terms of the impedance presented to a driving source. It is still possible for the circuit to carry on oscillating (for a time) after the driving source has been removed or it is subjected to a step in voltage (including a step down to zero).

The resonant frequency of the circuit is

$$\omega_0 = \sqrt{\frac{1}{LC} - \left(\frac{R}{L}\right)^2}$$

This is the resonant frequency of the circuit defined as the frequency at which the admittance has zero imaginary part. The frequency that appears in the generalised form of the characteristic equation (which is the same for this circuit as previously)

$$s^2 + 2\alpha s + \omega_0'^2 = 0$$

is not the same frequency. In this case it is the natural undamped resonant frequency

$$\omega_0' = \sqrt{\frac{1}{LC}}$$

The frequency ω_m at which the impedance magnitude is maximum is given by,

$$\omega_m = \omega_0' \sqrt{\frac{-1}{Q_L^2} + \sqrt{1 + \frac{2}{Q_L^2}}}$$

where $Q_L = \dfrac{\omega_0' L}{R}$ is the quality factor of the coil. This can be well approximated by,

$$\omega_m \approx \omega_0' \sqrt{1 - \frac{1}{2Q_L^4}}.$$

Furthermore, the exact maximum impedance magnitude is given by,

$$|Z|_{max} = RQ_L^2 \sqrt{\frac{1}{2Q_L\sqrt{Q_L^2+2} - 2Q_L^2 - 1}}$$

For values of Q_L greater than unity, this can be well approximated by,

$$|Z|_{max} \approx R\sqrt{Q_L^2(Q_L^2+1)}$$

- **Optocoupler:** an opto-isolator, also called an optocoupler, photocoupler, or optical isolator, is a component that transfers electrical signals between two isolated circuits by using light. Opto-isolators prevent high voltages from affecting the system receiving the signal. Commercially available opto-isolators withstand input-to-output voltages up to 10 kV and voltage transients with speeds up to 10 kV/µs. A common type of opto-isolator consists of an LED and a phototransistor in the same package. Opto-isolators are usually used for transmission of digital (on/off) signals, but some techniques allow use with analog (proportional) signals. The main electrical characteristics of an optocoupler are: *Current transfer ratio, isolation voltage, response time, forward current, collector current, Input and output tension.*
  In the circuit there are two LTV-846 optocoupler with the following characteristics:

PARAMETER		SYMBOL	RATING	UNIT
INPUT	Forward Current	I_F	50	mA
	Reverse Voltage	V_R	6	V
	Power Dissipation	P	70	mW
OUTPUT	Collector - Emitter Voltage	V_{CEO}	80	V
	Emitter - Collector Voltage	V_{ECO}	6	V
	Collector Current	I_C	50	mA
	Collector Power Dissipation	P_C	150	mW

Collector Current	I_C	2.5	—	30	mA	I_F=5mA V_{CE}=5V
*1 Current Transfer Ratio	CTR	50	—	600	%	

$$*1 \quad CTR = \frac{I_C}{I_F} \times 100\%$$

- **Charger gate:** Charger gate is a series of Input/output analog/digital gates. As for RIO gate it was designed as a series of simple switches for the digital outputs and as a series of

short circuit for the digital input. The analog I/O was not designed as already said. The transient time for the output switches is 10 us as for the RIO gate.

4.2.2 A/D circuit analysis

In order to understand if currents and tensions are within the limit imposed by each parts, DC transient simulation were done. Before were simulated the operation of each part separately using nominal condition of the circuit and sometimes parametric simulations were done to understand if there is a better solution for the operation. After a chronological simulation of the possible operation of the entire circuit was done. In this work will be explained the chronological analysis and parametric simulations only.

It is supposed that for *t<0s* conditions of the circuit are:

- Power supply OFF
- RIO gate OFF
- Relays OFF position (all the switches are in down position, close circuit)
- Charger gate OFF

For *t=0s*

- Power supply ON
- RIO gate OFF
- Relays OFF position (all the switches are in down position, close circuit)
- Charger gate ON

For t=0 power supply delivers current to the three switches through relays that are in OFF position since they are not yet energized. After a transient due to RLC circuit of the electrovalves, current of the power supply is at $I_{V1} \approx 240\,mA$ which is the sum of the three currents that flow into the three switches $I_{earth} = I_{dump} = I_{FIRE} \approx 80mA$ and:

$$I_{V1} = \frac{V}{R_{sw}/3}$$

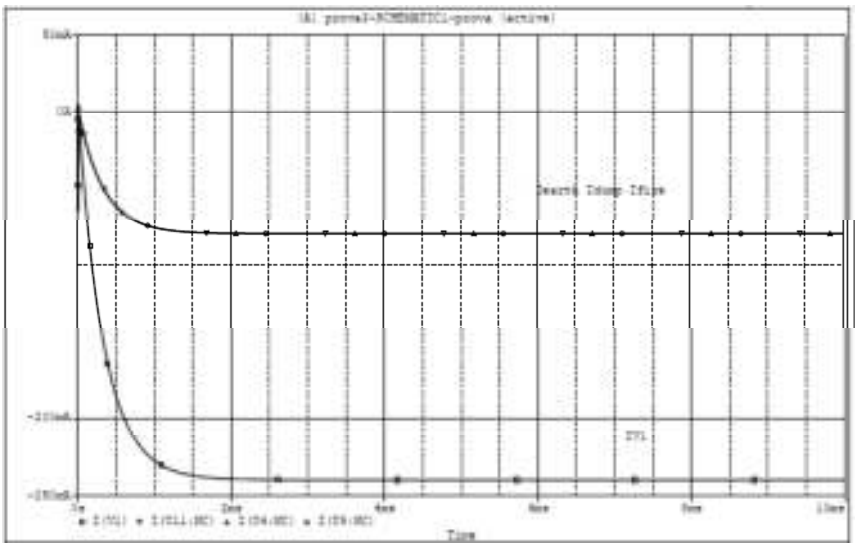

Fig 4.5: Current of the power supply and currents of the three switches

The next command is energize RIO gate through *air switch relay* that is piloted through *air switch.* It was supposed but almost certainly it is a proper supposition, that air switch change its state after a time in the order of seconds or tens seconds after t=0 at least. For this reason the two transients are not overlapped. It was chosen *t=500ms* to turn on *air switch.*

For *t=500ms*

- Power supply ON
- RIO gate ON
- Relays ON air switch relay OFF the rest
- Charger gate ON

Air switch allows the excitation of the *air switch relay* and so through the air switch flows a current with a transient of an RL DC circuit since the driver of the relay is a coil. The equation of the current is:

$$i(t) = \frac{V}{R}\left(1 - e^{-\frac{t}{\tau}}\right) + i(0)$$

Where:

$$i(0) \approx 0$$

$$\tau = \frac{L}{R} = \frac{4.21\ H}{1100\ \Omega} = 3.82\ ms\ (electric\ costant)$$

Time domain (transient) simulation condition:

- Start save data time: 495 ms
- Run to time: 530 ms
- Maximum step size: 0.05 ms

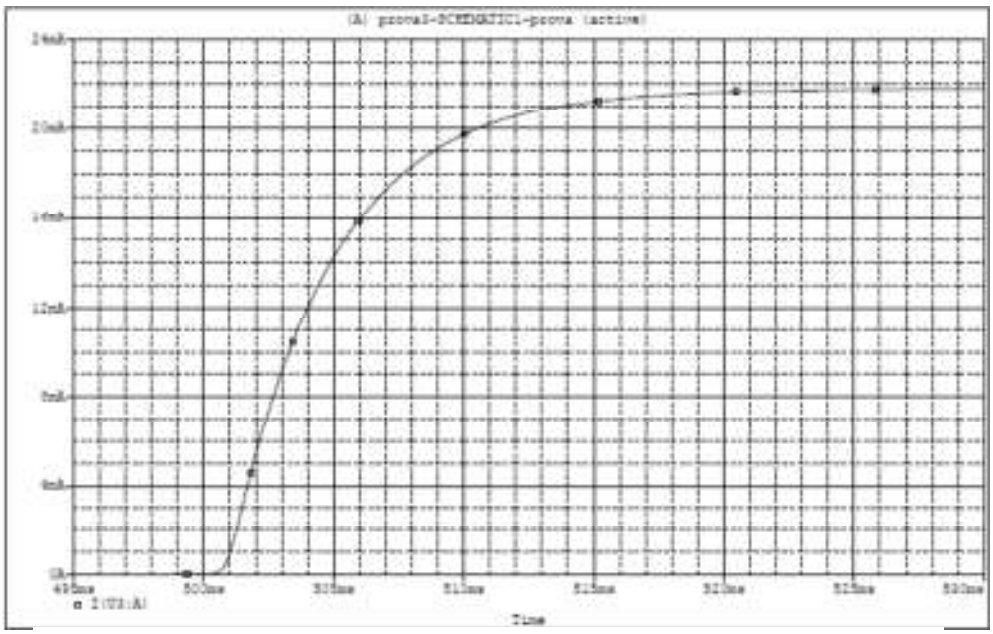

Fig.4.6: I exciting of the relay (pneumatic switch)

As is possible to see in Fig. 4.6 the current is slightly different, especially in the first part of the transient, from analytic trend due to switching time of the air switch that is comparable with electric constant of the circuit. In this case current cannot rise as in the equation but it has to follow the dynamic of the air switch. By the graph is possible to see that after 3τ current is almost at steady-state value that is:

$$I = \frac{V}{R_{coil}} = \frac{24}{1100} \approx 22mA$$

Current of the power supply is shown in Fig.4.7:

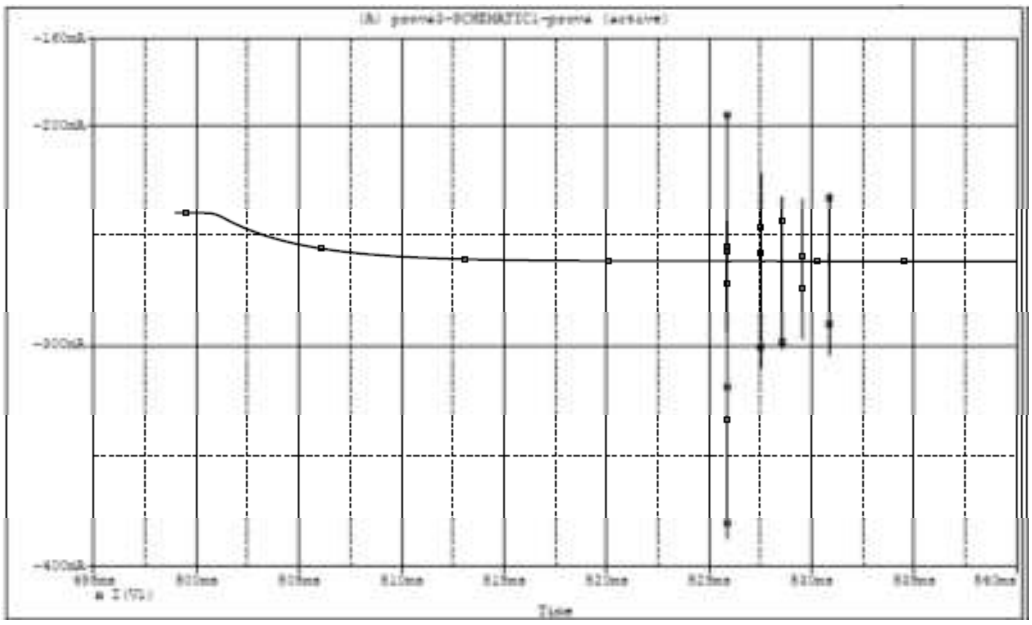

Fig. 4.7 Power supply current after air switch relay excitation

At the end of the transient current achieves value of $I_V \approx 262\ mA$.From datasheet of the relay is possible to see that $I_{pull} = 20mA$ and this value of current is achieved at t=510,5 ms (10,5 ms after switch closure). After other 15ms (Tmake) the pin can change is status from normally close to normally open at t=525,5 ms. As is possible to see from Fig.4.6, after pin change spikes of current occur due to a phenomen called *bounce*.

Contact bounce

Push-button switches, toggle switches, and electro-mechanical relays all have one thing in common: contacts. It's the metal contacts that make and break the circuit and carry the current in switches and relays. Because they are metal, contacts have mass. And since at least one of the contacts is on a movable strip of metal, it has springiness. Since contacts are designed to open and close quickly, there is little resistance (damping) to their movement.

Because the moving contacts have mass and springiness with low damping they will be "bouncy" as they make and break. That is, when a normally open (N.O.) pair of contacts is closed, the contacts will come together and bounce off each other several times before finally coming to rest in

a closed position. The effect is called "contact bounce" or, in a switch, "switch bounce" see Fig.4.8. Note that contacts can bounce on opening as well as on closing.

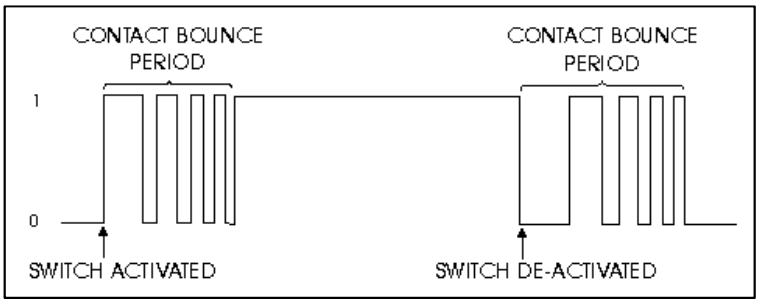

Fig.4.8: Bounce effect

If switch or relay is used turn on a lamp or start a fan motor, then contact bounce is not a problem. But if switch or relay is used as input to a digital counter, a personal computer, or a micro-processor based piece of equipment, then you must consider contact bounce. The reason for concern is that the time it takes for contacts to stop bouncing is measured in milliseconds. Digital circuits can respond in microseconds.

Bounce effect creates rapid variations of tension over C1 capacitance. From:

$$I_c = C\frac{dv_c}{dt}$$

Is possible to see that spikes of current depend from C value and rise/fall of the tension over the capacitance. C1 is used to decrease ripple of the tension at the output of power supply as a low pass filter. A parametric analysis shows how different value of C can change the ripple of the tension.Three different values of C are used: 0-10-100 nF with the follow results:

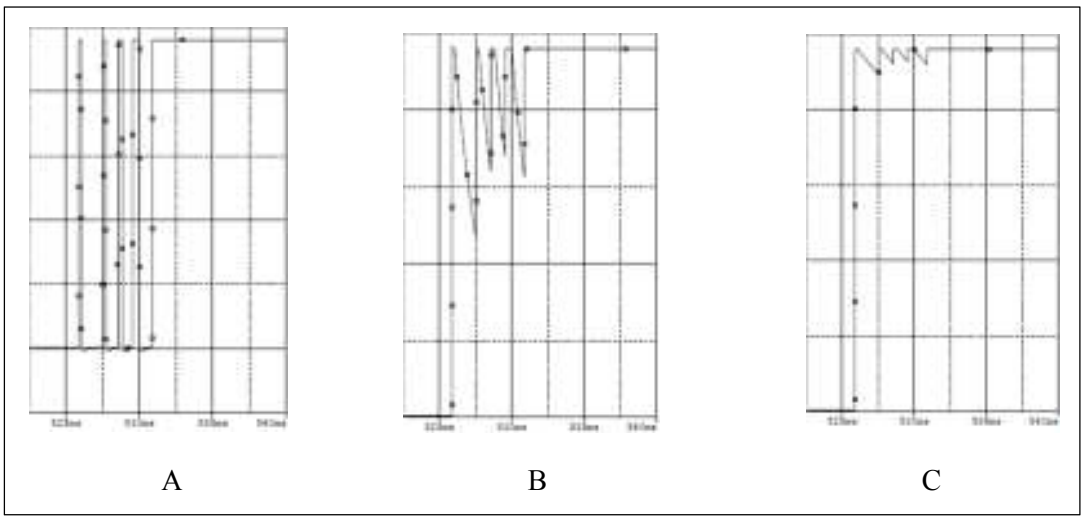

Fig.4.9: Bounce of tension over relay pin with different value of C1: A)0nF B)10nF C)100nF

As shown, more is C value less is ripple of tension but more is C value and higher are spikes of current as said before. 10nF is a common value to use in this kind of circuit. In any case gap time of bounce is 5 ms as datasheet. The others three relays have the same operation.

For *600<t<1200 ms*

- Power supply ON
- RIO gate ON
- Relays ON air switch relay OFF the rest
- Charger gate ON

HV On control – HV On monitor – EOC monitor

- *HV On control* is a signal from RIO gate to Charger gate that turn on the charger
- *HV On monitor* is a signal from Charger gate to RIO gate that shows in the LabVIEW software if the HV On led of the charger is on
- *EOC monitor* is a signal from Charger gate to RIO gate that is on at the end of the charge of the battery.

The three previous signals have to be on if the circuit is operating properly until the end of the charge of the bank of capacitances. If, for example, the charge of the capacitance is not successfully completed *EOC monitor* will be off and *Fault monitor* will be on anyway in this gap time three digital signals are on. Value of current of the digital signals is less than value of current of the relays because optocoupler needs very low level of current and so it need to limit current using resistance at the input/output of it. For the LTV-846 optocoupler was not found a model for PSpice Capture and so it was found a model quite similar for electrical characteristics, in the OPTO library of the software, called PS-2501 with the follow main characteristics:

Parameter		Symbol	Conditions	MIN.	TYP.	MAX.	Unit
Diode	Forward Voltage	V_F	I_F = 10 mA		1.17	1.4	V
	Reverse Current	I_R	V_R = 5 V			5	μA
	Terminal Capacitance	C_t	V = 0 V, f = 1.0 MHz		50		pF
Transistor	Collector to Emitter Dark Current	I_{CEO}	V_{CE} = 80 V, I_F = 0 mA			100	nA
Coupled	Current Transfer Ratio (I_C/I_F)*1	CTR	I_F = 5 mA, V_{CE} = 5 V	80	300	600	%
	Collector Saturation Voltage	$V_{CE(sat)}$	I_F = 10 mA, I_C = 2 mA			0.3	V
	Isolation Resistance	R_{I-O}	V_{I-O} = 1.0 kVDC	10^{11}			Ω
	Isolation Capacitance	C_{I-O}	V = 0 V, f = 1.0 MHz		0.5		pF
	Rise Time*2	t_r	V_{CC} = 10 V, I_C = 2 mA, R_L = 100 Ω		3		μs
	Fall Time*2	t_f			5		

Fig 4.10 shows dynamics of Input and Output current of the optocoupler and as said before transient of this part is much faster than relays transient.

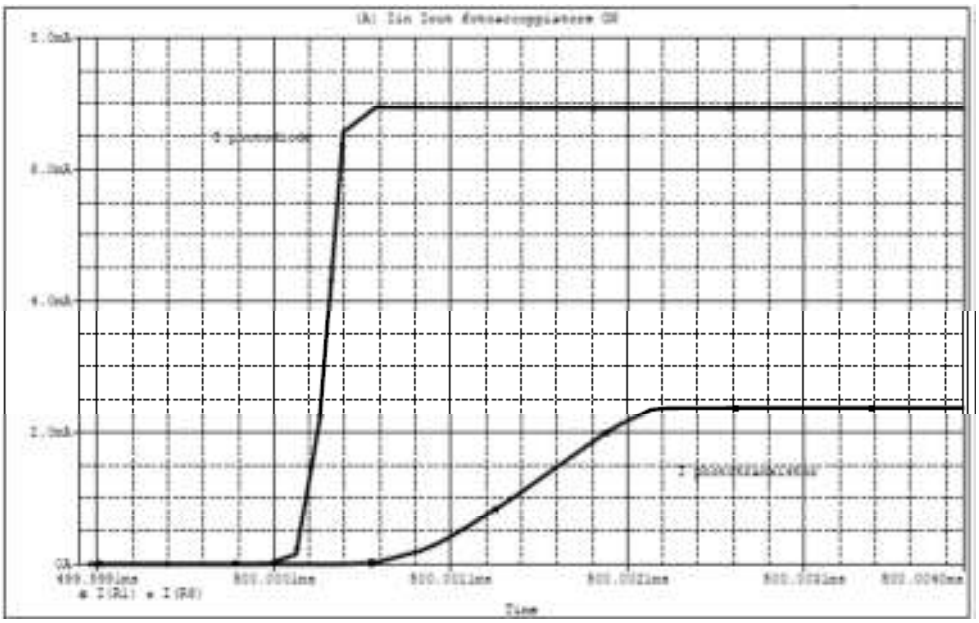

Fig.4.10: Transient of turn on of PS-2501 optocoupler

t_{rise} of output current is in the order of some microsecond.

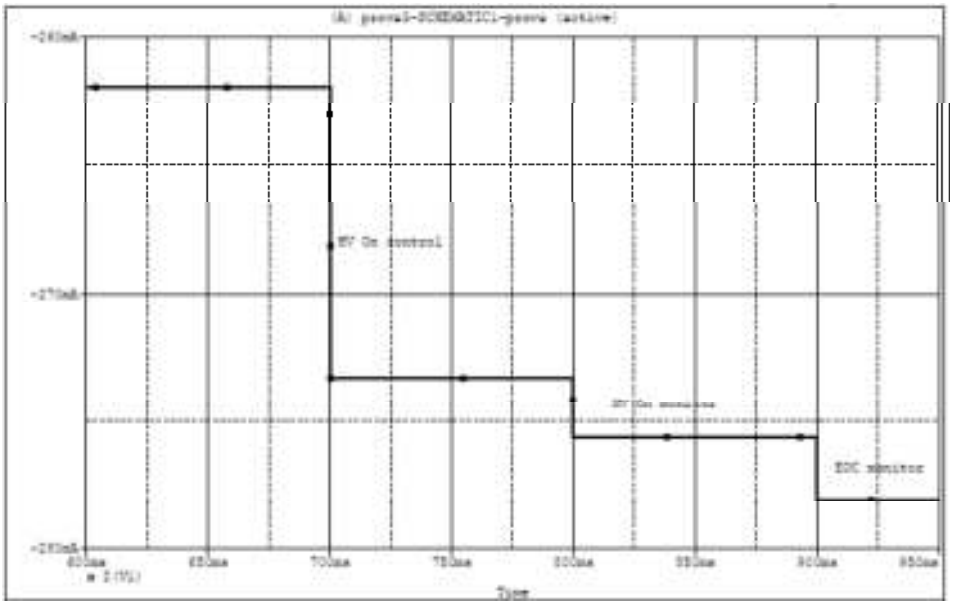

Fig.4.11: I power supply in the gap 600-950 ms

Analytically:

$$I_{HV\ On\ control} = \frac{V - V_F}{R} = \frac{24 - 1.17}{2k} = 11.41\ mA$$

$$I_{HV\ On\ monitor} = \frac{V - V_{ce\ sat}}{R} = \frac{24 - 0.3}{10k} = 2.37\ mA$$

$$I_{EOC\ monitor} = I_{HV\ On\ monitor}$$

From the graph is possible to see almost the same values.

$I_{EOC\ monitor} = I_{HV\ On\ monitor}$ are Input currents for RIO gate and from its datasheet is possible to see that the limit of the input current has to be between 3 and 7 mA and so is not sure that it will work properly.

For *t> 900ms*

Earth switch – Dump switch – FIRE switch

To fire the A/D waveforms needs before to open earth way through *Dump and earth switches* and after is possible to close *FIRE switch.*

Fig 4.12 shows power supply current in the gap of switching of *earth relay.*

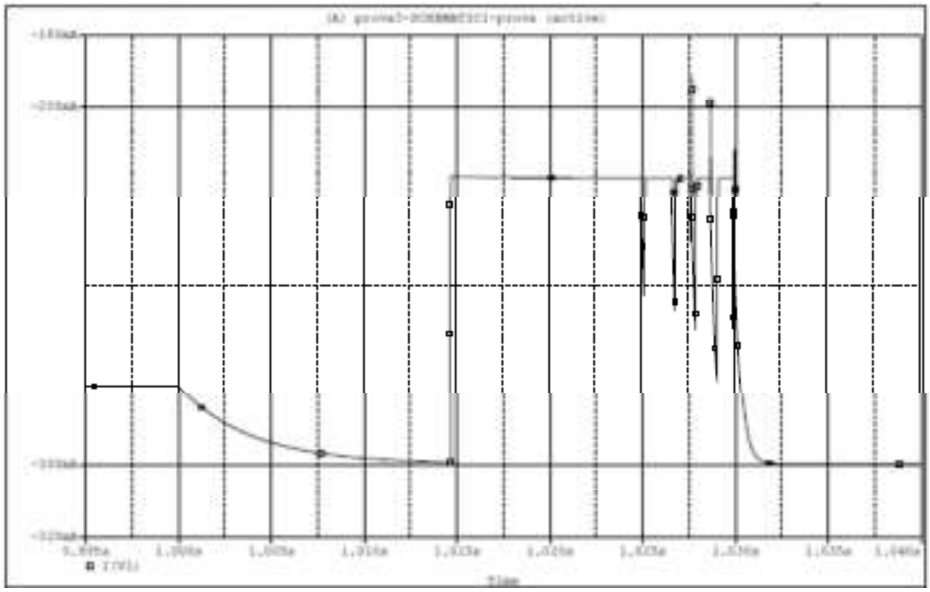

Fig.4.12: Power supply current during earth relay switching time

As is possible to see in the fig.4.12 there are:

the first transient due to excitation current of the relay, second part where current is decreased by 80 mA due to gap time between *T break* and *T make* where the out pin is floating and so no current is flowing through the it. After there is bounce time of 5ms about and at the end there is the transient of rise of current in the electrovalve.

Interesting to know is since electrovalve is an inductive load and high di/dt like that one of relay pin change causes high voltage peaks as shown in fig.4.13

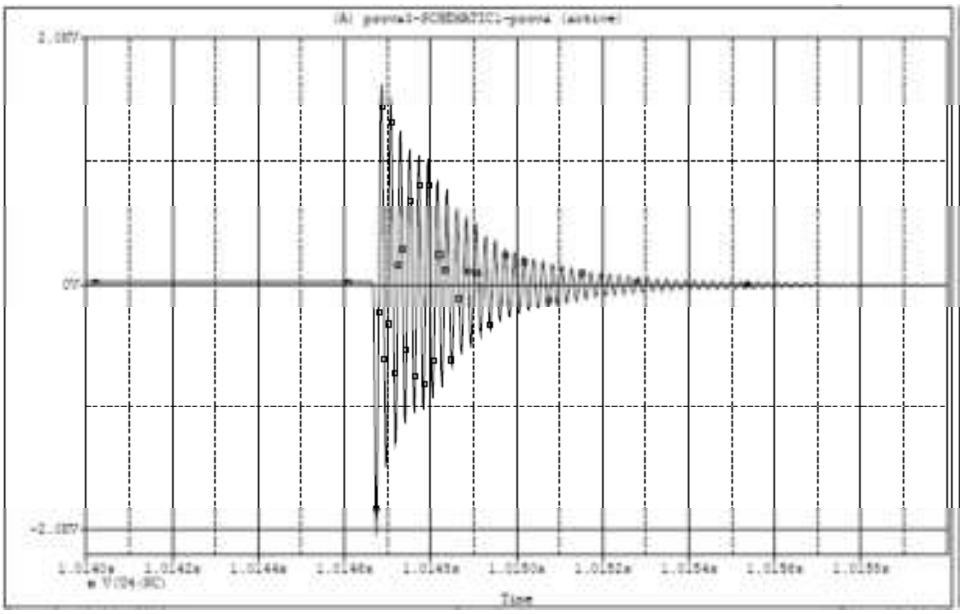

Fig.4.13: Voltage over electrovalve during relay pin swaping

As is possible to see from Fig.4.13 the voltage peak is almost 2kV and this could damage pin of the relay or isolation of the relay and electrovalve.

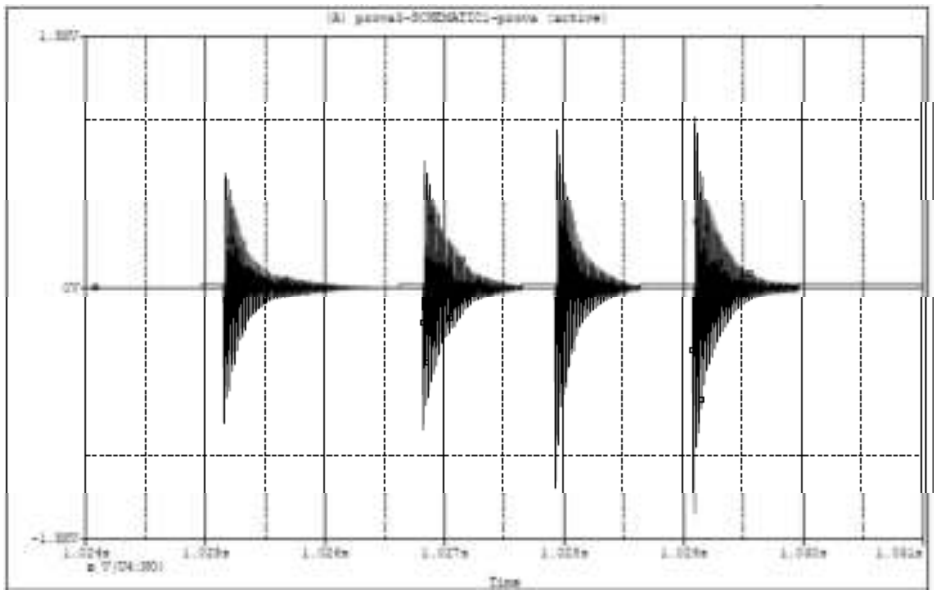

Fig.4.13: Voltage over electrovalve during relay pin swapping with bounce effect

In order to avoid voltage spikes over electrovalves during commutation of the relay is possible to use diodes to ensure that energy stored in the valve coil can flow next opening of the circuit.

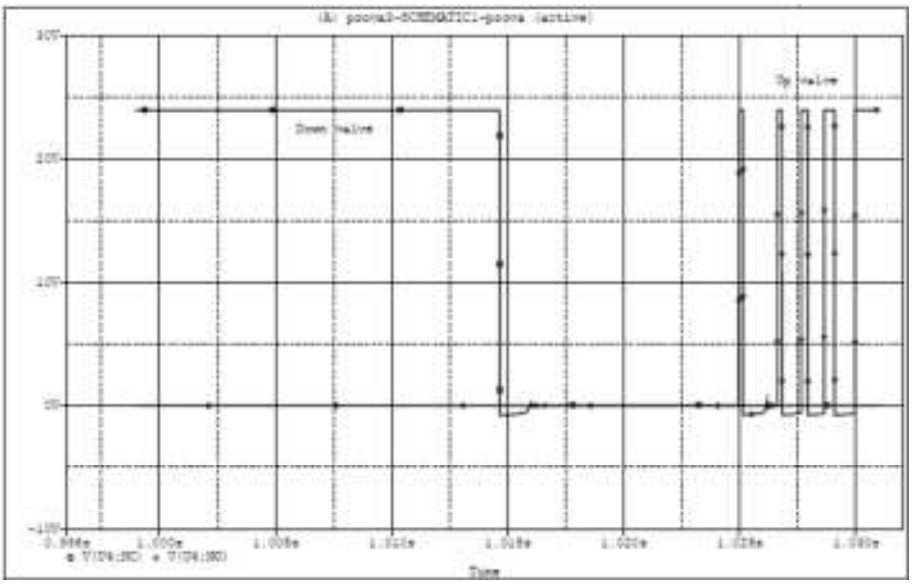

Fig.4.14: Voltage over electrovalve during relay pin swapping with diode

Total current delivered from power supply is shown in fig.4.15

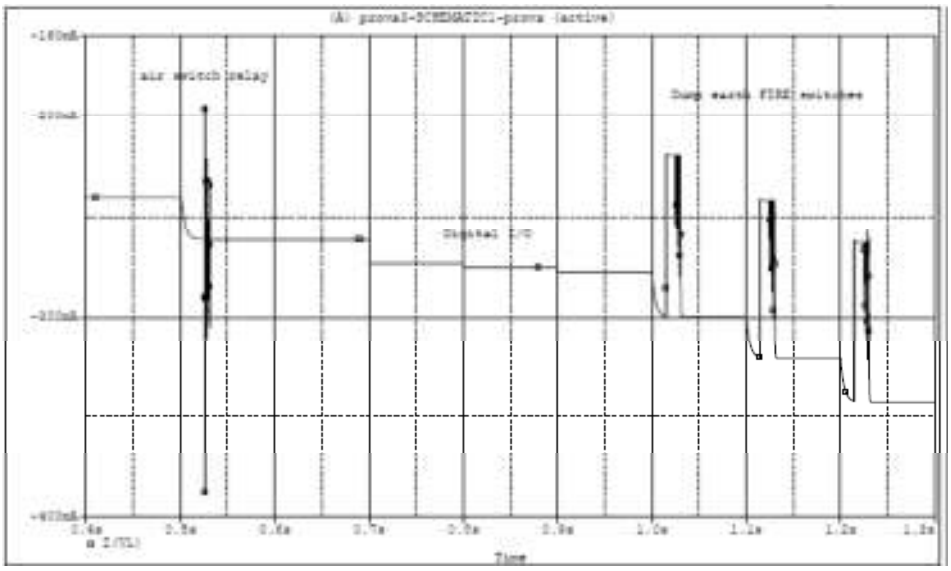

Fig4.15: trend of power supply current until end of fire of A/D waveform

After fire of A/D waveform there will be de excitation of the *FIRE – Dump – Earth relays* and there will be an opposite trend of the current. De excitation of relay has to be analyzed. Since during excitation of the relay, coil store energy $E = \frac{1}{2}LI^2$ that has to be disposed of for the de excitation. Presence of diode in antiparallel of the coil ensure that during switch off of the relay energy stored in the relay coil can flow form current through diode. If diode is not present over the coil there will be a tension:

$$v_L = L\frac{di}{dt}$$

Values of v_L depend by value of inductance (that for a 24 VDC coil is very high) and fall time of the current that depends by switch off time of the RIO gate. In the fig.4.16-4.17 is possible to see transient of switch off of the *FIRE relay* and current through the diode

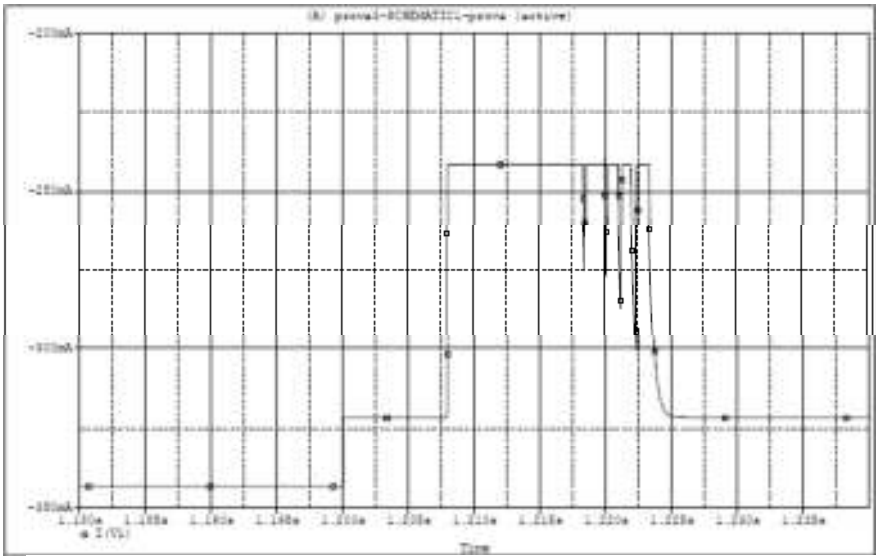

Fig.4.16: transient of de excitation of FIRE relay

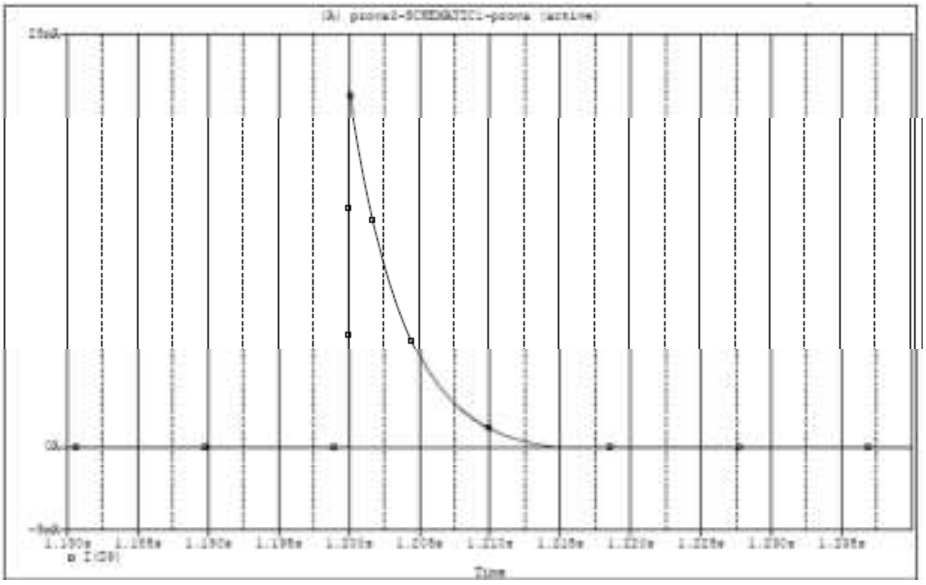

Fig.4.17: Diode current during de excitation

Without diode tension over the switch can achieve thousand volt, as shown in fig.4.18, and all the energy stored within the coil flows through RIO gate risking damage to it.

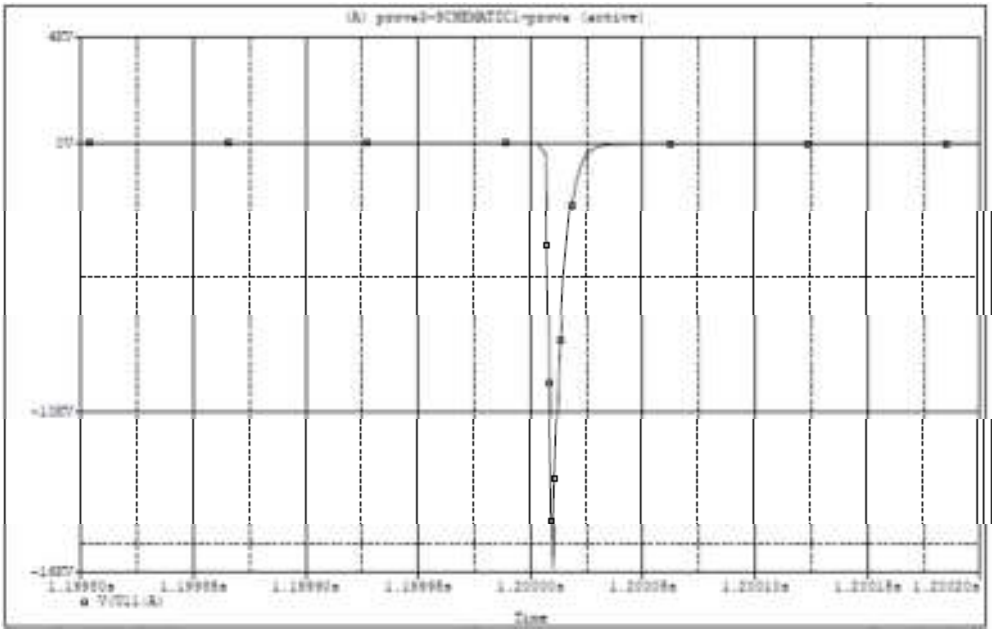

Fig.4.18: Tension over relay coil during de excitation without diode

4.3 B/C bank sizing and analisys

As explained in the third chapter, B/C bank has the operations of the A/D bank and it is made by the same components (RIO gate, relays electrovalves, air switch, Charger gates). Different between the two circuits are: one less relay one more RIO gate and one more charger gate and output optical gate. Dynamics of currents and tension of the circuit are quite the same. It needs to analyze current through optical output during transient time.

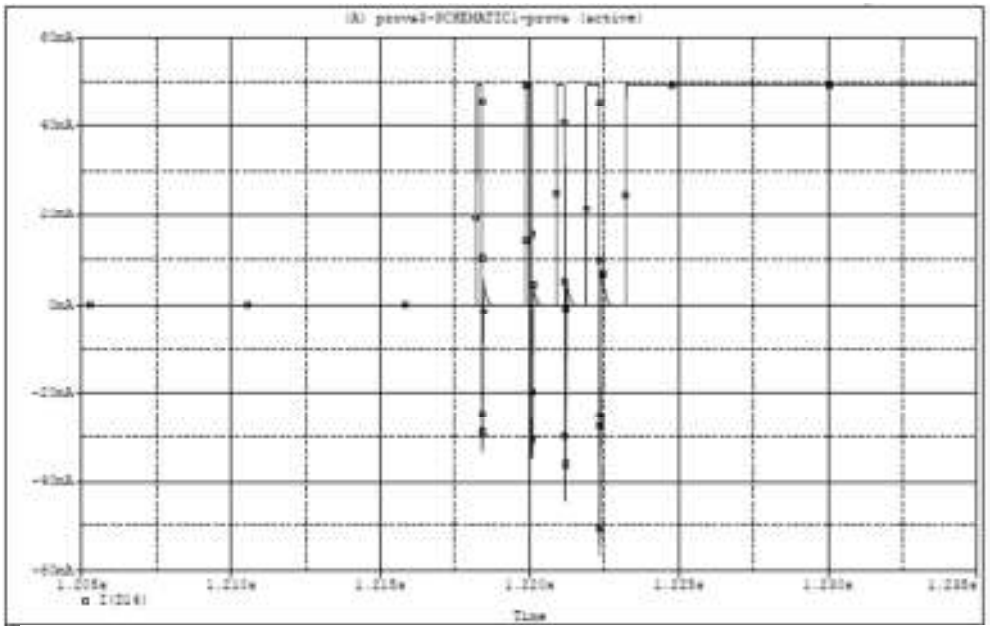

Fig.4.19: Switch on current of the phototrasmitter

As is possible to see in Fig.4.19 the bounce effect of the relay makes current spikes over photodiode.

4.4 Trigger circuit sizing and analysis

4.4.1 Trigger circuit sizing

In the trigger circuit need to analyze the sub circuit that provides to trigger A/D waveform through rogowski coil and make the 500ms signal to send to LabVIEW to Fire B/C waveform as said in chapter three.

- **Rogowski coil:** there is not a part in the PSpice libraries for this component but the output of the sensor is a tension that follows trend of the current that flow into the coil of the sensor. Is possible to model rogowski coil through a tension generator with an impulsive waveform with duration of the impulse equal to duration of A/D waveform (500us).
- **Rectifier:** is made by a Graetz bridge and so it was used four diodes to model it.
- **Optocoupler:** it was used a PS2501 like the others two circuits since it has quite the same characteristics of the real optocoupler SFH 618A/2
- **NE555 timer:** for this component it was used the equivalent from *ANALOG Library* and as said before the operation mode of the timer was monostable and to send a 500ms signal need to use a commercial resistance of 47k and a capacitance of 9.7 uF.
- **Optic trasmitter:** optic output is a simple photodiode. Difference between a diode and a photodiode from the electrical point of view that is interesting for the analysis is V_F for a photodiode is higher than a normal diode. In order to model this part it was used a normal diode with tension generator in series so that when photodiode is conducting its V_F is the sum of the tension generator and V_F of the diode.

4.4.2 Trigger circuit analysis

In the analysis it was studied input current of the optocoupler if it is within the limit or if need to change resistances but at the voltage peak of rogowski coil current is about 15 mA and this is enough to activate optocoupler. Vcc power supply delivers current for the output of the timer and its trend is the same of the output current and so all the considerations did for Iout are the same for Icc.

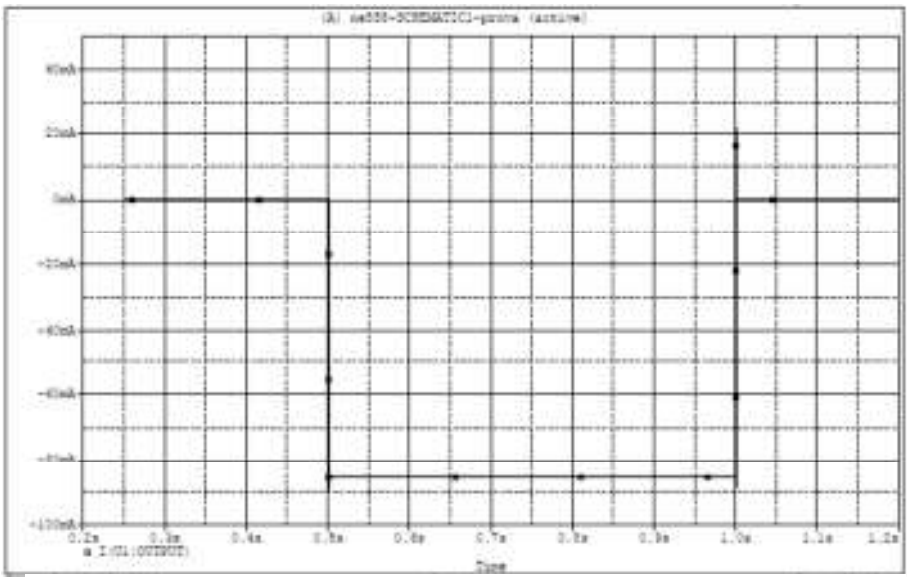

Fig.4.20: Output current of the NE555 timer

As is possible to see in Fig.4.20 from a 500us voltage pulse by using timer is possible to make a signal of 500ms. Furthermore Output current has to divide in the four parallel optotrasmitter (about 20mA each).

CONCLUSION

As said at the start of this work need to ensure safety for people, circuits, etc. has led to the need to design circuits very simple to manage. Interfacing with pneumatic control system through air switch ensure that people cannot use control system before all the safety protocols have been met. Communication by optical signals between chassis and control chamber is another point in favor of safety. Within the circuit safety level is ensured through using electromechanic relays instead, for example, state solid relays and using optocoupler between the two gates to ensure galvanic isolation. All the chassis are made to share with control chamber only command signals and not power signals (all the power supplies for the circuits are within the chassis).

To improve the operation of the control system consideration should be done:

- A/D chassis circuit: presence of electrovalves over output of the relays involves inductive loads for relays. Energy stored within valve coils during them on-state has to be disposed to go to off-state. For this reason could be better if free wheel diodes are positioned in antiparallel with valve coils. Current measured at the digital input of the RIO gate after signals from Charger gate does not achieve the minimum value at datasheet of RIO gate and this could induce no-activation of the gate. In this case resistances at the output of optocoupler should be changed in such a way to allows current to be within limits of RIO gate.
- B/C chassis circuit: presence of bounce effect for electromechanic relay causes current spikes at the input of the optotrasmitter that communicate with the IGBT in parallel with *Dump switch.* If spikes cause problem for the gate driver of the IGBT need to use a low pass filter at the input of the optotrasmitter.

BIBLIOGRAPHY

[1] AGATE, "Lightning Direct Effects Handbook," Ed Rupke Lightning Technologies Inc., Pittsfield, 2001

[2] V. Rakov, "Ligthning," 2006. [Online]. Available: http://www.plasmacoalition.org/plasma_writeups/lightning.pdf. [Accessed 20 Feb. 2012].

[3] T. Edwards, "Composite Materials Revolutionise Aerospace Engineering," Ingenia Mag., vol. 1, no. 36, pp. 50-57, Sept. 2008.

[4] C. Y. Niu, Composite Airframe Structures: Practical Design Information and Data, 1 ed., Wanchai: CONMILIT, 1992.

[5] B. C. Hoskin, "Introduction," in Composite Materials for Aircraft Structures, B. C. H. a. A. A. Baker, Ed., New York, AIAA, 1986, pp. 1-8.

[6] E. Guizzo, "Carbon take off [Carbon Fibre Composites]," IEEE Spectrum, vol. 43, no. 1, pp. 26-29, Jan. 2006.

[7] R. Wilkinson, Aircraft Structures and Systems, 1 ed., Essex: Longman, 1998.

[8] Ravi B. Deo, "Low-Cost Composite Materials and Structures for Aircraft Applications," RTO AVT Specialists' Meeting on "Low Cost Composite Structures", Vols. RTO-MP-069, no. II, May 7-11 2001.

[9] A. A. Baker, "Introduction," in Composite Materials for Aircraft Structures, 2nd ed., S. D. a. D. K. A. A. Baker, Ed., Reston, AIAA, 2004, pp. 1-21.

[10] N. Wright, "New technology drives indirect lightning test standards," in 10th International Conference on Electromagnetic Interference & Compatibility, 2008. INCEMIC 2008., Bangalore, 2008.

[11] J. Cutler and J. Liber, Understanding Aircraft Structures, 4th ed., Malden: Blackewell Publishing Inc., 2005.

[12] Standard - ED-14E - Section 23 - Lightning Direct Effects

[13] MBLL documentation

[14] High-Speed Imaging and Radiative Energy Measurements of a High-Current Pulsed Arc in Air H. Rabat, D. Hong, J.-M. Bauchire, and G. Riquel

[15] Characteristics of Lightning Discharges and Electric Structure of Thunderstorm Qie Xiushu, Zhang Yijun , and Zhang Qilin

[16] MBLL, "Background," 2011. [Online]. Available: http://www.mbll-cardiff.com/index.php/background. [Accessed 23 July 2012].

[17] C. U. N. Centre, "Lightning research advances," Oct. 2011. [Online]. Available: http://www.cardiff.ac.uk/news/articles/lightning-research-advances-7430.html. [Accessed 15 April 2012].

[18] C. U. N. Centre, "A year of achievement," March 2012. [Online]. Available: http://www.cardiff.ac.uk/news/articles/a-year-of-achievement-8437.html. [Accessed 15 April 2012].

[19] TECHNIX, "Operator Manual: SR60-P-20000 Model," TECHNIX, Creteil, 2012

[20] TECHNIX, "HIGH VOLTAGE GENERATORS," 20 September 2011. [Online]. Available: http://www.technix-hv.com/high_voltage_power_supplies/pdf/SR_15000_40000W_Series.pdf.

[21] IXYS, "Catalog," 2011. [Online]. Available: http://www.ixys.com/Documents/catalog_11-12.pdf.

[22] Bristish Standards Institution;, "BS 1977:1976 Specification for high conductivity copper tubes for electrical purposes," BSI, London, 1976.

[23] General Atomic Energy Products;, "Capacitor Specification: Part Number 32349," GAEP, San Diego, 2012.

[24] H. V. R. International, "Linear Disc Resistors," HVR, 14 February 2012. [Online]. Available: http://www.hvrint.com/lineardisc.htm.

[25] ELAND Cables, "H01N2-D Welding Cable," 4 May 2009. [Online]. Available: http://www.eland.co.uk/documents/H01N2D%20Cables.pdf.

[26] F. &. B. Ltd., “F-type: Foward Curve Multivane Fans,” 7 June 2011. [Online]. Available: http://www.fansandblowers.com/wp-content/files/BC_Fan_Range2.pdf.
[27] Athena Energy Corp, “High Performance, Wide Bandwidth Rogowski Coil and Amplifier: Instructions for Use,” July 2012. [Online]. Available: http://athenaenergycorp.com/htmlsite/docs/pubs/papers/Owner's_Manual.pdf.
[28] P. G. Leichauer, C. Stone and R. Rogers, “The Lightning Lab Control System: Setting up and running the control backbone,” MBLL, 2011.
[29] HIRSCHMANN, “Description and Operating Instructions: Optical Interface Converter OZDV 2451 G,” 2003. [Online]. Available: http://docs-europe.electrocomponents.com/webdocs/0d0c/0900766b80d0c38e.pdf.
[30] RS, “OZDV2451G V.24/RS232 to fibre converter,” 2012. [Online]. Available: http://radionics.rs-online.com/web/p/interface-converters/3672327/.
[31] Agilent Technologies Inc., “Versatile Link: The Versatile Fiber Optic Connection HFBR-0501 series,” 12 June 2001. [Online]. Available: http://pdf1.alldatasheet.com/datasheet-pdf/view/112355/HP/HFBR2522.html.
[32] EUROCAE WG-31/SAE AE4L, “ED-105: Aircraft Lightning Test Methods,” EUROCAE, Paris, April 2005.
[33] FLIR, “SC7600-MB: State-of-the-art Infrared Systems For R&D And Thermography Applications,” 2009. [Online]. Available: http://www.flir.com/uploadedFiles/Thermography/MMC/Brochures/T559240/T559240_EN.pdf.
[34] Photron, “FASTCAM SA5: ULTRA HIGH-SPEED VIDEO SYSTEM,” 2012. [Online]. Available: http://www.photron.com/datasheet/FASTCAM_SA5.pdf.
[35] Uvirco Technologies, “CoroCAM 504: The Ultimate Daylight Corona Imaging Camera,” June 2011. [Online]. Available: http://www.corocam.com/cc504/CoroCAM_504_brochure.pdf.
[36] Bitter, R.; Mohiuddin, T.; Nawrocki, M.;, LABVIEW ADVANCED PROGRAMMING TECHINIQUES, London: CRC Press LCC, 2001.
[37] http://en.wikipedia.org/wiki/LabVIEW
[38] http://www.technix hv.com/high_voltage_power_supplies/pdf/CCR_2500_5000_Js_Series.pdf
[39] https://eb.automation.siemens.com/mall/en/IT/Catalog/Product/6EP1333-2AA01
[40] Metal work catalog
[41] Liteon LTV-846 datasheet
[42] http://www.ni.com/compactrio/
[43] HFBR-0500ETZ Series datasheet
[44] http://en.wikipedia.org/wiki/Rogowski_coil
[45] ST microelectronics NE555P datasheet
[46] TRACOPOWER TEN25-1212 datasheet
[47] TRACOPOWER TML402 15C DATASHEET

ABSTRACT

Come tutti sanno l'energia fornita da un fulmine è molto più alta dell'energia gestita quotidianamente dall'uomo e quindi un laboratorio di fulmini deve soddisfare due requisiti: il primo e il più importante la sicurezza per le persone per gli edifici e per i circuiti elettrici. Dal primo requisito segue il secondo: quanto più semplicità nella progettazione dei circuiti.

INTRODUZIONE

Al giorno d'oggi, gli sforzi globali per ridurre i gas a effetto serra (GHG) in tutti i settori hanno rafforzato l'uso di nuovi compositi in Fibra di Carbonio (CFC) materiali nelle strutture della cellula. Tuttavia, dato che ogni aereo commerciale è colpito da un fulmine, almeno una volta l'anno, la sicurezza in volo di questi velivoli di nuova generazione diventa estremamente importante. Di conseguenza, Cardiff University ha creato una collaborazione con il produttore di aeromobili, EADS ®, e il governo gallese, per stabilire centro di ricerca di simulazioni di fulmini , chiamato Morgan-Botti Lightning Laboratory (MBLL). Dai due requisiti discussi nell'abstract il primo ha condotto a costruire un sistema di sicurezza a comando pneumatico che ha la caratteristica di essere quasi immune da disturbi elettromagnetici e può gestire la sicurezza del laboratorio durante gli esperimenti e durante il resto del tempo, ad esempio durante la manutenzione del circuito principale. L'aggiunta di una camera di controllo, dalla quale è possibile gestire tutto il laboratorio, che ha la caratteristica di essere una gabbia di Faraday e una trasmissione I / O di tipo ottico del sistema per comunicare dalla camera di controllo al circuito e viceversa garantisce la massima sicurezza per le persone all'interno del laboratorio. Il secondo requisito ha condotto alla realizzazione di semplici circuiti RLC che sono stati progettati per gestire correttamente elevati valori di correnti e tensioni (correnti nell'ordine delle centinaia di migliaia di ampere e tensioni nell'ordine delle decine di kilovolt).La necessità di gestire i circuiti principali in remoto (per garantire la sicurezza delle persone) ha richiesto la progettazione e costruzione di un sistema di controllo che consente di gestire tutte le funzionalità del circuito principale dalla camera di controllo tramite software di interfaccia LabVIEW. Ancora una volta, per garantire la semplicità del sistema di controllo, esso funziona in modalità DC e ad anello aperto. Nella prima parte di questo lavoro saranno spiegati i fenomeni della fulminazione dal punto di vista fisico, considerando come un fulmine può nascere e come può si propaga e le caratteristiche elettriche. Saranno fatte considerazioni generali sui CFRPs ,le loro caratteristiche meccaniche e le caratteristiche elettriche e le interazioni tra un fulmine e i CFRPs . Il MBLL sarà in grado di effettuare test che riproducono fedelmente un fulmine naturale. La forma corretta delle forme d'onda per le prove sono stati studiati da L'Organizzazione europea delle apparecchiature dell'aviazione civile (EUROCAE) e sono inclusi nella relazione ED84. Il MBLL sarà in grado di riprodurre le forme d'onda EUROCAE. Nella prima parte di questo lavoro sarà fatta una breve descrizione delle forme d'onda EUROCAE. Nel secondo capitolo saranno discusse le caratteristiche del MBLL considerando i principali circuiti elettrici e il loro funzionamento atto a riprodurre i diversi tipi di forme d'onda. Le forme d'onda create dai circuiti principali devono essere opportunamente coordinate in modo da simulare un fulmine per questo motivo il laboratorio è dotato di un sistema di controllo che è in grado di gestire il funzionamento dei circuiti elettrici. Il terzo capitolo sarà focalizzato sul sistema di controllo, in particolare, il circuito elettrico e il funzionamento dei tre chassis. Nel quarto capitolo verranno spiegate le simulazioni di funzionamento del sistema di controllo correlate da grafici e dei relativi risultati. Le simulazioni sono state effettuate con il software Orcad PSpice 9.1 per Windows